APPLICATION OF MAGNETO-RHEOLOGICAL DAMPER ON RISER TENSIONER SYSTEM FOR LOW-HEAVE SEMISUBMERSIBLE TO REDUCE RISER STROKE

A Thesis

by

MUHAMMAD ZAID BIN ZAINUDDIN

Submitted to the Office of Graduate and Professional Studies of
Texas A&M University
in partial fulfillment of the requirements for the degree of

MASTER OF SCIENCE

Chair of Committee,	Moo Hyun Kim
Committee Members,	Richard Mercier
	Alejandro Orsi
Head of Department,	Sharath Girimaji

December 2017

Major Subject: Ocean Engineering

ABSTRACT

The push for optimizing current technology in semisubmersible system enables reduction in semisubmersible overall size. One field that see potential optimization is the riser operation philosophy, which in certain cases become the restricting factor of utilizing smaller semisubmersible. In adverse sea-state riser stroke becomes large such that it results in large topside deck, hence large hull. The objective of this thesis is to employ the magneto-rheological damper (MR Damper) in riser system to ameliorate the riser stroke in storm event in order to reduce the deck spacing. This leads to reduction in deck size. In addition, this thesis looks into suitable semisubmersible that generates favorable motion to be used hand-in-hand with the MR damper. Finally, this thesis investigates the operational philosophy of the riser tensioner system and MR Damper that result in the most optimum riser stroke. The analysis develops a new shallow draft low-heave semisubmersible with the resulting favorable riser stroke of 7.55m (24.76ft) without MR Damper. Using this as the host vessel, the analysis finds that the most optimum use of MR Damper on riser tensioner system is by having the MR Damper constantly engage to the riser tensioner ring so that it can dissipate energy when the stroke is at its highest speed, that is when the stroke is at nominal (at zero stroke). Then applying linear damping coefficient of 9000 kN/ms^{-1} onto the MR Damper reduces riser stroke from 7.55m (24.76ft) to 4.52m (14.81ft), well within the target stroke of 4.57m (15ft). The reduction of the stroke is attributed to the energy dissipation in semisubmersible heave motion and riser top motion, leading to lower heave motion and riser top motion. Implementing an up-scaled MR Damper numerical model results in total stroke close to linear damping MR Damper model, that is 4.91m (16.11ft). In conclusion, the

application of MR damper in riser tensioner system results in a lower riser stroke, the utilization of a low-heave semisubmersible also results in a lower riser stroke, and the constantly-engaged MR Damper during storm event allows an effective use of MR Damper.

DEDICATION

This thesis is dedicated to my parents whom I respect and love, and have shown the path to success is through education.

ACKNOWLEDGEMENTS

I would like to express my utmost gratitude to my advisor, Dr. Moo-Hyun Kim and Dr. Shankar Bhat for their guidance, benevolent support and continuous encouragement throughout this study. Their expertise and knowledge from academia and industry have enlightened me in the field of offshore engineering.

A sincere appreciation to my committee members, Dr. Richard Mercier and Dr. Alejandro Orsi for the insightful guidance and generous support.

Also, a thousand thanks to Dr. Heon-Yong Kang and Dr. Hooi-Siang Kang for their advise and support throughout my study that helps me develop my technical competency.

Lastly, many thanks to my peers Byungjin Kim and Hyung-Chul Kim for their support and for sharing their valuable knowledge and experience that assisted me in my research.

CONTRIBUTORS AND FUNDING SOURCES

This work was supervised by a thesis committee consisting of Professor Dr. Moo-Hyun Kim (committee chairperson, Professor at Ocean Engineering Department), Dr. Richard Mercier (committee member, Professor at Zachry Civil Engineering Department and Director of Offshore Technology Research Center), Dr. Alejandro Orsi (committee member, Professor at Oceanography Department) and Dr. Shankar Bhat (special committee member, Global and Riser Engineer at Sarawak Shell Berhad, Malaysia).

The works performed in Chapter 3 and Chapter 4 were under the guidance of Dr. Heon-Yong Kang (Research Assistant Professor at Ocean Engineering Dept), Byungjin Kim (PhD Student at Ocean Engineering Dept) and Hyung Chul Kim (PhD Student at Ocean Engineering Dept). The MR Damper parameters presented in Section 2.4.3 is provided by Dr. Hooi-Siang Kang (Professor at Department of Ocean, Aeronautics & Automotive Engineering, Universiti Teknologi Malaysia).

All other work conducted for the thesis (or) dissertation was completed by the student independently.

There are no outside funding contributions to acknowledge related to the research and compilation of this document.

NOMENCLATURE

CHARM3D	Texas A&M Ocean Engineering in-house finite element program for coupled moored offshore structures
HP	High Pressure
ISOPE	International Society of Offshore and Polar Engineers
LP	Low Pressure
MODU	Mobile Offshore Drilling Unit
MR	Magneto-Rheological
RAO	Response Amplitude Operator
SPE	Society of Petroleum Engineers
TTR	Top-Tensioned Riser

TABLE OF CONTENTS

LIST OF FIGURES

LIST OF TABLES

1. INTRODUCTION

The need to improve semisubmersible operation in deep water and in harsher environment necessitates an out-of-box solution to the current technology. This is a challenging undertaking as it involves thorough analysis of the system integrity of the floating production-drilling facility. One system in question is the riser system. Riser operation is highly dependent on the environment. One factor that dictates this is the relative motion between the riser and the semisubmersible at the riser-semisubmersible interface point, which is at the topside deck. The relative motion is called riser stroke. In harsher environment the riser stroke becomes large and this stroke has to be accommodated by the topside deck. This leads to big spacing between topside deck and causes weight penalty that has to be absorbed by hull. A solution to improve this is to introduce a smart damper that can lower the stroke. The overall outcomes are the possibilities of a smaller topside deck and smaller hull.

Smart damper has been used in civil engineering and automotive engineering as a mean to dampen motion and subsequently reducing the motion magnitude. One particular damper is Magneto-Rheological Damper or MR Damper. MR Damper is a semi-active damper that can produce various damping coefficient depending on the requirement programmed into its control algorithm. This research focuses on deploying MR Damper technology into semisubmersible system by analyzing its numerical model, with the goal to reduce the relative motion at harsh environment. The following subsections provide brief introduction to the semisubmersible system.

1.1 Production Semisubmersible

Production semisubmersible is a type of moored vessel with hull consisting of columns and pontoons (see Figure 1 for generic semisubmersible configuration). It has the advantage over other type of floating production system ie. Tensioned-Leg Platform and Spar, as it is able to operate in deeper water and has wider deck spacing that can accommodate more equipment (Ajimoko 2016) (Muehlner and Banumurthy 2015).

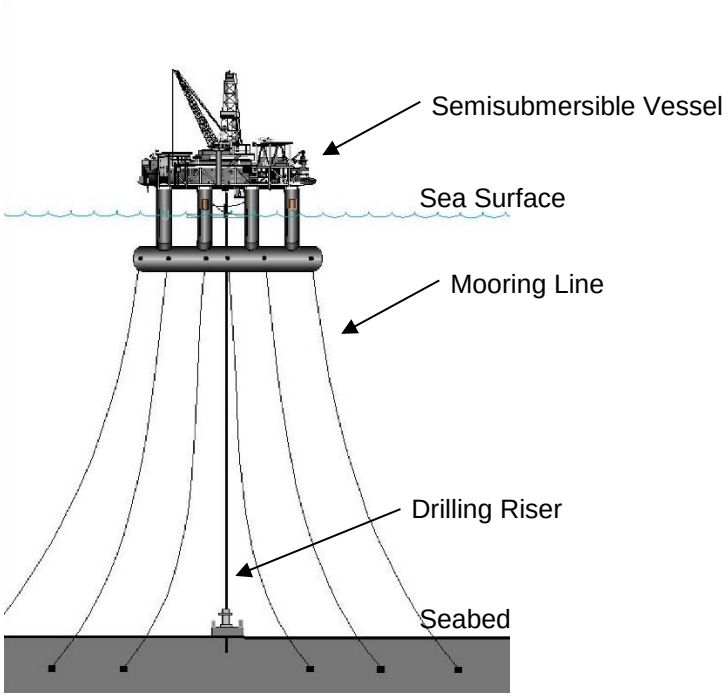

Figure 1 Main parts of semisubmersible (Reprinted with permission from Bureau of Ocean Energy Management (Minerals Management Service, Gulf of Mexico OCS Region 2000))

However semisubmersible has an inherently large heave motion which adversely impact the operation ie operation suspension in harsh environment (Muehlner and Banumurthy 2015). Due to this, the industry put a lot effort in the design of the

semisubmersible hull that results in a low heave motion. This is done by manipulating the shape and/or dimension of the hull column and pontoon.

A deep-draft semisubmersible is a low-heave type semisubmersible used for production platform. However deep-draft semisubmersible hull is relatively large compared to shallow-draft semisubmersible hull. But, leveraging the knowledge and the principle from the low-heave deep-draft production semisubmersible can lead to a small low-heave semisubmersible.

1.2 Top-Tensioned Riser System

Top-tensioned riser (TTR) is a near-vertical tubular casing that connects the wellhead on the seabed to the Topside deck. The TTR acts as an interface between topside deck and the wells, and as a pressure and hydrocarbon containment. It has a fixed connection at the seabed and a hydro-pneumatic support system called tensioner system at the top. The tensioner system behaves like a non-linear spring system.

A unique feature of TTR is that it is always under tension throughout its vertical column. This tension is provided by the tensioner. The necessary for the tension is the avoidance of column buckling in the riser casing wall. The column buckling is a type of structural failure caused by compression force.

When subject to environment (current, wave and wind) both semisubmersible and TTR move towards the direction of the environment. Due to having different mass shape and connection, TTR and semisubmersible have different set of vertical motions, but the TTR moves/deflects in compliance to the semisubmersible owing to its connection to the semisubmersible. The relative motion between top of TTR and semisubmersible or riser stroke (sometimes called tensioner stroke) is critical because of its impact on topside deck spacing and design. In addition to this the stroke is one of the factors that dictate the operation envelope of the TTR and consequently, the operation envelope of wells. In storm event, the stroke becomes large as the magnitude of the seastate becomes large.

1.3 Top-Tensioned Riser Tensioner

A TTR tensioner system is generally made of a few subassemblies called cylinder assembly (see Figure 2). A cylinder assembly normally consists of 3 main parts, namely a pressurized barrel that connects to topside deck, a piston that connects to the riser, and a pressurized accumulator that connects pneumatically to the barrel. The barrel houses the piston (see Figure 3). The barrel and the piston form a pneumatic-mechanical link between riser and topside deck. The accumulator bottle acts as nitrogen gas storage, which volumes determines the stiffness of the tensioner system. The schematic below shows the main components of the tensioner system:

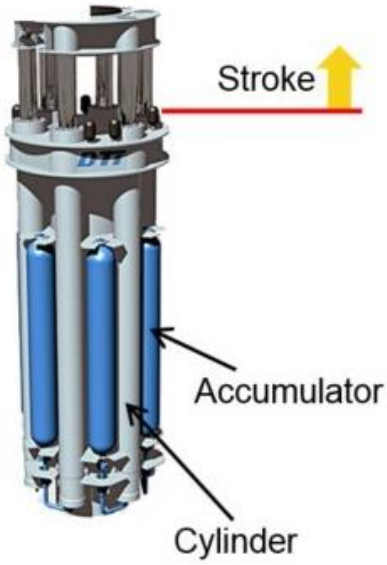

Figure 2 Typical view of tensioner system (Push-style or ram-style)

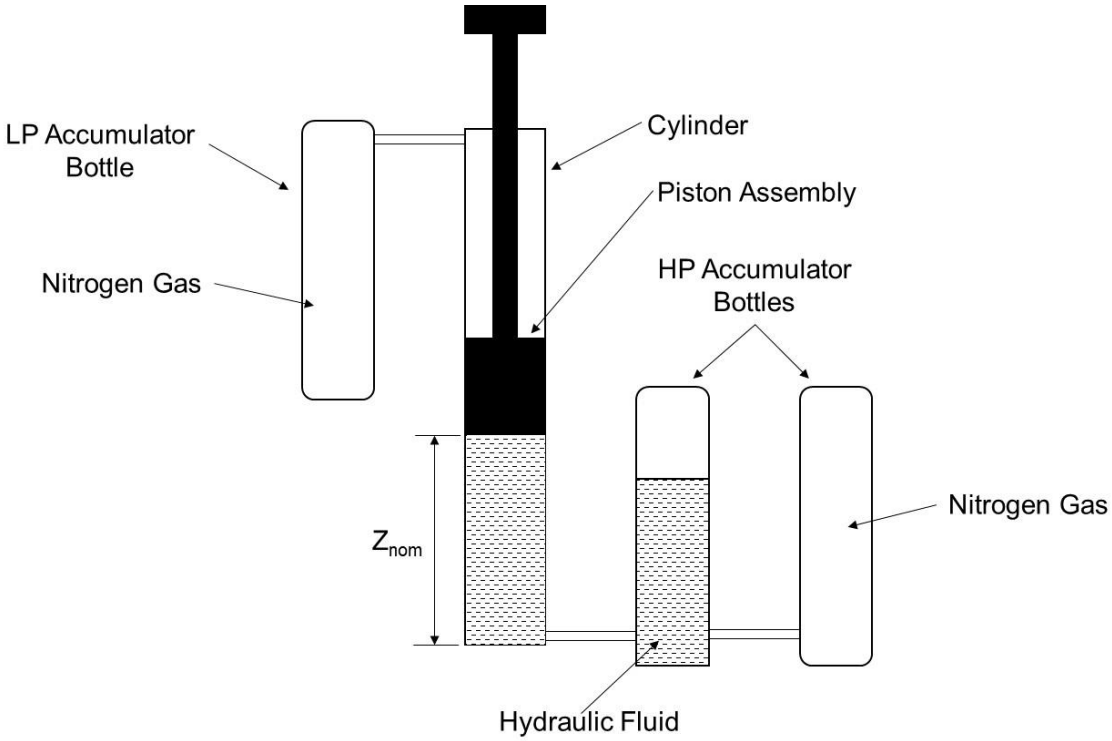

Figure 3 Typical schematic of ram-style cylinder subassembly

The tensioner system generates tension by applying pressure at the bottom side of the piston. This leads to an upward force by the piston, which is then transmitted to the riser through the piston rod. The pressure is contained within the barrel and the accumulator bottle. A sufficient amount of pressure has to be applied to generate the required tension.

The riser stroke is accommodated by the tensioner system through the movement of the barrel and the piston. The barrel moves according to the semisubmersible deck, and the piston moves according to the riser. To accommodate the stroke, the barrel and the piston rod must be at certain length, or else the piston will bottom out, or in laymen term the piston will hit the barrel top or bottom wall, causing structural damage and subsequently loss of pressure containment, and hence loss of tension in the riser.

A long stroke requires long tensioner barrel and long tensioner piston. This adds complexity in the manufacturing process of the tensioner, especially the piston rod. Complexity in manufacturing translates into higher cost. Therefore, it is desirable to keep the tensioner stroke short so as to simplify the manufacturing process and to keep the cost low.

When the tensioner strokes down (or when the piston moves down or the barrel moves up or combination of both), the piston compresses the nitrogen gas in the accumulator bottle, increasing the inner pressure of the barrel and the accumulator. This leads to an increase of pressure applied to the piston, and hence an increase of tension applied to the

riser. It is a common practice not to intervene with the tensioner system in stroke event due to various reason including safety. This makes the tensioner a passive system.

1.4 Tensioner-TTR-Semisubmersible System

As in most system the TTR tensioner system can be represented with spring-mass system. Hence, the stroke motion of the TTR can also be represented by spring mass system (see Figure 4).

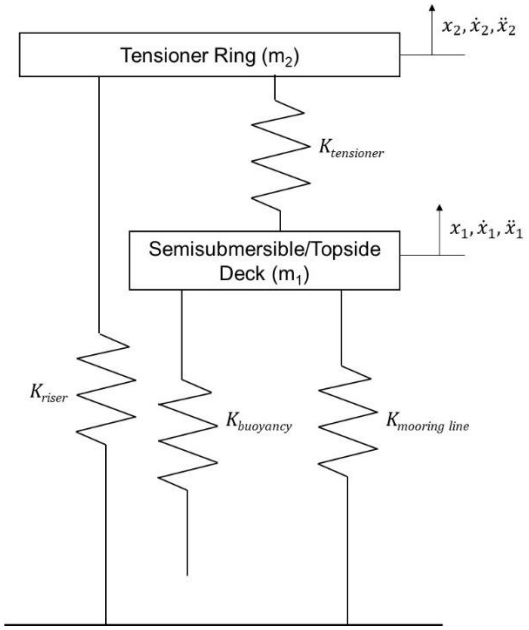

Figure 4 Schematic of riser tensioner and semisubmersible spring-mass system

$$\sum F = m_2\ddot{x}_2 = k_{tensioner}(x_2 - x_1) - k_{riser}x_2$$

Equation 1

Equation 1 represents the forces acted on tensioner ring. The mass m_2 is the physical mass of the tensioner ring. The restoring forces are the tensioner restoring force ($k_{tensioner}(x_2 - x_1)$) and riser restoring force ($k_{riser}x_2$). A more detail equation of motion is discussed in section 4.3.

1.5 Magneto-Rheological Damper (MR Damper)

In any spring-mass system a damper can be introduced to suppress the resulting cyclic behavior. As such, in Semisubmersible Riser Tensioner system, the resulting cyclic behavior of the stroke can also be dampened or suppressed by a damper.

An MR Damper is a semi-active structural damper filled with magneto-rheological fluid (MR fluid), a type of fluid that exhibits viscoelastic behavior when subject to magnetic field (Yang, et al. 2004). The magnetic field is generated when applying current to the MR damper. The viscoelasticity of the MR fluid then determines the damping coefficient of the MR Damper. The advantage of MR Damper lies in the MR fluid, which viscoelastic can be adjusted by manipulating the magnetic field strength or the input current. This means that the MR Damper damping coefficient can also be adjusted by adjusting the current that induces the magnetic field. This results in a type of smart damper.

MR Damper has seen application in civil and automotive engineering. In civil engineering, MR Damper is used to suppress vibration in building structure, creating a form of seismic protection for the building (Bitaraf, et al. 2009). It is used to absorb the cyclic

seismic energy applied on the structure ie. Building without transferring the energy back to the system, creating an overall stable seismic protection system. In automotive engineering, MR damper is used in car suspension system, as a form of damper or shock absorbers. MR Damper strength is adjusted according to the vertical motion of the car, resulting in less vibrating motion.

2. THEORETICAL BACKGROUND

2.1 Dynamic of Offshore Structures

The analysis of low-heave semisubmersible utilized two numerical program: the frequency-domain WAMIT and the time-domain CHARM3D. The semisubmersible hydrodynamic coefficient was obtained by performing frequency domain free floating analysis on WAMIT. Afterwards, fully coupled (semisubmersible-riser-mooring) time domain analysis were performed to obtain the overall system performance.

2.1.1 Basic Parameters

The following parameters are the basic parameters used in the subsequent discussion:
Incident wave velocity potential:

$$\phi_1 = -\frac{\xi_a g e^{kz}}{\omega} sin(kx + \omega t)$$

Equation 2

Free surface elevation:

$$\xi = \xi_a cos(kx + \omega t)$$

Equation 3

Horizontal wave speed

$$u = \frac{\partial \phi_1}{\partial x} = -\frac{\xi_a g k e^{kz}}{\omega} cos(kx + \omega t)$$

Equation 4

Vertical wave speed

$$w = \frac{\partial \phi_1}{\partial z} = -\frac{\xi_a g k e^{kz}}{\omega} sin(kx + \omega t)$$

Equation 5

Horizontal wave acceleration:

$$a_1 = \frac{\partial u}{\partial t} = \frac{\partial^2 \phi_1}{\partial t \partial x} = \xi_a g k e^{kz} cos(kx + \omega t)$$

Equation 6

Vertical wave acceleration:

$$a_3 = \frac{\partial w}{\partial t} = \frac{\partial^2 \phi_1}{\partial t \partial z} = -\xi_a g k e^{kz} cos(kx + \omega t)$$

Equation 7

2.1.2 Hydrodynamic Coefficients of the Semisubmersible

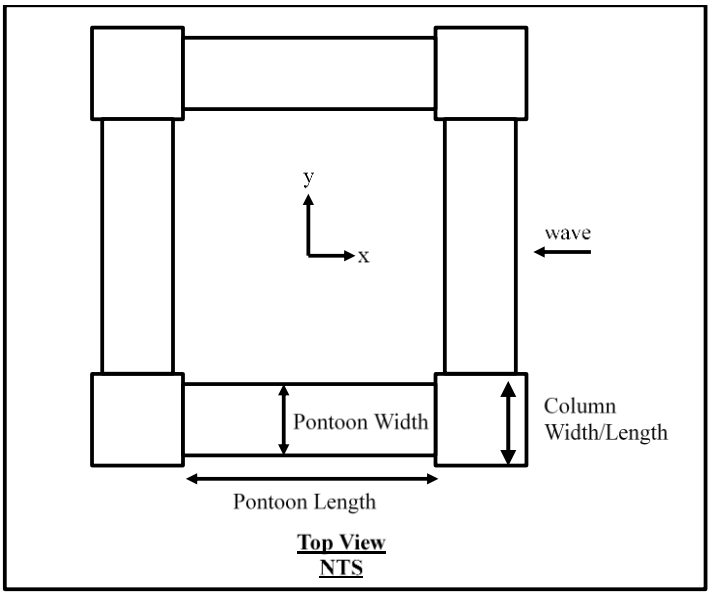

Figure 5 Schematic of generic four column semisubmersible (Top view)

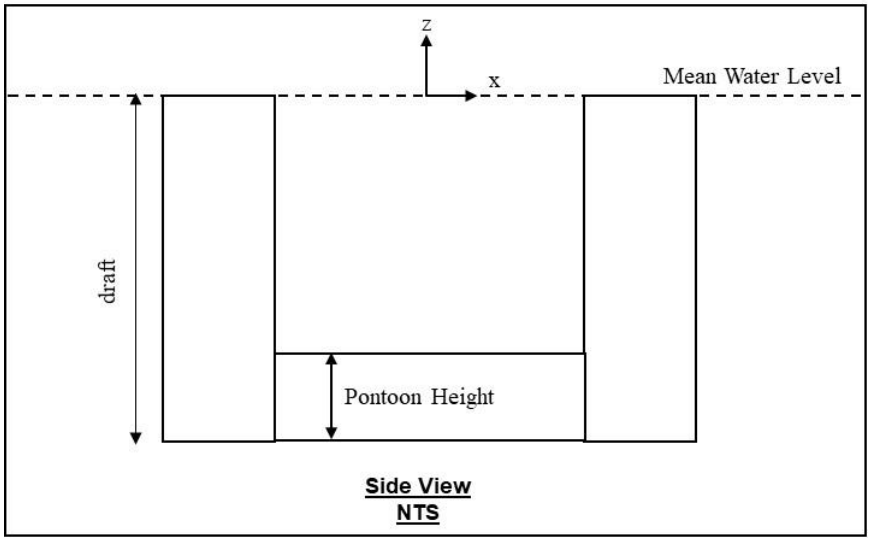

Figure 6 Schematic view of generic four columns semisubmersible (Side view)

WAMIT frequency domain analysis utilize the concept of potential flow, in which the flow is assumed incompressible (no separation and formation of boundary layer), and irrotational; the fluid domain satisfies Laplace Equation (WAMIT 2015):

$$\nabla^2\Phi = 0$$

Equation 8

The harmonic time dependence allows the definition of a complex velocity potential ϕ, related to Φ by the following equation:

$$\Phi = Re\left(\phi e^{i\omega t}\right)$$

Equation 9

where Re denotes the real part, ω is the frequency of the incident wave and t is time. The incident wave velocity potential is described in Equation 2. The wave number k is the real root of the dispersion relation:

$$\frac{\omega^2}{g} = k\tanh(kh)$$

Equation 10

where g is the gravitational acceleration and h is the water depth.

In analyzing semisubmersible motion, it is normal to assume that the semisubmersible is in steady state solution, that is the semisubmersible is oscillating at the frequency of regular wave that excite the semisubmersible (Faltinsen 1990). The resultant hydrodynamic forces and moments are:

1. Froude-Kriloff and diffraction forces and moments. The loads are calculated under the assumption that the semisubmersible is restrained and it is subjected to incident wave.
2. Radiation force and moments. The loads are calculated under the assumption that the semisubmersible is oscillating at the excitation frequency in calm water (no incident wave). This results in the added mass, damping and restoring terms of the semisubmersible.

Due to linearity of the two forces, they can be added to give the total hydrodynamic force. This provide a convenience in describing the waves generated by the two above mentioned assumption on semisubmersible motion (fixed and oscillated). The generated waves are diffraction wave and radiation wave. The velocity potentials of the two waves can be added together:

$$\phi = \phi_R + \phi_D$$

Equation 11

where

$$\phi_R = i\omega \sum_{j=1}^{6} \xi_j \phi_j$$

Equation 12

ξ_j: complex amplitudes of the semisubmersible oscillatory motion in its six degree of freedom

ϕ_j: unit amplitude radiation potential

$$\phi_D = \phi_1 + \phi_S$$

Equation 13

ϕ_1: incident wave potential (see Equation 2)

ϕ_S: scattered disturbance of the incident wave by the fixed semisubmersible

hence:

$$\phi = \left(i\omega \sum_{j=1}^{6} \xi_j \phi_j \right) + (\phi_1 + \phi_S)$$

Equation 14

Since the velocity potential satisfies Laplace equation, the following boundary condition must be satisfied:

1. Linearized free surface boundary condition:

$$-\omega^2 \phi + g \frac{\partial \phi}{\partial z} = 0 \text{ at } z = 0$$

Equation 15

2. Bottom boundary condition due to impermeability assumption:

$$\frac{\partial \phi}{\partial z} = 0 \text{ at } z = -h$$

Equation 16

3. Wetted semisubmersible surface; the fluid velocity is normal to the surface:

$$\frac{\partial \phi}{\partial \mathrm{n}} = \left(i\omega \sum_{j=1}^{6} \xi_j n_j \right) + \left(\frac{\partial \phi_1}{\partial n} + \frac{\partial \phi_S}{\partial n} \right)$$

Equation 17

n: unit vector normal to the surface

Since the semisubmersible surface is impermeable, hence:

$$\frac{\partial \phi_D}{\partial n} = \frac{\partial \phi_1}{\partial n} + \frac{\partial \phi_S}{\partial n} = 0$$

Equation 18

Plug in Equation 18 into Equation 17:

$$\frac{\partial \phi}{\partial \mathrm{n}} = i\omega \sum_{j=1}^{6} \xi_j n_j$$

Equation 19

4. At far field, the radiated and scattered wave velocity diminish, hence:

$$\lim_{r\to\infty} \sqrt{r}\left(\frac{\partial \phi_R}{\partial r} - ik\,\phi_R\right) = 0$$

Equation 20

$$\lim_{r\to\infty} \sqrt{r}\left(\frac{\partial \phi_S}{\partial r} - ik\,\phi_S\right) = 0$$

Equation 21

To obtain the velocity potentials, WAMIT used a three dimensional source technique. From this, a linearized hydrodynamic pressure equation can be derived from Bernoulli equation (quadratic velocity term is neglected (Faltinsen 1990)):

$$p = -\rho \frac{\partial \phi}{\partial t} = -\rho \left[-\omega^2 \left(\sum_{j=1}^{6} \xi_j \phi_j \right) + \frac{\partial \phi_1}{\partial t} + \frac{\partial \phi_S}{\partial t} \right]$$

Equation 22

To obtain first order diffraction force:

$$F_D = -\rho \int_{S_B} \left(\frac{\partial \phi_1}{\partial t} + \frac{\partial \phi_S}{\partial t} \right) n_k \, dS$$

Equation 23

To obtain hydrodynamic reaction force:

$$F_R = \rho \int_{S_B} \omega^2 \left(\sum_{j=1}^{6} \xi_j \phi_j \right) n_k \, dS$$

Equation 24

Added mass and damping coefficient can be obtained from the reaction force:

$$A_{kj} = \rho \, Re \left[\frac{\int_{S_B} \left(\sum_{j=1}^{6} \xi_j \phi_j \right) n_k \, dS}{e^{-i\omega t}} \right]$$

Equation 25

$$B_{kj} = \rho\, Im\left[\frac{\int_{S_B}\left(\sum_{j=1}^{6}\xi_j\phi_j\right)n_k\, dS}{e^{-i\omega t}}\right]$$

Equation 26

where:

A_{kj}: added mass coefficient in the k-th mode due to motion in j-th mode

B_{kj}: damping coefficient in the k-th mode due to motion in j-th mode

2.2 Wave Loads on Structures in Time Domain

In CHARM3D linear wave forces are computed at a specified wave frequency, and the second order sum and difference frequency forces are obtained from the interactions of bichromatic waves. The linear and second-order hydrodynamics forces on a body due to stationary Gaussian random seas can in general be expressed as a two term Voterra series in time-domain:

$$F^{(1)}(t) + F^{(2)}(t) = \int_{-\infty}^{\infty} h_1(\tau)\eta(t-\tau)\, d\tau + \int_{-\infty}^{\infty}\int_{-\infty}^{\infty} h_2(\tau_1,\tau_2)\eta(t-\tau_1)\eta(t-\tau_2)d\tau_1 d\tau_2$$

Equation 27

where:

$h_1(\tau)$: linear impulse response function

$h_2(\tau_1,\tau_2)$: Quadratic impulse response function

$\eta(t)$: ambient wave free surface position at the reference point

For unidirectional seas with N wave components, the wave exciting forces from incident wave potential and diffraction potential in unidirectional waves can be addressed as following:

$$F_I^{(1)}(t) = \mathrm{Re}\left[\sum_{i=1}^{N} A_i \mathbf{L}(\omega_i) e^{i\omega t}\right]$$

Equation 28

$$F_I^{(2)}(t) = \mathrm{Re}\left[\sum_{i=1}^{N}\sum_{j=1}^{N} A_i A_j^* \mathbf{D}(\omega_i, -\omega_j) e^{i(\omega_i - \omega_j)t} + \sum_{i=1}^{N}\sum_{j=1}^{N} A_i A_j \mathbf{S}(\omega_i, \omega_j) e^{i(\omega_i + \omega_j)t}\right]$$

Equation 29

where:

A_i: wave amplitude

$\mathbf{L}(\omega_i)$: linear transfer function

$\mathbf{D}(\omega_i, -\omega_j)$: Difference frequency quadratic force transfer function

$\mathbf{S}(\omega_i, \omega_j)$: Sum frequency quadratic force transfer function

The forces from radiation potential have the following form in time domain:

$$F_R(t) = -m(\infty)\ddot{\xi} - \int_{-\infty}^{t} \mathbf{R}(t-\tau)\dot{\xi} d\tau$$

Equation 30

where:

$m(\infty)$: semisubmersible added mass at infinite frequency (see Equation 32)

$\mathbf{R}(t-\tau)$: Retardation function (see Equation 31)

$\ddot{\xi}$: semisubmersible oscillatory acceleration

$\dot{\xi}$: semisubmersible oscillatory velocity

$$\mathbf{R}(t) = \frac{2}{\pi}\int_0^\infty C(\omega)\frac{\sin(\omega t)}{\omega}d\omega$$

Equation 31

where:

$C(\omega)$: Damping coefficient at frequency ω

$$m(\infty) = m_{add}(\omega) - \int_0^\infty \mathbf{R}(t)\cos(\omega t)\,dt$$

Equation 32

where:

$m_{add}(\omega)$: semisubmersible added mass at frequency ω

The total wave loads in the time domain can be obtained by adding the wave exciting force and wave radiation force:

$$F_{total}(t) = F_I(t) + F_R(t)$$

Equation 33

2.2.1 Morison's Equation

The Morison Equation is commonly used for evaluating wave load for slender cylindrical members on the floating platform where the diameter of the member is small compared to the wave length. The Morison's formula states that the wave load per unit length of the structure normal to the elemental section with diameter *D* is obtained by the sum of an inertial, added mass, and drag force:

$$F_M(t, \dot{x}_n) = C_m \rho \frac{\pi D^2}{4} \dot{u}_n - C_a \rho \frac{\pi D^2}{4} \ddot{x}_n + \frac{1}{2} \rho C_D D_S (u_n - \dot{x}_n)|u_n - \dot{x}_n|$$

Equation 34

where:

C_m: inertia coefficient, $C_m = 1 + C_a$

C_a: added mass coefficient

C_D: drag coefficient

D_S: breadth or diameter of the structure

ρ: density of the fluid

u_n: velocity of the fluid normal to the body

$\dot{u}_n$: acceleration of the fluid normal to the body

$\dot{x}_n$: velocity of the structure

$\ddot{x}_n$: acceleration of the structure

The first two terms on the right hand side of Equation 34 are inertia force including Froude-Kriloff force and added mass effect. The last term is the drag force in the relative velocity form. This relative-velocity form indicates that the drag force contributes to both exciting force and damping to the motion of the platform.

2.3 Semisubmersible Motion in Time Domain

The equation of motion of the semisubmersible in time-domain can be represented as following:

$$(\mathbf{M} + \mathbf{M}_{add}(\infty))\ddot{\xi} + \mathbf{K}\xi = F_I(t) + F_c\left(t, \dot{\xi}\right) + F_M(t, \dot{\xi})$$

Equation 35

$$F_c\left(t, \dot{\xi}\right) = -\int_{-\infty}^{t} \mathbf{R}(t-\tau)\dot{\xi}d\tau$$

Equation 36

where:

$F_I(t)$: wave exciting force

$F_M(t, \dot{\xi})$: nonlinear drag force term from Morison's equation

M: Semisubmersible physical mass matrix

$\mathbf{M}_{add}(\infty)$: Semisubmersible added mass matrix at infinite frequency

K: Semisubmersible stiffness matrix including mooring line, riser and hydrodynamic stiffness

Adams-Moulton method (or mid-point method) is used to solve the equation of motion. The first step of the solution is to reduce Equation 35 to first order differential equation by applying the following:

$$\zeta = \dot{\xi}$$

Equation 37

Hence Equation 35 becomes:

$$\bar{\mathbf{M}}\dot{\zeta} + \mathbf{K}\xi = F_I(t) + F_c\left(t, \dot{\xi}\right) + F_M(t, \dot{\xi})$$

Equation 38

or

$$\bar{\mathbf{M}}\dot{\zeta} = F_I(t) + F_c\left(t, \dot{\xi}\right) + F_M\left(t, \dot{\xi}\right) - \mathbf{K}\xi$$

Equation 39

where:

$$\bar{\mathbf{M}} = \mathbf{M} + \mathbf{M}_{add}(\infty)$$

Equation 40

Then, integrating Equation 39 from $t^{(n)}$ to $t^{(n+1)}$:

$$\bar{\mathbf{M}}\left(\zeta^{(n+1)} - \zeta^{(n)}\right) = \int_{t^{(n)}}^{t^{(n+1)}} F_I(t) + F_c\left(t, \dot{\xi}\right) + F_M\left(t, \dot{\xi}\right) - \mathbf{K}\xi \, dt$$

Equation 41

$$\xi^{(n+1)} - \xi^{(n)} = \int_{t^{(n)}}^{t^{(n+1)}} \zeta \, dt$$

Equation 42

Applying Adam-Moulton scheme ($\int_{t^{(n)}}^{t^{(n+1)}} x\,dt = \frac{\Delta t}{2}\left[x^{(n)} + x^{(n+1)}\right]$) into Equation 41 and Equation 42:

$$\bar{\mathbf{M}}\zeta^{(n+1)} = \bar{\mathbf{M}}\zeta^{(n)} + \frac{\Delta t}{2}\left[F_I^{(n+1)} + F_I^{(n)} + F_C^{(n+1)} + F_C^{(n)} + F_M^{(n+1)} + F_M^{(n)}\right] - \frac{\Delta t}{2}\mathbf{K}\left(\xi^{(n+1)} + \xi^{(n)}\right)$$

Equation 43

$$\xi^{(n+1)} - \xi^{(n)} = \frac{\Delta t}{2}\left[\zeta^{(n)} + \zeta^{(n+1)}\right]$$

Equation 44

Or

$$\zeta^{(n+1)} = \frac{2}{\Delta t}\left[\xi^{(n+1)} - \xi^{(n)}\right] - \zeta^{(n)}$$

Equation 45

The right hand sides of Equation 43 and Equation 45 contain an unknown variable $\xi^{(n+1)}$ and terms that depend on unknown variables at time step $(n+1)$. To solve the equations, Adams-Bashford scheme is implemented to the following nonlinear force terms:

$$\int_{t^{(n)}}^{t^{(n+1)}} F_c\left(t, \dot{\xi}\right) dt = \frac{\Delta t}{2}\left(3F_C^{(n)} - F_C^{(n-1)}\right) \text{ for } n \neq 0$$

Equation 46

and

$$\int_{t^{(n)}}^{t^{(n+1)}} F_c\left(t, \dot{\xi}\right) dt = \Delta t F_C^{(0)} \text{ for } n = 0$$

Equation 47

$$\int_{t^{(n)}}^{t^{(n+1)}} F_M\left(t, \dot{\xi}\right) dt = \frac{\Delta t}{2}\left(3F_M^{(n)} - F_M^{(n-1)}\right) \text{ for } n \neq 0$$

Equation 48

and

$$\int_{t^{(n)}}^{t^{(n+1)}} F_M\left(t, \dot{\xi}\right) dt = \Delta t F_M^{(0)} \text{ for } n = 0$$

Equation 49

Combining Equation 43, Equation 44, Equation 46 and Equation 48 to achieve the following:

$$\left[\frac{4}{\Delta t^2}\bar{\mathbf{M}} + \mathbf{K}\right]\Delta\xi = \frac{4}{\Delta t}\bar{\mathbf{M}}\zeta^{(n)} + \left(F_I^{(n+1)} + F_I^{(n)}\right) + \left(3F_C^{(n)} - F_C^{(n-1)}\right)$$
$$+ \left(3F_M^{(n)} - F_M^{(n-1)}\right) - 2\mathbf{K}\xi^{(n)} + 2F_0$$

Equation 50

where:

$$\Delta\xi = \xi^{(n+1)} - \xi^{(n)}$$

Equation 51

F_0: Constant forces (ie buoyancy force)

To obtain $\xi^{(n+1)}$, solve $\Delta\xi$ in Equation 50, and plug it in Equation 51.

2.4 Dynamic of Mooring Line and Riser System

Both mooring line and risers are considered as slender structures with equal principal bending stiffness (or zero bending stiffness for chain). The restoring effects of these lines to the platform come from combination of the gravity force of the line, line geometry and line tension. The bending stiffness of the line contributes little to the restoring effects but it is a

structural concern for the riser. In CHARM3D, a three-dimensional elastic rod theory is chosen to model the mooring lines and risers. Finite element method is used to interpret the theory in numerical form.

2.4.1 Theory of Rod

In the theory of rod, the behavior of the slender rod is described in terms of the position of the centerline of the rod. The centerline of the rod in the deformed state is described by a space curve $\mathbf{r}(s,t)$, as illustrated in Figure 7. The space curve is defined by the position vector $\mathbf{r}$, which is a function of the arc-length s and time t.

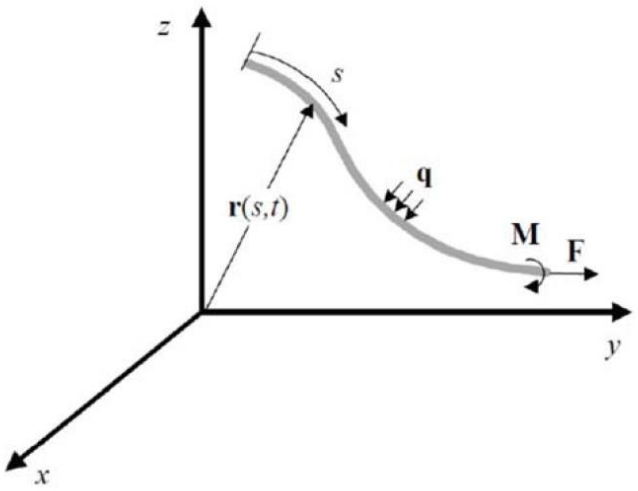

Figure 7 Coordinate system of slender rod

Initially the rod is assumed inextensible, meaning that the overall arc-length does not change in undeformed shape and deformed shape. The unit tangent vector of the space curve

is $\mathbf{r}'$, and the principal normal vector is directed along $\mathbf{r}''$ and the bi-normal is directed along $\mathbf{r}' \times \mathbf{r}''$, where the prime denotes the differentiation with respect to arc-length.

The internal state of stress at a point on the rod is described by the resultant force, **F** and moment **M** acting along the centerline. The equilibrium of the linear force and moment for a segment of rod with unit arc-length leads to the following equation of motion:

$$\mathbf{F}' + \mathbf{q} = \rho \ddot{\mathbf{r}}$$

Equation 52

$$\mathbf{M}' + \mathbf{r}' \times \mathbf{F} + \mathbf{m} = 0$$

Equation 53

where:

q: applied force per unit length

ρ: rod mass per unit length

m: applied moment per unit length

For elastic rod with equal principal stiffness, where the bending moment is proportional to curvature and is directed along the bi-normal, the resultant moment **M** is:

$$\mathbf{M} = \mathbf{r}' \times EI\mathbf{r}'' + H\mathbf{r}'$$

Equation 54

where:

EI: rod bending stiffness

H: torque

Differentiate Equation 54 with respect to arc-length and substitute the result into Equation 53 to achieve the following:

$$\mathbf{r}' \times [(EI\mathbf{r}'') + \mathbf{F}] + H'\mathbf{r}' + H\mathbf{r}'' + \mathbf{m} = 0$$

Equation 55

The mooring lines, tethers and riser have no distributed torsional motion from the hydrodynamic forces owing to their cross-sectional shape. In addition, the torque in the lines are usually small, hence negligible. Therefore the terms H and $\mathbf{m}$ are assumed zero. Thus Equation 55 becomes:

$$\mathbf{r}' \times [(EI\mathbf{r}'') + \mathbf{F}] = 0$$

Equation 56

Introducing a scalar function $\lambda(s,t)$ to rewrite term $\mathbf{F}$ in Equation 56:

$$\mathbf{F} = -(EI\mathbf{r}'')' + \lambda\mathbf{r}'$$

Equation 57

The inextensibility condition on rod leads to:

$$\mathbf{r}' \cdot \mathbf{r}' = 1$$

Equation 58

Rearranging Equation 57 so that $\lambda\mathbf{r}'$ is on left hand side and the remaining terms are on the right hand side, and then taking dot product with $\mathbf{r}'$ leads to:

$$\lambda = \mathbf{F} \cdot \mathbf{r}' + (EI\mathbf{r}'')' \cdot \mathbf{r}'$$

Equation 59

or

$$\lambda = T + EI\kappa^2$$

Equation 60

where:

T: line tension

κ: line curvature

Combining Equation 57 and Equation 52 to express the rod equation of motion in EI and λ:

$$-(EI\mathbf{r}'')'' + \lambda\mathbf{r}'' + \mathbf{q} = \rho\ddot{\mathbf{r}}$$

Equation 61

If the rod is stretchable and the stretch is linear and small, the above inextensibility condition (Equation 58) can be approximated by:

$$\frac{1}{2}(\mathbf{r}' \cdot \mathbf{r}' - 1) = \frac{T}{EA} \approx \frac{\lambda}{EA}$$

Equation 62

Equation 61 and Equation 58 (or Equation 62) combined with initial conditions and applied force, $\mathbf{q}$ are sufficient to determine the dependent variables $\mathbf{r}(s,t)$ and $\lambda(s,t)$. In most offshore applications, the applied force on the rod (mooring line, riser and tether) comes from the hydrostatic and hydrodynamic forces from external and internal fluid, and the weight of the rod itself. Thus the applied force, $\mathbf{q}$ can be written as:

$$\mathbf{q} = \mathbf{w} + \mathbf{F^s} + \mathbf{F^d}$$

Equation 63

where:

$\mathbf{w}$: rod weight per unit length

$\mathbf{F^s}$: hydrostatic force per unit length

$\mathbf{F^d}$: hydrodynamic force per unit length

The hydrostatic force is due to buoyancy of the rod and hydrostatic pressure from the external fluid:

$$\mathbf{F^s} = \mathbf{B} - (P\mathbf{r}')'$$

Equation 64

where:

$\mathbf{B}$: rod buoyancy force per unit length

P: hydrostatic pressure at point $\mathbf{r}$ on the rod

The hydrodynamic force is due to the external fluid motion, and is calculated using Morison's equation:

$$\begin{aligned}\mathbf{F^d} &= -C_A\ddot{\mathbf{r}}^n + C_M\dot{\mathbf{V}}^n + C_D|\mathbf{V}^n - \dot{\mathbf{r}}^n|(\mathbf{V}^n - \dot{\mathbf{r}}^n)\\ &= -C_A\ddot{\mathbf{r}}^n + \bar{\mathbf{F}}^d\end{aligned}$$

Equation 65

where:

C_A: Added mass coefficient (added mass per unit length)

C_M: Inertial coefficient (inertia force per unit length per unit acceleration)

C_D: Drag coefficient (drag force per unit length per unit normal velocity)

$\mathbf{V}^n$: fluid velocity normal to rod centerline

$\dot{\mathbf{V}}^n$: fluid acceleration normal to rod centerline

$\dot{\mathbf{r}}^n$: rod velocity normal to its centerline

$\ddot{\mathbf{r}}^n$: rod acceleration normal to its centerline

Combining Equation 61, Equation 63, Equation 64 and Equation 65 to get the rod overall equation of motion:

$$\rho\ddot{\mathbf{r}} + C_A\ddot{\mathbf{r}}^n + (EI\mathbf{r}'')'' + \left(\bar{\lambda}\mathbf{r}'\right)' = \bar{\mathbf{w}} + \bar{\mathbf{F}}_d$$

Equation 66

$$\bar{\lambda} = T + P - EI\kappa^2 = \bar{T} - EI\kappa^2$$

Equation 67

$$\bar{\mathbf{w}} = \mathbf{w} + \mathbf{B}$$

Equation 68

where:

$\bar{T}$: rod effective tension

$\bar{\mathbf{w}}$: rod effective weight or rod wet weight

Equation 66 and Equation 58 are the governing equations for the statics and dynamics of the submerged rods.

2.4.2 Ram-Style Hydro-Pneumatic Tensioner System

Top-tensioned riser is equipped with hydro-pneumatic tensioner system at the top to provide the required tension and to accommodate the relative motion between riser top motion and semisubmersible motion (see section 1.3). In CHARM3D, tensioner system can be modelled as:

1. Linear spring

2. Hydro-pneumatic tensioner without effect of backside pressure (or low pressure side)
3. Hydro-pneumatic tensioner with significant effect of backside pressure (or low pressure side)

This section will discuss option 2 and option 3 for ram-style tensioner. The more conventional pull-style tensioner has the same system principal as the ram style but with different mechanical design.

Figure 8 shows schematic of ram style tensioner system. The piston assembly is structurally connected to the top of riser and the cylinder and the accumulator bottles (high pressure bottle and low pressure bottle) are mounted on semisubmersible topside deck.

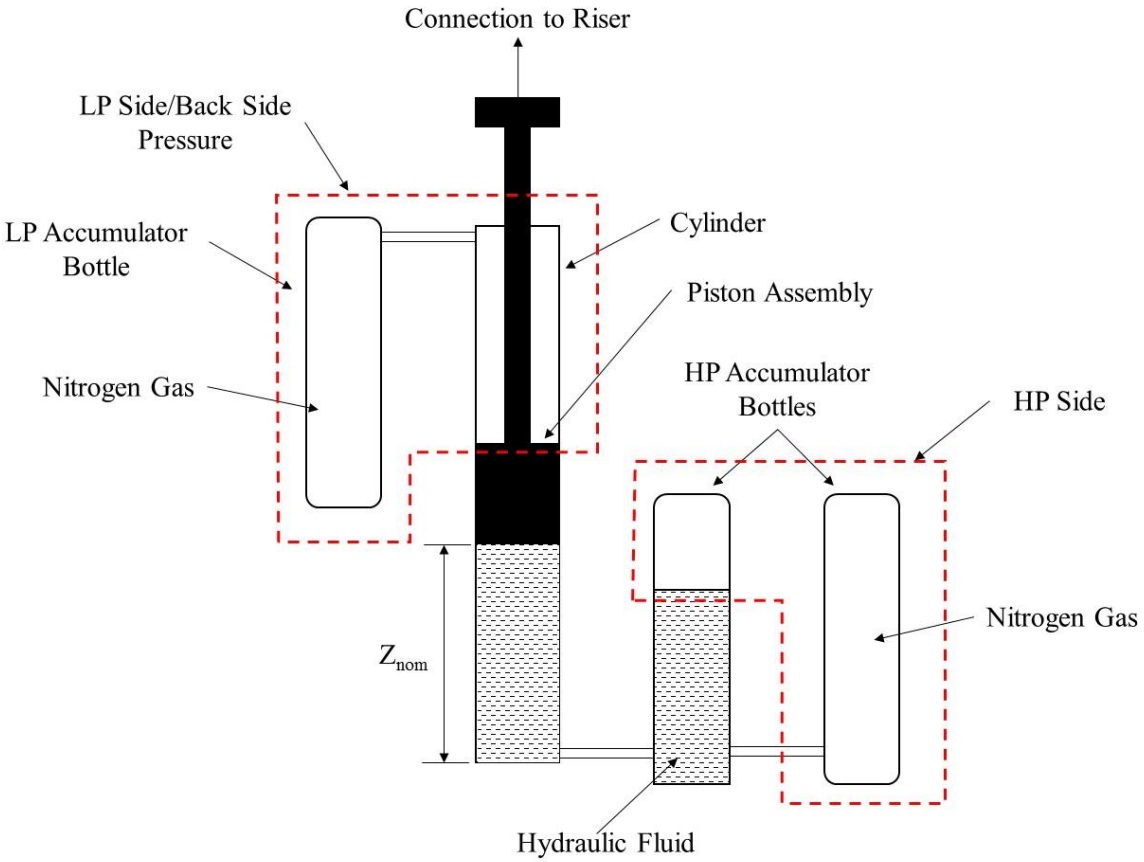

Figure 8 Schematic of ram-syle tensioner system cylinder assembly

There are two type of fluids in tensioner system: hydraulic fluid, used to lubricate and wet the seal of the piston and cylinder, and nitrogen gas, used to generate tension and stiffness for the system.

Normally, a tensioner system consists of a few cylinder assemblies, ranging from 4 to 8 assemblies. Each cylinder assembly consists of a cylinder with inner-travelling piston, and a few accumulator bottles. The accumulator bottles are used to provide storage for hydraulic

fluid and nitrogen gas. This is to ensure that the overall cylinder assembly height is not too big or else the deck cannot accommodate it.

2.4.2.1. Hydro-Pneumatic Tensioner System without the Effect of Backside Pressure

The effect of back-side pressure on the overall tensioner tension is small such that it is ignored most of the time, especially in the early stage of design. Therefore the tensioner tension is generated purely from the pressurized nitrogen gas in high pressure side (HP side, see Figure 8). This section discusses the derivation of tensioner tension without the effect of backside pressure.

Using the natural gas law to relate the HP side pressure at nominal (no stroke) to HP side pressure at stroke:

$$P_0(V_0)^\gamma = P_1(V_1)^\gamma$$

Equation 69

where:

P_0: Set pressure or nominal pressure in cylinder and accumulator bottle

V_0: Nominal nitrogen gas volume in cylinder and accumulator bottle

P_1: Pressure at stroke condition in cylinder and accumulator bottle

V_1: Stroke nitrogen gas volume in cylinder and accumulator bottle

γ: Gas constant

From force-pressure relationship:

$$P = \frac{F}{A}$$

Equation 70

therefore

$$P_0 = \frac{T_{0\_cyl}}{A_i}$$

Equation 71

and

$$P_1 = \frac{T_{1\_cyl}}{A_i}$$

Equation 72

where:

T_{0_cyl}: nominal cylinder tension (not to be confused with nominal tensioner tension)

T_{1_cyl}: stroke cylinder tension

A_i: annulus cross section area of the cylinder (HP side)

Substituting Equation 71 and Equation 72 into Equation 69:

$$\frac{T_{0\_cyl}}{A_i}(V_0)^\gamma = \frac{T_{1\_cyl}}{A_i}(V_1)^\gamma$$

Equation 73

To develop a tensioner system equation that workable for numerical analysis, two assumptions have to be made on the hardware design of the tensioner. The first assumption is that the tensioner system has no accumulator bottle, but the nominal volume (zero stroke volume) of the nitrogen gas remains the same. This is illustrated in Figure 9 below. The reason to keep the gas volume the same is to conserve the resulting tensioner stiffness and

tensioner tension at stroke. The second assumption is that the hydraulic fluid in the HP side is incompressible, hence its volume can be ignored. This is illustrated in Figure 10.

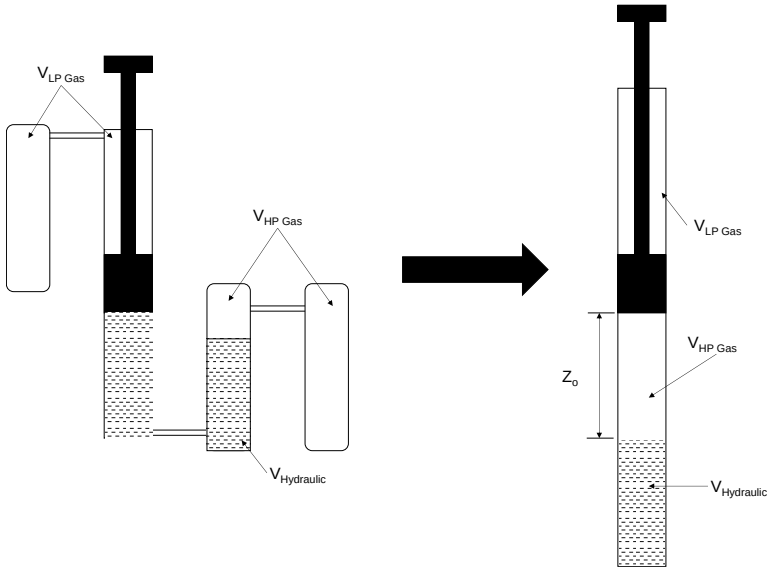

Figure 9 Conversion of tensioner system without accumulator bottle (Piston at nominal position)

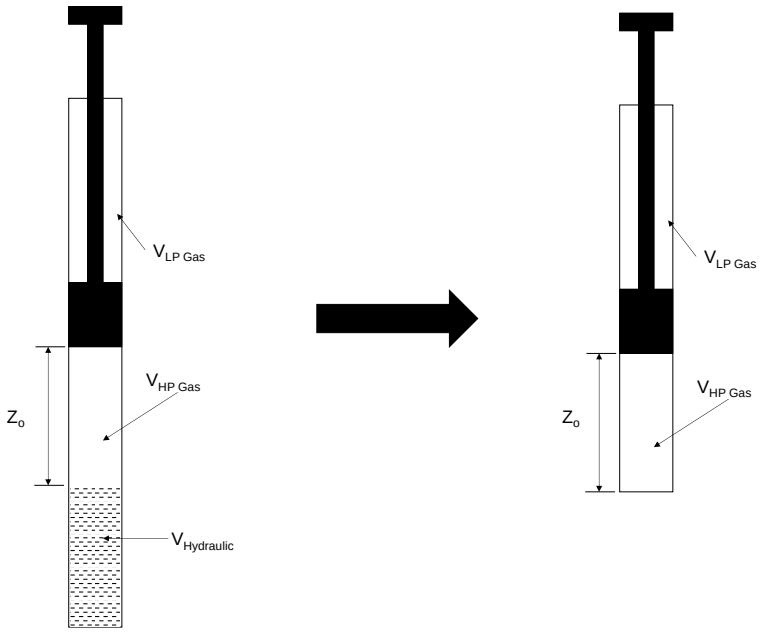

Figure 10 Conversion of tensioner system without hydraulic fluid volume

In Figure 10, a new parameter is introduced: Z_0. Z_0 can be determined from the equation below if the HP side nominal volume is known:

$$V_{HP\ Gas} = V_0 = Z_0 A_i$$

Equation 74

If the volume is absence, then Z_0 can be determined from the desired nominal tensioner stiffness (see Equation 83).

When the cylinder strokes (or when the riser strokes down) the $V_{HP\ Gas}$ term changes as follows:

$$V_{HP\ Gas} = V_1 = (Z_0 + \Delta Z) A_i$$

Equation 75

where:

ΔZ: cylinder stroke or riser stroke

Note that ΔZ is positive when the cylinder/riser strokes up, and negative when the cylinder/riser strokes down.

Substituting Equation 74 and Equation 75 into Equation 73 to obtain the following relationship:

$$T_{0\_cyl}A_i(Z_0A_i)^\gamma = T_{1\_cyl}A_i((Z_0 + \Delta Z)A_i)^\gamma$$

Equation 76

or

$$T_{1\_cyl} = T_{0\_cyl}\frac{(Z_0A_i)^\gamma}{((Z_0 + \Delta Z)A_i)^\gamma}$$

Equation 77

Simplifying Equation 77 by cancelling common term (A_i), and expressed T_{1_cyl} as a function of the remaining terms:

$$T_{1\_cyl} = T_{0\_cyl}\left(\frac{Z_0}{(Z_0 + \Delta Z)}\right)^\gamma$$

Equation 78

or

$$T_{1\_cyl} = T_{0\_cyl}\left(1 + \frac{\Delta Z}{Z_0}\right)^{-\gamma}$$

Equation 79

To get the overall tensioner tension and stiffness, multiply T_{1_cyl} with the number of cylinder assembly:

$$T_1 = nT_{0\_cyl}\left(1 + \frac{\Delta Z}{Z_0}\right)^{-\gamma}$$

Equation 80

or

$$T_1 = T_0\left(1 + \frac{\Delta Z}{Z_0}\right)^{-\gamma}$$

Equation 81

where:

T_1: tensioner tension at stroke

T_0: tensioner tension at nominal

n: number of cylinder assembly

If the number of cylinder assembly is unknown, one can determine T_0 from the riser weight and the overall pull factor or tension factor:

$$T_0 = W_{Above\_Tension\_Ring} + (TF \times W_{Below\_Tension\_Ring})$$

Equation 82

where:

$W_{Above\_Tension\_Ring}$: Riser joint, riser component and riser inner fluid effective weight above tensioner ring

$W_{Below\_Tension\_Ring}$: Riser joint, riser component and riser inner fluid effective weight below tensioner ring

TF: riser tension factor

The tensioner ring is a piece of structure that connects the tensioner cylinder piston with the riser joint.

The tensioner stiffness is obtained by differentiating Equation 81 with cylinder/riser stroke (ΔZ):

$$K_{ten} = \frac{dT_1}{d\Delta Z} = \frac{T_0 \gamma}{Z_0}\left(1 + \frac{\Delta Z}{Z_0}\right)^{-\gamma-1}$$

Equation 83

Note that from Equation 83 the tensioner stiffness is proportionate to nominal tension T_0 and gas constant γ, but is inversely proportionate to parameter Z_0. Also, Equation 81 and Equation 83 show that the tensioner is a nonlinear spring, in which the stiffness increases as the down-stroke increases.

2.4.2.2. Hydro-Pneumatic Tensioner System with the Effect of Backside Pressure

In some cases, the back side or the LP side may participate in the tensioner tension. This effect is significant in large upstroke event. To account for this, the force generated by the back side pressure has to be accounted in Equation 73. The force generated by the back side is as following:

$$T_{1_{LP\_cyl}} = \left(P_{0_{LP}} A_{LP}\right) \frac{\left(V_{0_{LP}}\right)^{\gamma}}{\left(V_{0_{LP}} - \Delta Z A_{LP}\right)^{\gamma}}$$

Equation 84

where:

$P_{0_{LP}}$: the back side nominal pressure or set pressure

$V_{0_{LP}}$: the back side nitrogen gas nominal volume

A_{LP}: annulus cross section area of the cylinder (LP side)

The tensioner tension equation becomes:

$$T_1 = n\left[(P_0 A_i)\frac{(V_0)^\gamma}{(V_0 + \Delta Z A_i)^\gamma} - \left(P_{0_{LP}} A_{LP}\right)\frac{\left(V_{0_{LP}}\right)^\gamma}{\left(V_{0_{LP}} - \Delta Z A_{LP}\right)^\gamma}\right]$$

Equation 85

or

$$T_1 = n\left[(P_0 A_i)\left(1 + \frac{\Delta Z A_i}{V_0}\right)^{-\gamma} - \left(P_{0_{LP}} A_{LP}\right)\left(1 - \frac{\Delta Z A_{LP}}{V_{0_{LP}}}\right)^{-\gamma}\right]$$

Equation 86

Differentiating Equation 86 to obtain the tensioner stiffness:

$$K_{ten} = -n\gamma\left[\frac{P_0 A_i^2}{V_0}\left(1 + \frac{\Delta Z A_i}{V_0}\right)^{-\gamma-1} + \frac{P_{0_{LP}} A_{LP}^2}{V_{0_{LP}}}\left(1 - \frac{\Delta Z A_{LP}}{V_{0_{LP}}}\right)^{-\gamma-1}\right]$$

Equation 87

Equation 86 and Equation 87 have the advantage of having more accurate representation of the tensioner than Equation 81 and Equation 83. But they require more user defined input such as nominal pressure and nominal gas volume; they are normally used if the tensioner design is known.

2.4.3 Magneto-Rheological Damper in Riser Tensioner System

MR Damper changes its damping coefficient by changing the current that energizes the MR fluid in its barrel (see section 1.5). Various numerical model has been suggested and tested to better estimate the system curve of MR Damper. Yang et al (Yang, Li and Chen 2013) describes the various numerical model of MR Damper, of two are of interest in this study:

1. Bingham Model – used by MR Damper supplier LORD corp
2. Non-Linear Hysteretic Arctan function model – used by Dr. Hooi-Siang Kang in his research on MR Damper (Kang 2015)

The following equation describes the Bingham model:

$$F_{MR\ Damper} = f_c sgn(\dot{x}) + c_0\dot{x} + f_0$$

Equation 88

where:

f_c: knee force or yield force as a function of energizing current

$sgn(\dot{x})$: signum function

c_0: damping coefficient as a function of energizing current

f_0: offset damping force

A major feature in Bingham model is the knee force f_c that represents the visco-elastic behavior of the MR fluid. According to Yang, the knee force is proportionate to the energizing current (Yang, Li and Chen 2013). However, Bingham model does not capture the

hysteretic feature of MR Damper (Yang, Li and Chen 2013). Another interesting feature about Bingham model is that the damping force is linear. This allows for simplification of MR Damper numerical model to linear model, particularly in early stage of front-end design, where system design is generated first and dictates hardware design. Figure 11 below illustrates MR Damper system curve with Bingham model and comparison with experimental result.

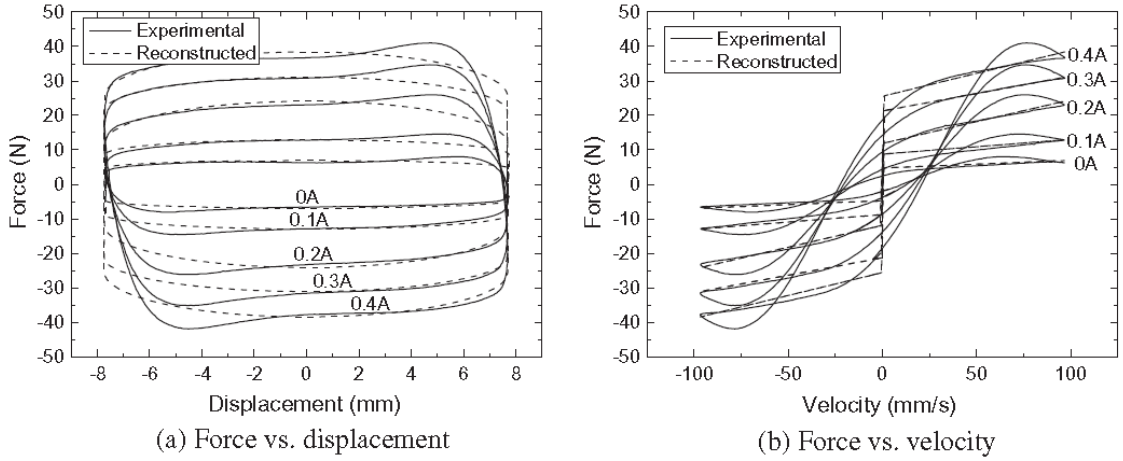

Figure 11 Bingham model system curve (Yang, Li and Chen 2013). Reconstructed curve is the numerical model based on Equation 88. (Reprinted with permission from Elsevier)

Another MR Damper numerical model is Non-Linear Hysteretic Arctan function model, which is described by the following equation:

$$F_{MR\ Damper} = c\dot{x} + kx + \alpha \tan^{-1}\left(\beta\dot{x} + \delta sgn(x)\right)$$

Equation 89

where:

c: damping coefficient

k: stiffness coefficient

α, β, δ: hysteresis parameters

Figure 12 illustrates MR Damper system curve with Non-Linear Hysteretic Arctan function and comparison with experimental result. This model captures they hysteretic feature of MR Damper.

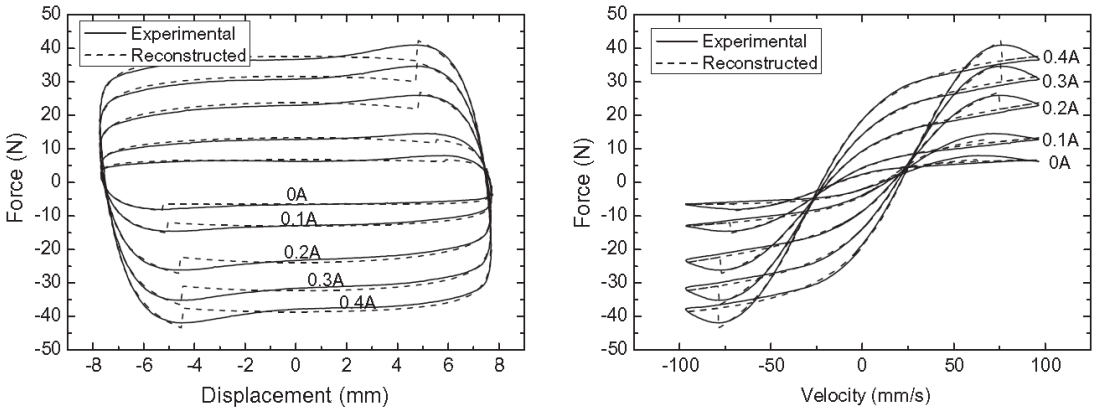

(a) Force vs. displacement (b) Force vs. velocity

Figure 12 Non-linear hysteretic arctangent function model system curve (Yang, Li and Chen 2013). Reconstructed curve is the numerical model based on Equation 89. (Reprinted with permission from Elsevier)

Dr. Kang determined the MR Damper parameters based on Non-Linear Hysteretic Arctan function model and based on existing small scale MR Damper as following (Kang 2015):

$$c = (8.5 \times 10^5 \times i^2) + (1.4 \times 10^7 \times i) + (6.0 \times 10^6)$$

Equation 90

$$k = (1.2 \times 10^5 \times i) + (9.8 \times 10^3)$$

Equation 91

$$\alpha = (2.571 \times 10^6 \times i^2) + (4.11 \times 10^6 \times i) + (8.0 \times 10^4)$$

Equation 92

$$\beta = (22.05 \times i) + 17.82$$

Equation 93

$$\delta = 2.6i + 2.3$$

Equation 94

where:

i: input/energizing current

Equation 90 through Equation 94 indicate that the dominant parameters in this model are linear damping coefficient c and hysteresis parameter α. Aside the hysteresis parameter, the non-linear hysteretic arctan function model is also biased towards the linear damping coefficient as the Bingham model.

The bias of linear damping in Bingham model and Non-Linear Hysteretic Arctan Function model, and the absence of large scale MR Damper for offshore application allows for assumption of MR Damper numerical model to be a linear damping model:

$$F_{MR\ Damper} = C_{MR\ Damper}\dot{x}$$

Equation 95

This provides flexibility to independently determine the required damping coefficient $C_{MR\ Damper}$ without complicating other parameters, which can be dealt at later design stage.

2.4.4 Coupling of Mooring and Riser with Semisubmersible

The numerical model of the connection between the rods (mooring lines and risers) and the semisubmersible is a combination of linear spring, rotational spring and nonlinear spring. The linear spring defines the translational motion between the platform's connecting point and the top of the line, the rotational spring represents the rotation of the platform and the tangential direction of the line, and the nonlinear spring represents the tensioner for the riser system (see section 2.4.2).

CHARM3D models the rods using finite element method. The top node (also the end node) is connected to the semisubmersible through the spring connection, and is subjected to force and moment from the springs. Under the assumption of small angular motions of the platform, the force exerted on the node by the linear connector is defined as following:

$$\boldsymbol{N} = [\boldsymbol{K^L}](\boldsymbol{X} + \boldsymbol{p} + (\boldsymbol{\theta} \times \boldsymbol{p}) - \boldsymbol{r})$$

Equation 96

where:

$[\boldsymbol{K^L}]$: 3×3 diagonal stiffness matrix of the linear spring

$\boldsymbol{X}$: translational motion of the semisubmersible

$\boldsymbol{p}$: position vector of the spring connection in the semisubmersible coordinate system

$\boldsymbol{\theta}$: angular motion of the semisubmersible

$\boldsymbol{r}$: position of the rod top node or end node where the spring is attached

The spring forces onto the semisubmersible are following:

$$\boldsymbol{F^L} = -\boldsymbol{N}$$

Equation 97

$$\boldsymbol{M^L} = \boldsymbol{p} \times (-\boldsymbol{N})$$

Equation 98

The moment applied on the end node by the rotational spring connector is proportional to the angle between the direction vector of the spring and the tangent of the line at the connection. Under the assumption of small angular motions of the platform:

$$\boldsymbol{L} = \boldsymbol{K^\theta}\left(\boldsymbol{e} + (\boldsymbol{\theta} \times \boldsymbol{e}) - \frac{\boldsymbol{r'}}{|\boldsymbol{r'}|}\right)$$

Equation 99

where:

$\boldsymbol{K^\theta}$: rotational spring constant

$\boldsymbol{e}$: unit vector in the rigid body coordinates

$\boldsymbol{r'}$: rod centerline tangent

The spring forces onto the semisubmersible are following:

$$F^\theta = 0$$

Equation 100

$$\boldsymbol{M^{\theta} = L \times r' \approx L \times e}$$

Equation 101

The equation of the line at the connected rod is coupled with the unknown motion of the platform by using symbol K_{ij}^{AB} to indicate the tangential stiffness coefficient for degree of freedom B_j, in equation A_i:

$$K_{ij}^{rr} = -\frac{\partial N_i}{\partial r_j} = K_i^L \delta_{ij}$$

Equation 102

$$K_{ij}^{rX} = -\frac{\partial N_i}{\partial X_j} = -K_i^L \delta_{ij}$$

Equation 103

$$K_{ij}^{r\theta} = -\frac{\partial N_i}{\partial \theta_j} = -K_i^L C_{ij}$$

Equation 104

$$K_{ij}^{r'r'} = -\frac{\partial L_i}{\partial r_j} = K^{\theta}\left[\frac{\delta_{ij}}{(r_m' r_m')^{\frac{1}{2}}} - \frac{r_i' r_j'}{(r_n' r_n')^{\frac{3}{2}}}\right]$$

Equation 105

$$K_{ij}^{r'\theta} = -\frac{\partial L_i}{\partial \theta_j} = -K^{\theta} D_{ij}$$

Equation 106

$$[C] = \begin{bmatrix} 0 & -p_3 & p_2 \\ p_3 & 0 & -p_1 \\ -p_2 & p_1 & 0 \end{bmatrix}$$

Equation 107

$$[D] = \begin{bmatrix} 0 & -e_3 & e_2 \\ e_3 & 0 & -e_1 \\ -e_2 & e_1 & 0 \end{bmatrix}$$

Equation 108

The Newton's method is applied to solve the equations of the semisubmersible, which is coupled with the lines. The connector force exerted on the rigid body at iteration $n+1$ is approximated by following equations:

$$F_i^{(n+1)} = F_i^{(n)} + \frac{\partial F_i}{\partial r_j}\Delta r_j + \frac{\partial F_i}{\partial X_j}\Delta X_j + \frac{\partial F_i}{\partial \theta_j}\Delta\theta_j + \cdots$$

$$= F_i^{(n)} - K_{ij}^{Xr}\Delta r_j - K_{ij}^{XX}\Delta X_j - K_{ij}^{X\theta}\Delta\theta_j + \cdots$$

Equation 109

$$M_i^{(n+1)} = M_i^{(n)} + \frac{\partial M_i}{\partial r_j}\Delta r_j + \frac{\partial M_i}{\partial r_j'}\Delta r_j' + \frac{\partial M_i}{\partial \theta_j}\Delta\theta_j + \frac{\partial M_i}{\partial X_j}\Delta X_j + \cdots$$

$$= M_i^{(n)} - K_{ij}^{\theta r}\Delta r_j - K_{ij}^{\theta r'}\Delta r_j' - K_{ij}^{\theta\theta}\Delta\theta_j - K_{ij}^{\theta X}\Delta X_j + \cdots$$

Equation 110

where:

$$K_{ij}^{Xr} = -K_i^L\delta_{ij}$$

Equation 111

$$K_{ij}^{XX} = K_i^L \delta_{ij}$$

Equation 112

$$K_{ij}^{X\theta} = K_i^L C_{ij}$$

Equation 113

$$K_{ij}^{\theta r} = K_i^{\theta} C_{ji}$$

Equation 114

$$K_{ij}^{\theta r'} = K_i^{\theta} D_{ji}$$

Equation 115

$$K_{ij}^{\theta\theta} = -\frac{\partial M_i}{\partial \theta_j} = K_i^L C_{ki} C_{kj} + K_i^{\theta} D_{ki} D_{kj}$$

Equation 116

The line/rod stiffness coefficients: K_{ij}^{rr} and $K_{ij}^{r'r'}$ are included in the rod/line element equation that is connected to the platform. The rigid body stiffness coefficients: K_{ij}^{XX}, $K_{ij}^{X\theta}$ and $K_{ij}^{\theta\theta}$ are included in the semisubmersible equation of motion. The coupling stiffness coefficients: K_{ij}^{rX}, K_{ij}^{Xr}, $K_{ij}^{r\theta}$, $K_{ij}^{r'\theta}$, $K_{ij}^{\theta r}$ and $K_{ij}^{\theta r'}$ are included in the coupling matrix. The force vectors $N_i^{(n)}$, $L_i^{(n)}$, $F_i^{(n)}$ and $M_i^{(n)}$ are added to the force vector of line/rod and semisubmersible equations of motion.

3. DESIGN OF LOW-HEAVE SEMISUBMERSIBLE

3.1 Overview

As mentioned in section 1.1, semisubmersible is chosen because of its advantages over other type of Floating Production System. However it exhibits large heave motion, which adversely affects the riser operation. Initial investigation of MR Damper by Dr. Hooi-Siang Kang utilized a drilling semisubmersible that was deemed generic (Kang 2015). Hand-calculation of semisubmersible wave excitation force and heave response were performed to make quick verification of the design before performing frequency-domain free floating analysis. The equation for wave excitation force of semisubmersible is:

$$F_3 = \rho \xi_a g e^{-kz_m} \cos(\omega t) \left[\begin{array}{c} \left(-2kL_P \cos\left(\frac{k}{2}(L_P + L_C) \right) - 4\sin\left(k\frac{L_P}{2} \right) \right) \left(h_P w_P + \frac{A_{33}^{(2D)}}{\rho} \right) + \\ 4L_c w_c e^{-k(h_{draft} - z_m)} \cos\left(\frac{k}{2}(L_P + L_C) \right) \end{array} \right]$$

Equation 117

The equation for semisubmersible heave response is:

$$\eta_3 = \frac{\rho \xi_a g e^{-kz_m} \cos(\omega t) \left[\begin{array}{c} \left(-2kL_P \cos\left(\frac{k}{2}(L_P + L_C) \right) - 4\sin\left(k\frac{L_P}{2} \right) \right) \left(h_P w_P + \frac{A_{33}^{(2D)}}{\rho} \right) + \\ 4L_c w_c e^{-k(h_{draft} - z_m)} \cos\left(\frac{k}{2}(L_P + L_C) \right) \end{array} \right]}{-\omega^2 (M + A_{33}) + (4\rho g L_C w_c + k_{riser} + k_{mooring})}$$

Equation 118

where:

ρ: seawater density

ξ_a: wave amplitude

g: gravity acceleration

k: wave number

ω: wave frequency in rad/s

L_P: pontoon length

L_C: column length

h_P: pontoon height

w_P: pontoon width

$A_{33}^{(2D)}$: pontoon 2-dimnesional added mass

L_c: column length

w_c: column width

h_{draft}: semisubmersible draft

z_m: distance between mean water level to pontoon centerline

M: semisubmersible and topside physical mass

A_{33}: semisubmersible heave added mass

k_{riser}: riser stiffness

$k_{mooring}$: mooring stiffness

Derivation of these equations are included in Appendix 1.

The term $\left(-2kL_P \cos\left(\frac{k}{2}(L_P + L_C)\right) - 4\sin\left(k\frac{L_P}{2}\right)\right)\left(h_P w_P + \frac{A_{33}^{(2D)}}{\rho}\right)$ in Equation 117 and Equation 118 are the pontoon contribution to the excitation force. The term $4L_c w_c e^{-k(h_{draft}-z_m)} \cos\left(\frac{k}{2}(L_P + L_C)\right)$ are the column contribution to the excitation force.

Careful inspection of Equation 117 shows that the pontoon contributed force works against the column contributed force. There is at least one frequency where the pontoon-contributed force cancels out column-contributed force. This frequency is called cancellation frequency (the term cancellation period will be used instead from this point onwards). Note that the column excitation force is inversely proportionate to wave number k. In deepwater, k becomes small as wave period, T increases. Therefore the column excitation force increases as k becomes small or T becomes large. To suppress column excitation force, the region where column is dominating the excitation force must have lower wave amplitude. This philosophy will be used as guidance in examining the semisubmersible.

3.2 Design Objective

This exercise seeks to obtain a shallow-draft low-heave semisubmersible with the draft to be within 30 m (98.5ft) and the column spacing to be at 55m ballpark (180.5 ft).

3.3 Literature Review and Feasibility Analysis

Several low-heave semisubmersibles from offshore journals were investigated for this exercise. They are:

1. McDermott Deepdraft Semisubmersible (Chen, Mei and Mills 2007)
2. Floatec Offset-Pontoon Semisubmersible (Muehlner and Banumurthy 2015)

Option 1 semisubmersible has conventional four square cross section columns with four pontoons linking the column at the bottom. Option 2 semisubmersible has four square-cross-section columns with offset pontoon. Both options are production semisubmersibles. The

semisubmersibles' dimensions and heave performance are compared against the generic semisubmersible (Base Case). Figure 13 shows dimensional comparison between these cases. Details of the dimension are included in Appendix 2.

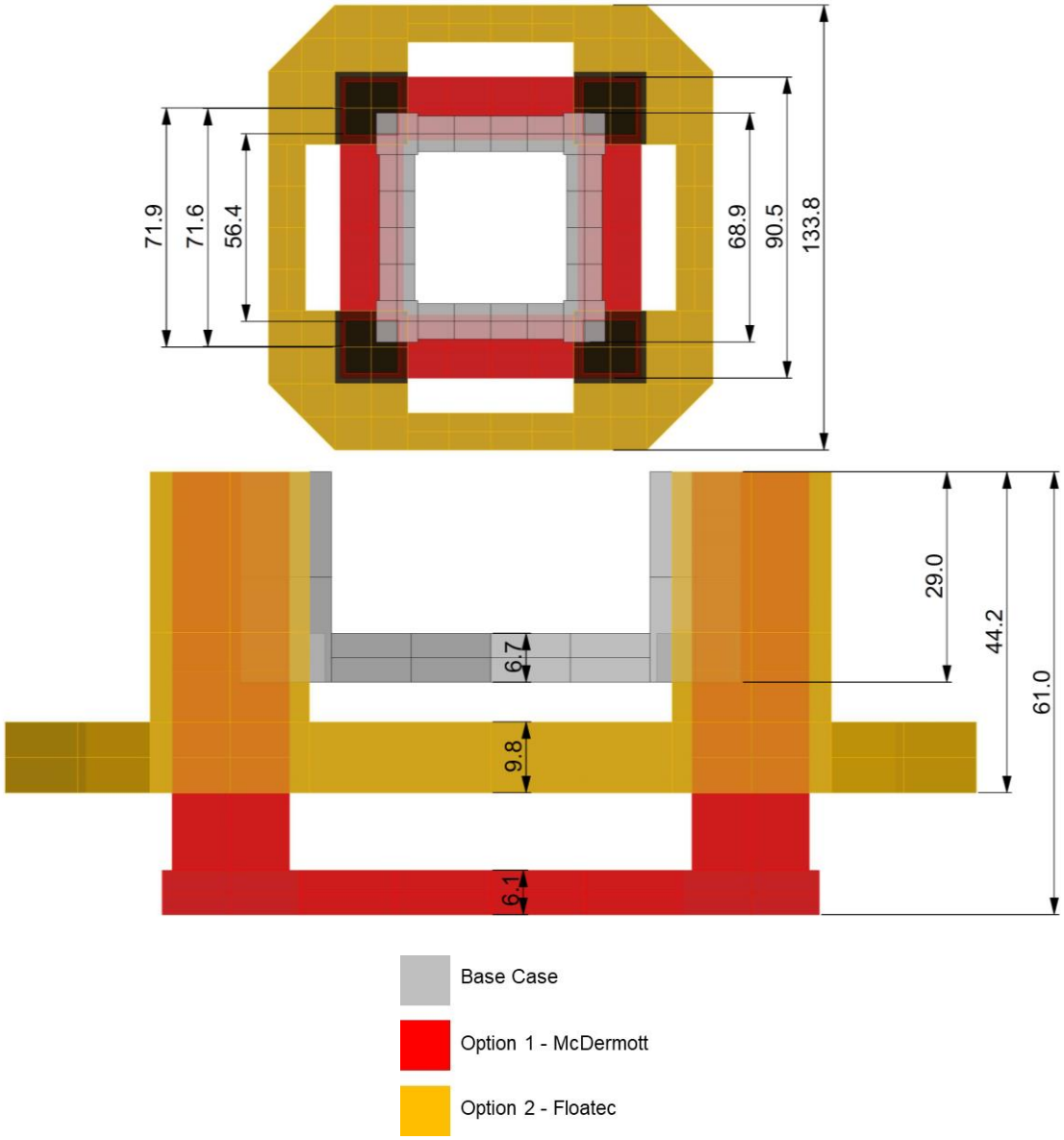

Figure 13 Size and shape comparison between Base Case, Option 1 and Option 2 semisubmersibles (Dimensions in meter)

The table below summarizes the major parameters of the three options:

Parameter	Base Case	Option 1 – McDermott	Option 2 - Floatec
Draft	28.96 m (95.02 ft)	60.96 m (200 ft)	44.19 m (145.00 ft)
Column Spacing	56.39 m (185 ft)	71.62 m (235 ft)	71.93 m (236 ft)
Column (Length x Width)	12.5 m x 12.5 m (41.01 ft x 41.01 ft)	16.15 m x 16.15 m (53 ft x 53 ft)	21.94 m x 21.94 m (72.00 ft x 72.00 ft)
Pontoon Width	10.67 m (35.00 ft)	18.90 m (62.00 ft)	11.13 m (36.50 ft)
Pontoon Height	6.72 m (22.05 ft)	6.10 m (20 ft)	9.75 m (32.00 ft)
Pontoon Length	43.89 m (144.00 ft)	52.73 m (173 ft)	133.80 m (439.00 ft)
Waterplane Area	625 m^2 (6728 ft^2)	1044 m^2 (11,236 ft^2)	1926 m^2 (20,736 ft^2)
Submerged Volume	30,688 m^3 (1,083,898 ft^3)	87,919 m^3 (3,105,280 ft^3)	148,788 m^3 (5,255,168 ft^3)

Table 1 Parameters for Base-Case Semisub, Option-1 McDermott Semisub (Chen, Mei and Mills 2007) and Option-2 Floatec Semisub (Muehlner and Banumurthy 2015). (Part of Option-1 McDermott Semisub figures and Option-2 Floatec Semisub figures are reprinted with permission from ISOPE and Society of Petroleum Engineers respectively)

Option-1 semisubmersible has the deepest draft among the three options, and bigger waterplane area than Base Case. Having deeper draft results in lower wave excitation force, which then leads to lower heave response. Option 2 has the largest waterplane area, and

deeper draft than Base Case. Having large waterplane area leads to large heave hydrodynamic buoyancy stiffness, as shown in the equation below:

$$K_{buoyancy} = \rho g A_w$$

Equation 119

where:

A_w: waterplane area

Having large heave buoyancy stiffness normally leads to lower heave response, but there is a weight penalty that needs to be balanced.

A free floating frequency-domain analysis was performed to validate and understand Option-1 and Option-2 designs, focusing on the heave performance (Response Amplitude Operator (RAO) and natural period). The plot below shows the heave RAO of the three options:

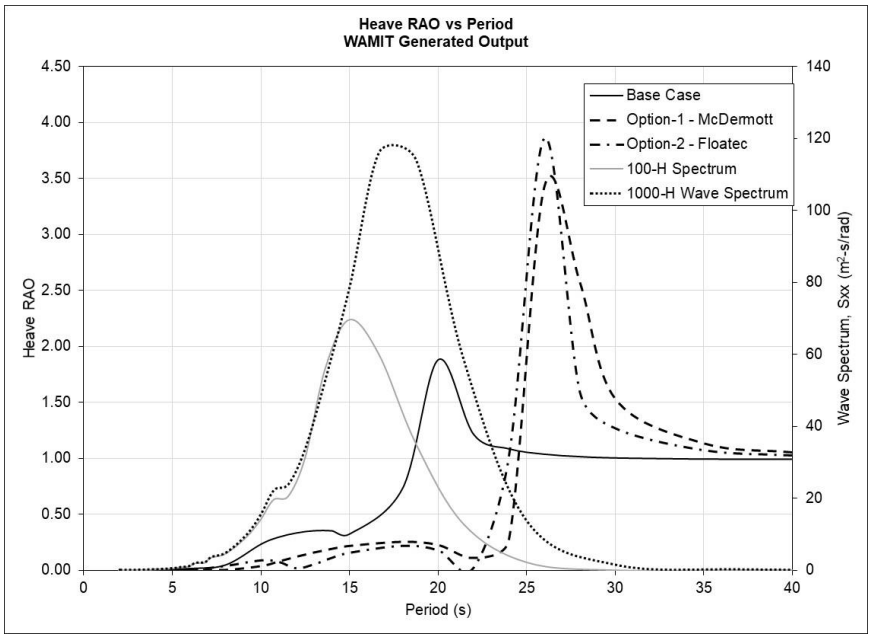

Figure 14 Heave RAO comparison plot for Base Case, Option-1 and Option-2

As shown in Figure 14, Option-1 and Option-2 heave RAO have lower values than Base Case RAO at most period within 100-H and 1000-H wave excitation regions. The peak in the heave RAO curves indicate heave natural period. From Figure 14, Option-1 and Option-2 heave natural periods are outside 100-H wave excitation region, and at the higher period and low energy spectrum of 1000-H wave excitation region. This shows that Option-1 and Option-2 natural period will not be excited in 100-H storm, and lower wave energy to excite the heave natural period in 1000-H environment.

Option-2 was chosen as the basis for the design of shallow-draft low-heave semisubmersible. It has lower heave RAO, and better design, based on the following criteria:

1) Shallower draft
2) Higher heave natural frequency

3) Higher cancellation period
4) Higher waterplane area

3.4 Description of Shallow Draft Low-Heave Semisubmersible System

A shallow-draft low-heave smaller semisubmersible was developed by scaling down the overall shape of Option-2 semisubmersible. This is to ensure that the shape benefits in lowering heave motion is preserved. The shallow-draft low-heave semisubmersible is called Mid-Case from this point onwards. Not all dimensions are scaled-down accordingly due to certain necessity, ie the column cross sectional size is driven by heave buoyancy stiffness requirement. The Mid-Case semisubmersible is juxtaposed with Base Case and Option-2 in Figure 15 below.

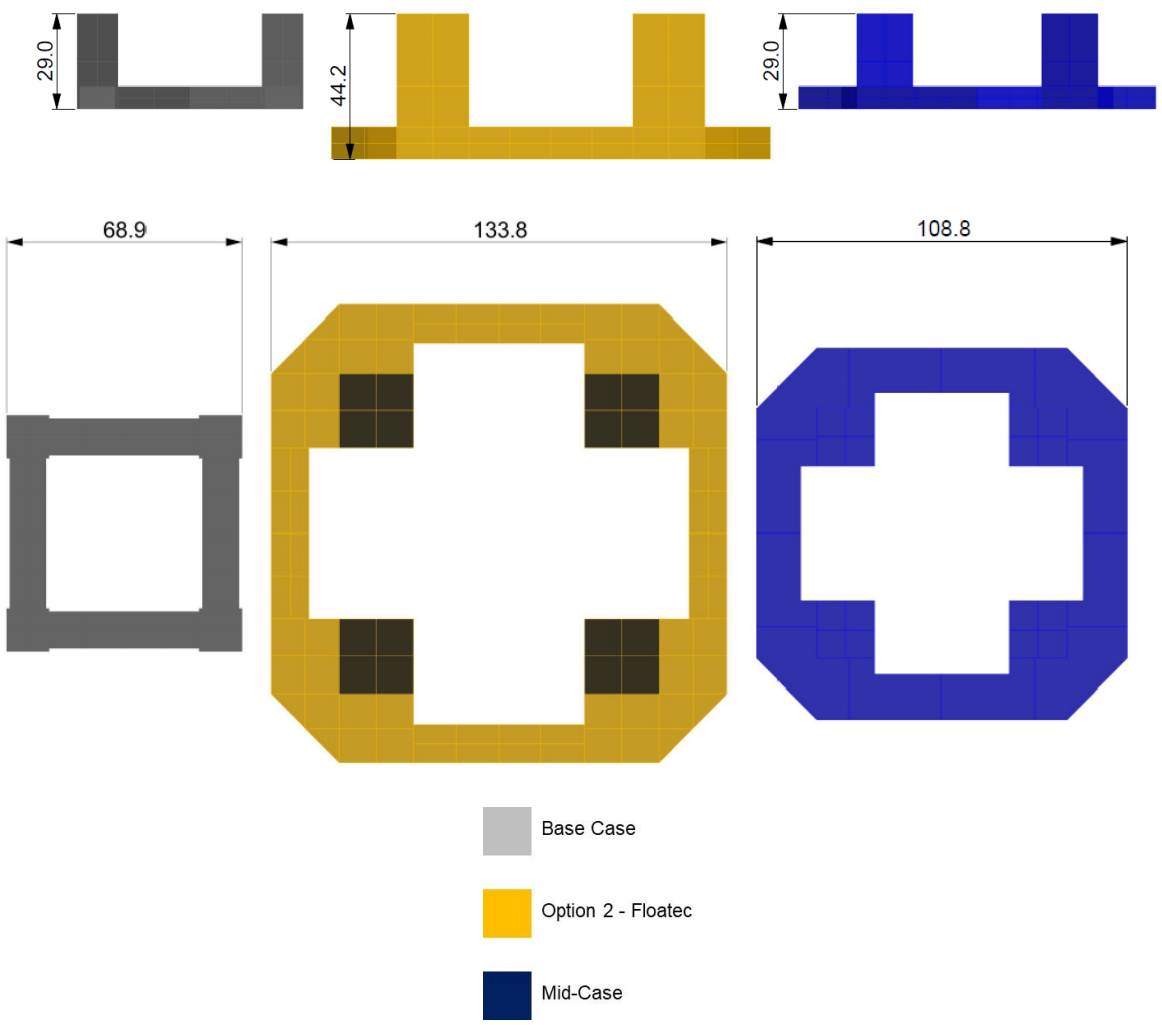

Figure 15 Base-Case, Option-2 and Mid-Case semisubmersibles juxtapose for comparison

The table below summarizes the major dimensions of Base-Case, Option-2 and Mid-Case Semisubmersibles.

Parameter	Base Case	Option 2 – Floatec	Mid-Case
Water Depth	1219.2 m (4000 ft)	1219.2 m (4000 ft)	1219.2 m (4000 ft)
Draft	28.96 m (95.02 ft)	44.19 m (145.00 ft)	28.96 m (95.02 ft)
Column Spacing	56.39 m (185 ft)	71.93 m (236 ft)	56.39 m (185 ft)
Column (Length x Width)	12.5 m x 12.5 m (41.01 ft x 41.01 ft)	21.94 m x 21.94 m (72.00 ft x 72.00 ft)	17.0 m x 17.0 m (55.78 ft x 55.78 ft)
Pontoon Width	10.67 m (35.00 ft)	11.13 m (36.50 ft)	13.00 m (42.65 ft)
Pontoon Height	6.72 m (22.05 ft)	9.75 m (32.00 ft)	6.72 m (22.05 ft)
Pontoon Length	43.89 m (144.00 ft)	133.80 m (439.00 ft)	108.81 m (357 ft)
Waterplane Area	625 m^2 (6728 ft^2)	1926 m^2 (20,736 ft^2)	1156.00 m^2 (12,444 ft^2)
Submerged Volume	30,688 m^3 (1,083,898 ft^3)	148,788 m^3 (5,255,168 ft^3)	67,644 m^3 (2,389,159 ft^3)

Table 2 Parameter comparison of Base-Case semisub, Option-2 Floatec semisub (Muehlner and Banumurthy 2015) and Mid-Case semisub (Part of Option-2 Floatec figures are reprinted with permission from SPE)

3.4.1 Mooring System

The semisubmersible is equipped with 12 mooring lines and 2 top-tensioned risers. Figure 16 below shows the hang-off points of the mooring lines and top-tensioned risers with respect to the semisubmersible. Details of hang-off points can be found in Appendix 3.

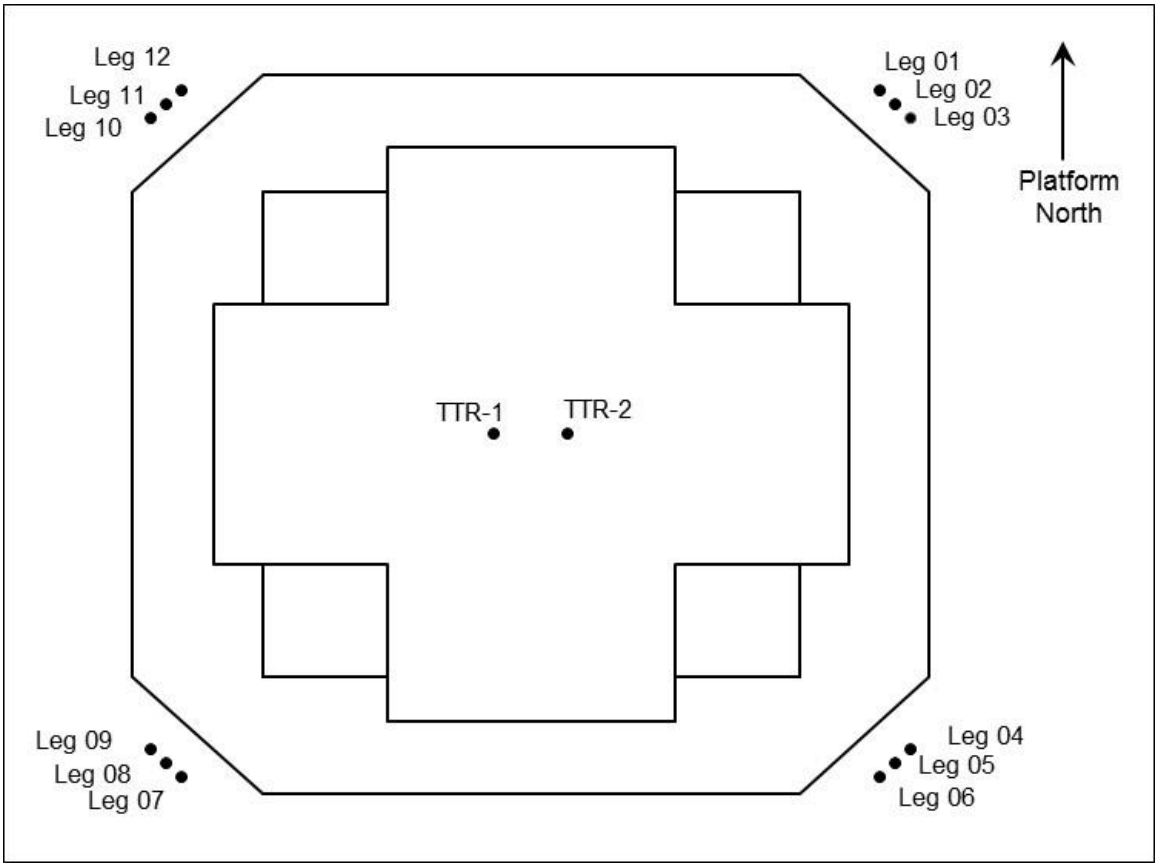

Figure 16 Hang off points of mooring lines (Called "Leg") and top-tensioned riser (TTR)

The table below summarizes the mooring lines information:

Parameters	Value
No of Mooring Lines	12
Pretension per Mooring Line	2,030 kN (456.36 kip)
Mooring Line Length	2,031.80 m (6,666.32 ft)

Table 3 Summary of mooring legs for Mid-Case semisub

3.4.2 Riser System

The top-tensioned risers are dual-casing drilling riser with ram-style tensioner at the top to provide the required tension. The riser is assumed to have a constant profile throughout its column. Figure 17 shows the cross section of the riser.

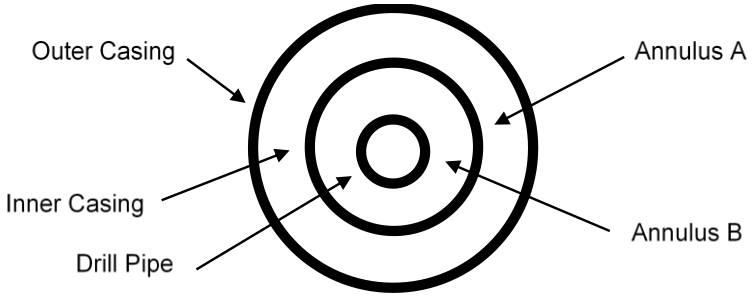

Figure 17 Riser cross section diagram

The table below summarizes the TTR information:

Parameters		Value
Type		Drilling
Content	Annulus-A	Drilling Fluid (1434 kg/m^3)
	Annulus-B	
	Drilling Tube	
Weight	Above Tensioner Ring	0 kN (0 kip)
	Below Tensioner Ring	3744.26 kN (841.74 kip)
Tension Factor		1.32
Nominal Top Tension		4928.60 kN (1108.00 kip)
Outer Casing	Outer Diameter	351 mm (13.82 in)
	Wall Thickness	19 mm (0.75 in)
Inner Casing	Outer Diameter	273 mm (10.75 in)
	Wall Thickness	19 mm (0.75 in)
Drilling Tubing	Outer Diameter	140 mm (5.51 in)
	Wall Thickness	18 mm (0.71 in)

Table 4 Summary of riser parameters for Mid-Case semisub

3.4.3 Riser Tensioner System

Riser Tensioner system provides the required tension to the riser (see section 1.3). The nominal top-tension is dictated by the riser weight requirement. The nominal top-tension then determines the initial pressure in the riser tensioner (see section 2.4.2).

A sensitivity analysis was performed to determine the most optimum tensioner stiffness that which can provide the lowest stroke. The sensitivity analysis also looked into higher tension factor to investigate its effect on riser stroke. Generally, the higher the stiffness, the more restrictive the riser stroke is. However higher stiffness contributes to the semisubmersible natural period, that it reduces the natural period. If the natural period falls within the wave energy period, it will result in bigger heave motion, hence bigger riser stroke. Therefore, a balance between tensioner stiffness and heave motion is required to get the lowest possible stroke. The sensitivity analysis utilized Mid-Case vessel, which performance is described in subsequent section.

Table 5 and Table 6 below show the result from tensioners stiffness sensitivity analysis. The stiffness that provides the lowest total riser stroke is Case-2 stiffness, which has 492.86 kN/m stiffness (33.77 kip/ft stiffness). Increasing the stiffness from Case 2 leads to higher total stroke. Having nominal tension or tension factor also do not result in lower total stroke (Case 6 and Case 7). The increase of total stroke is attributed to the increase of heave motion as shown in Table 7 and Table 8 below.

Mode	Load Case	Metocean	C_f	Health Case	Nominal Tensioner Values				Stroke		
					Top Tension (kN)	Tension Factor	Tensioner Stiffness (kN/m)	Tensioner Stiffness Fraction	Max Upstroke (m)	Max Downstroke (m)	Total Stroke (m)
Drilling	1	1000-H	1.2	Intact	4928.60	1.32	444.67	9.02%	4.16	-3.52	7.68
	2						492.86	10.00%	4.12	-3.43	7.55
	3						591.43	12.00%	4.22	-3.39	7.61
	4						690.00	14.00%	4.51	-3.40	7.91
	5						788.58	16.00%	5.06	-3.44	8.51
	6				5241.97	1.4	472.95	9.02%	4.13	-3.46	7.59
	7				5990.82	1.6	540.51	9.02%	4.21	-3.40	7.61

Table 5 Tensioner sensitivity study load case matrix and stroke result (SI unit)

Mode	Load Case	Metocean	C_f	Health Case	Nominal Tensioner Values				Stroke		
					Top Tension (kip)	Tension Factor	Tensioner Stiffness (kip/ft)	Tensioner Stiffness Fraction	Max Upstroke (ft)	Max Downstroke (ft)	Total Stroke (ft)
Drilling	1	1000-H	1.2	Intact	1107.99	1.32	30.47	9.02%	13.63	-11.56	25.19
	2						33.77	10.00%	13.50	-11.26	24.76
	3						40.52	12.00%	13.86	-11.12	24.97
	4						47.28	14.00%	14.80	-11.16	25.95
	5						54.03	16.00%	16.61	-11.29	27.91
	6				1178.44	1.4	32.41	9.02%	13.55	-11.36	24.91
	7				1346.79	1.6	37.03	9.02%	13.80	-11.16	24.96

Table 6 Tensioner sensitivity study load case matrix and stroke result (Imperial unit)

Mode	Load Case	Metocean	C_f	Health Case	Nominal Tensioner Values				Heave Natural Period (s)	Heave		
					Top Tension (kN)	Tension Factor	Tensioner Stiffness (kN/m)	Tensioner Stiffness Fraction		Max Upward Heave (m)	Max Downward Heave (m)	Total Heave (m)
Drilling	1	1000-H	1.2	Intact	4928.60	1.32	444.67	9.02%	24.35	3.70	-4.22	7.91
	2						492.86	10.00%	24.25	3.69	-4.21	7.90
	3						591.43	12.00%	24.07	3.76	-4.26	8.02
	4						690.00	14.00%	23.88	3.95	-4.56	8.51
	5						788.58	16.00%	23.70	4.22	-5.16	9.38
	6				5241.97	1.4	472.95	9.02%	24.29	3.69	-4.21	7.89
	7				5990.82	1.6	540.51	9.02%	24.16	3.69	-4.20	7.90

Table 7 Mid-case semisubmersible heave motion (SI unit)

Mode	Load Case	Metocean	C_f	Health Case	Nominal Tensioner Values				Heave Natural Period (s)	Heave		
					Top Tension (kip)	Tension Factor	Tensioner Stiffness (kip/ft)	Tensioner Stiffness Fraction		Max Upward Heave (ft)	Max Downward Heave (ft)	Total Heave (ft)
Drilling	1	1000-H	1.2	Intact	1107.99	1.32	30.47	9.02%	24.35	12.13	-13.84	25.96
	2						33.77	10.00%	24.25	12.12	-13.81	25.93
	3						40.52	12.00%	24.07	12.34	-13.98	26.32
	4						47.28	14.00%	23.88	12.97	-14.95	27.92
	5						54.03	16.00%	23.70	13.86	-16.93	30.79
	6				1178.44	1.4	32.41	9.02%	24.29	12.09	-13.80	25.90
	7				1346.79	1.6	37.03	9.02%	24.16	12.12	-13.79	25.91

Table 8 Mid-case semisubmersible heave motion (Imperial unit)

Case-2 stiffness is then used as criteria for determining the nitrogen gas volume in tensioner. The result is tabulated in Table 9 below.

Parameters	Value
Nominal Top Tension	4928.60 kN (1108.00 kip)
Nominal Tensioner Stiffness	492.86 kN/m (33.77 kip/ft)
No. Of Cylinder Assembly	6
Z_0[1]	11.02 m (36.17 ft)
Nitrogen Gas Constant	1.1
HP Side Annulus Area	0.25 m^2 (2.65 ft^2)
LP Side Annulus Area	0.20 m^2 (2.20 ft^2)
HP Side Nitrogen Gas Volume	2.72 m^3 (717 gal)
LP Side Nitrogen Gas	2.5 m^3 (660 gal)
HP Side Nitrogen Set Pressure	3418.25 kPa (495.78 psi)
LP Side Nitrogen Set Pressure	100.00 kPa (14.50 psi)

Note:
[1] See section 2.4.2 for details

Table 9 Summary of tensioner system for riser system

Figure 18 and Figure 19 show Case-2 Tensioner System Curve with no backside pressure or no LP side pressure (see section 1). In downstroke event, the tensioner tension and stiffness increase in nonlinear fashion. This is due to the compression of the gas in the high-pressure side of the tensioner system. In upstroke event the tensioner tension and stiffness decreases due to increase in HP side nitrogen volume, which leads to lower

pressure. Incorporation of back side pressure do not affect the tensioner tension and tensioner stiffness in downstroke event, but a small effect is seen on high upstroke side (numerical model is discussed in section 2.4.2.2). For comparison between tensioner system curve with and without back-side pressure, see Appendix 4. TTR-1 tensioner system was modeled based on tensioner with no-backside pressure whereas TTR-2 tensioner system was modeled based on tensioner with backside pressure. The reason of this is because of the interest in inner pressure of TTR-2 tensioner system, which will be equipped with MR Damper.

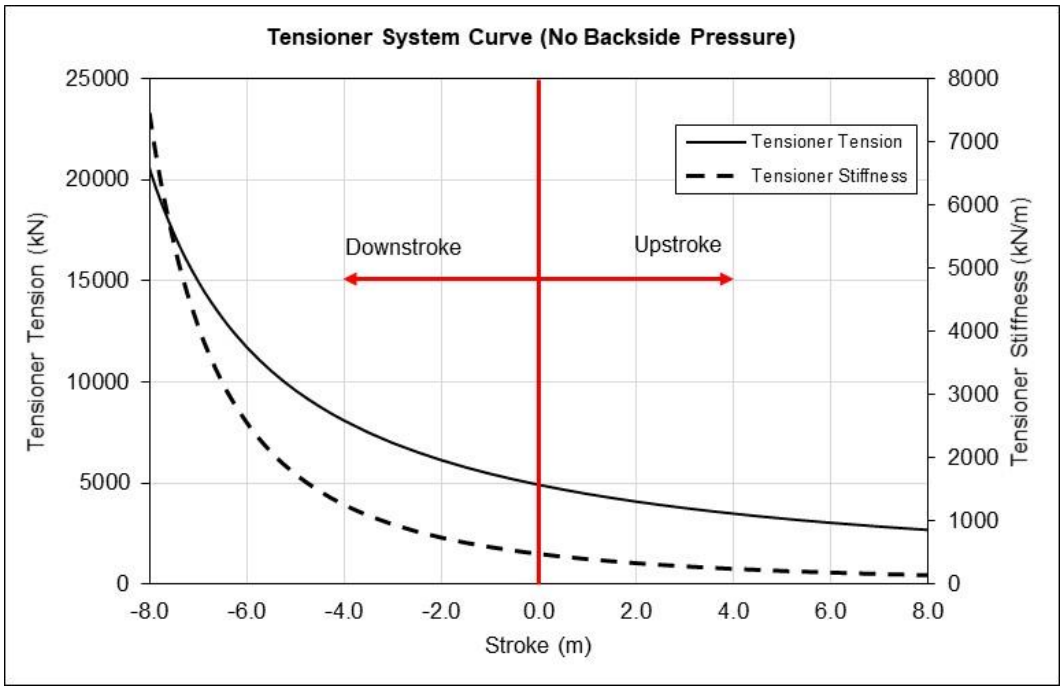

Figure 18 Case-2 tensioner system curve with no backside pressure (SI unit)

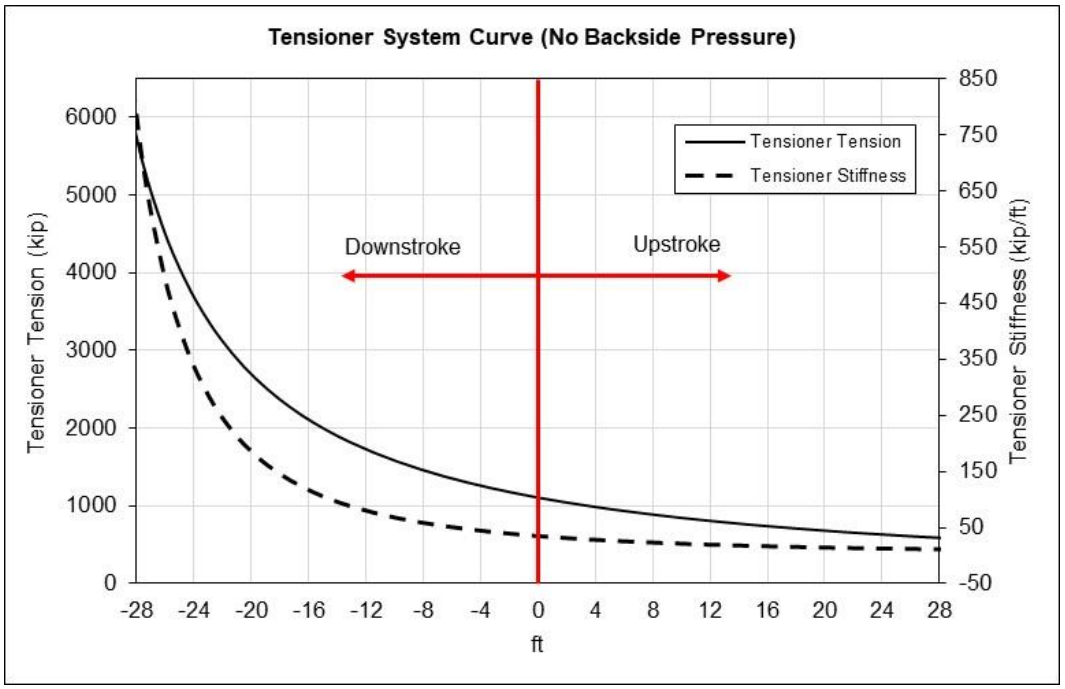

Figure 19 Case-2 tensioner system curve with no backside pressure (Imperial unit)

3.4.4 Metocean Condition

Gulf-Of-Mexico 1000-H return period metocean is chosen to validate the performance of the semisubmersible and the riser. The reason of choosing 1000-H storm is to validate MR Damper do-ability to suppress riser in the most severe storm. The table below summarizes the Metocean condition:

Parameters		1000-H
Significant Wave Height		19.8 m (64.7 ft)
Peak Period		17.2 s
Overshooting Parameter, γ		2.4
Main Direction of Waves		180 deg
Direction of Current		180 deg
Current Profile	Surface Speed	3 m/s (9.8 ft/s)
	Speed at Mid-Profile	2.25 m/s (7.4 ft/s)
	Zero-speed Depth	126 m (413.4 ft)
Wind Speed	10 m Elevation (1 hour speed)	60 m/s (196.9 ft/s)

Table 10 Summary of 1000-H GoM metocean

3.5 Shallow-Draft Low-Heave Semisubmersible System Performance

Figure 20 below shows heave RAO comparison between Base Case, Option-2 and Mid-Case from frequency-domain free floating analysis using WAMIT. The overall heave RAO of Mid-Case semisub has better performance than Base-Case semisubmersible. The heave natural period of Mid-Case lies outside 100-H wave excitation period, and lies at the lower energy of 1000-H wave excitation period.

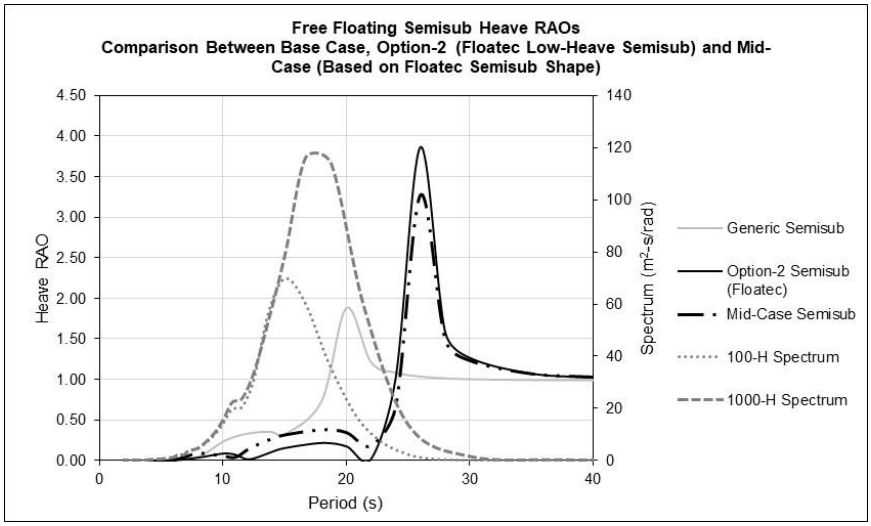

Figure 20 Free floating heave RAO for Base-Case (Generic semisub), Option-2 Floatec semisub and Mid-Case semisub

A coupled time-domain analysis was performed to validate the performance of Mid-Case semisubmersible. Particular attention was paid to the semisubmersible heave motion and riser stroke. The table below summarizes the Mid-Case motion and comparison with Base Case and Option-2.

Motion Mode	Base Case	Option-2 Floatec	Mid-Case
Surge	34.58 m (113.45 ft)	28.04 m (91.99 ft)	34.61 m (113.57 ft)
Sway	0.06 m (0.21 ft)	0.06 m (0.18 ft)	0.11 m (0.37 ft)
Heave	14.80 m (48.55 ft)	5.45 m (17.89 ft)	7.91 m (25.95 ft)
Pitch	9.00 deg	4.86 deg	6.63 deg
Roll	0.14 deg	0.04 deg	0.05 deg
Yaw	0.11 deg	0.15 deg	0.21 deg

Table 11 Total motion of Base-Case, Option-2 and Mid Case semisubmersibles (See Appendix 5 for detail results)

The Mid-Case total heave motion from Table 11 is significantly lower than Base-Case, which confirms the result from the frequency-domain free-floating case discussed above. This improvement helped in reducing the riser stroke to a manageable level, as riser stroke in semisubmersible system is heavily influenced by the heave motion. There is no significant improvement on the surge between Mid-Case and Base Case. The sway motion is small as there is no environment heading in the sway direction.

Table 12 below summarizes riser total stroke. The total stroke of Mid-Case is 7.55m (24.76ft), 5.98m (19.6ft) reduction from Base-Case. The reduction occurs in both upstroke and downstroke direction, which inline with the reduction in heave upward and downward

motion (see appendix 5 for motion details). Note that Tensioner system Case-2 is used in Mid-Case semisubmersible.

Case	Stroke		
	Max Upstroke	**Max Downstroke**	**Total Stroke**
Base Case	7.85 m (25.77 ft)	-5.68 m (-18.63 ft)	13.53 m (44.40 ft)
Option-2 - Floatec	2.72 m (8.93 ft)	-2.45 m (-8.04 ft)	5.17 m (16.98 ft)
Mid Case	4.12 m (13.50 ft)	-3.43 m (-11.26 ft)	7.55 m (24.76 ft)

Table 12 Riser stroke for Base Case, Option-2 and Mid Case

4. MAGNETO-RHEOLOGICAL DAMPER IN RISER TENSIONER SYSTEM

4.1 Overview

Section 1.5 describes the overall mechanism of MR Damper and the use of it in civil and automotive engineering as a mean to dampen vibration. Section 2.4.3 describes the theoretical background of MR Damper. MR Damper has the advantage over passive damper, that its damping coefficient can be varied according to the need. This makes MR Damper a suitable vibration suppressor for earthquake and car motion. The benefit of having able to vary the damping coefficient leads to finding the required damping coefficient to damp the stroke motion from Mid-Case Semisubmersible riser (see section 3.5), which then can be turned to the basis for designing MR Damper for tensioner system.

4.2 System Description

MR Damper is incorporated into the riser tensioner system. In this research only riser 2 (TTR-2) tensioner system is equipped with MR Damper (see Figure 16). The MR Damper for tensioner system overall design is envisioned to be the same as existing MR Damper albeit in a bigger scale. The sketch below envisions the MR Damper incorporation into the riser tensioner system:

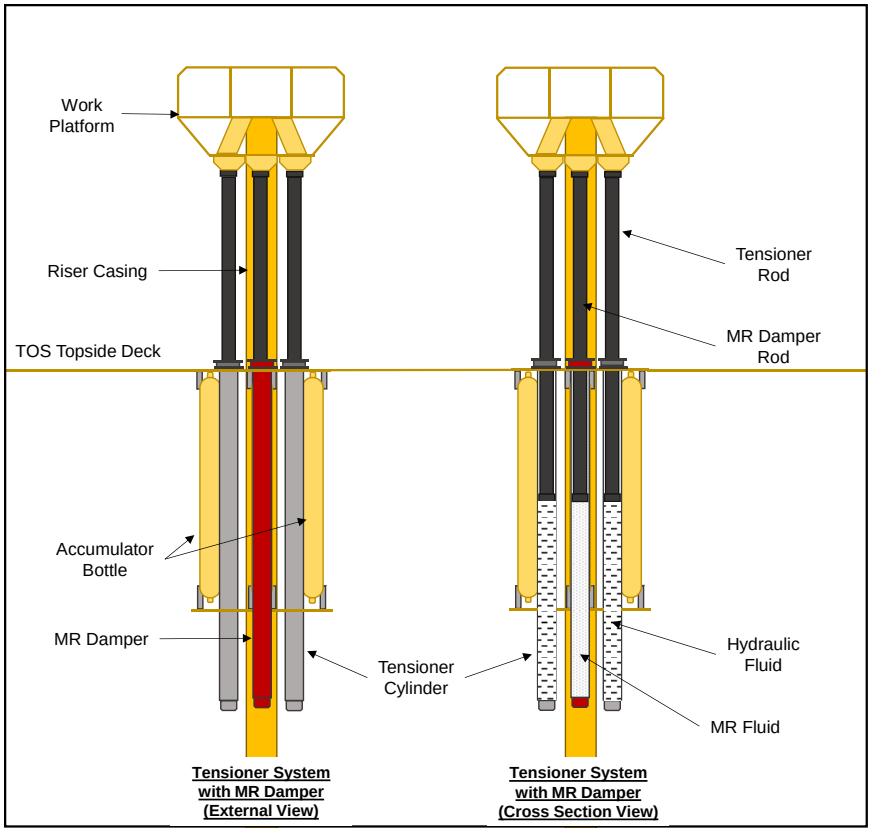

Figure 21 View of ram-style riser tensioner system with MR damper (Surface kits are not shown)

MR Damper barrel, where MR fluid is stored, is mounted onto the topside deck, similar to the tensioner cylinder. As such, it is subjected to the semisubmersible motion owing to the structural connection between topside deck and semisubmersible hull. MR damper rod assembly, consisting of a rod and a piston is attached to the riser tensioner ring, in which a work platform is mounted on it. Consequently, its motion is subjected to the riser top motion. Having connected to two different structures or bodies means that the MR Damper has to accommodate the relative motion between the two bodies (relative vertical

displacement and relative vertical velocity). Note that in this research, the MR Damper is constantly engaged to the tensioner ring/work platform (see section 4.4).

4.3 Numerical Model

Transforming the hardware system into spring-mass system for numerical model:

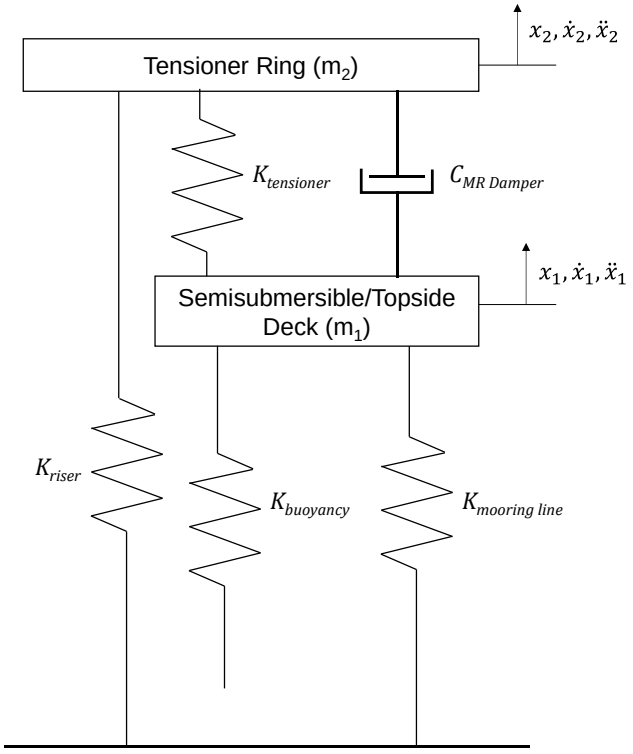

Figure 22 Representation of riser tensioner and MR damper system in spring mass system

Note 2-bodies in Figure 22: tensioner ring and semisubmersible. Dissecting the system to gain understanding of tensioner and MR Damper actions on the bodies:

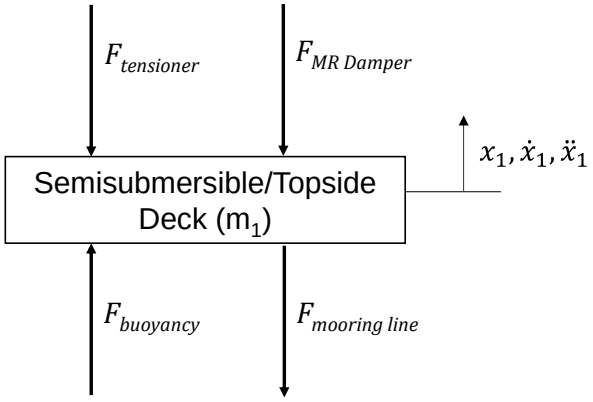

Figure 23 Free-body diagram of semisubmersible and interaction with riser tensioner system and MR Damper

and for tensioner ring:

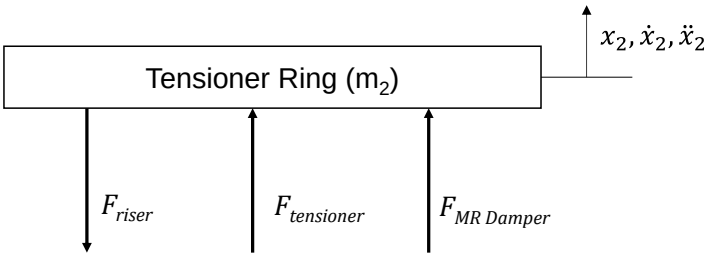

Figure 24 Free-body diagram of riser tensioner ring with interaction with riser tensioner system and MR Damper

The equation of motion for the semisubmersible is constructed based on Figure 23:

$$-F_{tensioner} - F_{MR\ Damper} + F_{buoyancy} - F_{mooring\ line} = m_1\ddot{x}_1$$

Equation 120

where:

$F_{tensioner}$: see Equation 86

$F_{MR\ Damper}$: see Equation 95

$$F_{buoyancy} = K_{buoyancy} x_1$$

Equation 121

where:

$K_{buoyancy}$: see Equation 119

$$F_{mooring\ line} = K_{mooring\ line} x_1$$

Equation 122

where:

$K_{mooring\ line}$: mooring line structural stiffness

The final form of the equation of motion:

$$-n\left[(P_0 A_i)\left(1 + \frac{(x_2 - x_1)A_i}{V_0}\right)^{-\gamma} - \left(P_{0_{LP}} A_{LP}\right)\left(1 - \frac{(x_2 - x_1)A_{LP}}{V_{0_{LP}}}\right)^{-\gamma}\right]$$
$$- C_{MR\ Damper}(\dot{x}_1 - \dot{x}_2) + K_{buoyancy} x_1 - K_{mooring\ line} x_1 = m_1 \ddot{x}_1$$

Equation 123

The equation of motion for riser tensioner ring is constructed based on free body diagram in Figure 24:

$$F_{tensioner} + F_{MR\ Damper} - F_{riser} = m_2 \ddot{x}_2$$

Equation 124

$$F_{riser} = K_{riser} x_2$$

Equation 125

The final form of the equation motion is:

$$n\left[(P_0A_i)\left(1+\frac{(x_2-x_1)A_i}{V_0}\right)^{-\gamma}-\left(P_{0_{LP}}A_{LP}\right)\left(1-\frac{(x_2-x_1)A_{LP}}{V_{0_{LP}}}\right)^{-\gamma}\right]$$

$$+C_{MR\ Damper}(\dot{x}_1-\dot{x}_2)-K_{riser}x_2=m_2\ddot{x}_2$$

Equation 126

4.4 MR Damper Operational Philosophy

It is essential to determine how to utilize MR Damper. MR Damper may not be needed in low sea-state as the heave motion and the resulting stroke are not big. In storm event, it may not be desirous to engage and/or energize MR Damper all the time unless the stroke exceeds certain limit. However, the 1000-H GoM Metocean condition used in this thesis is a severe environment; this necessitates constant engagement and constant energization of MR Damper (see justification below).

MR Damper primary objective is to restrict riser stroke. The riser stroke takes a form of random responses, hence it can be represented as a summation of sinusoidal equations:

$$\Delta Z=\sum_{i=1}^{N}|Z_i|\cos(\omega_i+\alpha_i)$$

Equation 127

However, MR Damper is a function of riser stroke velocity, which is a time derivative of riser stroke:

$$V_{\Delta Z} = -\sum_{i=1}^{N} |Z_i|\, \omega_i \sin(\omega_i + \alpha_i)$$

Equation 128

Equation 127 and Equation 128 show that stroke and stroke velocity are orthogonal to each other. Therefore, the maxima or minima of stroke occurs at zero stroke velocity and vice versa. This is evident in the Case-2 run, which stroke time series is plotted below:

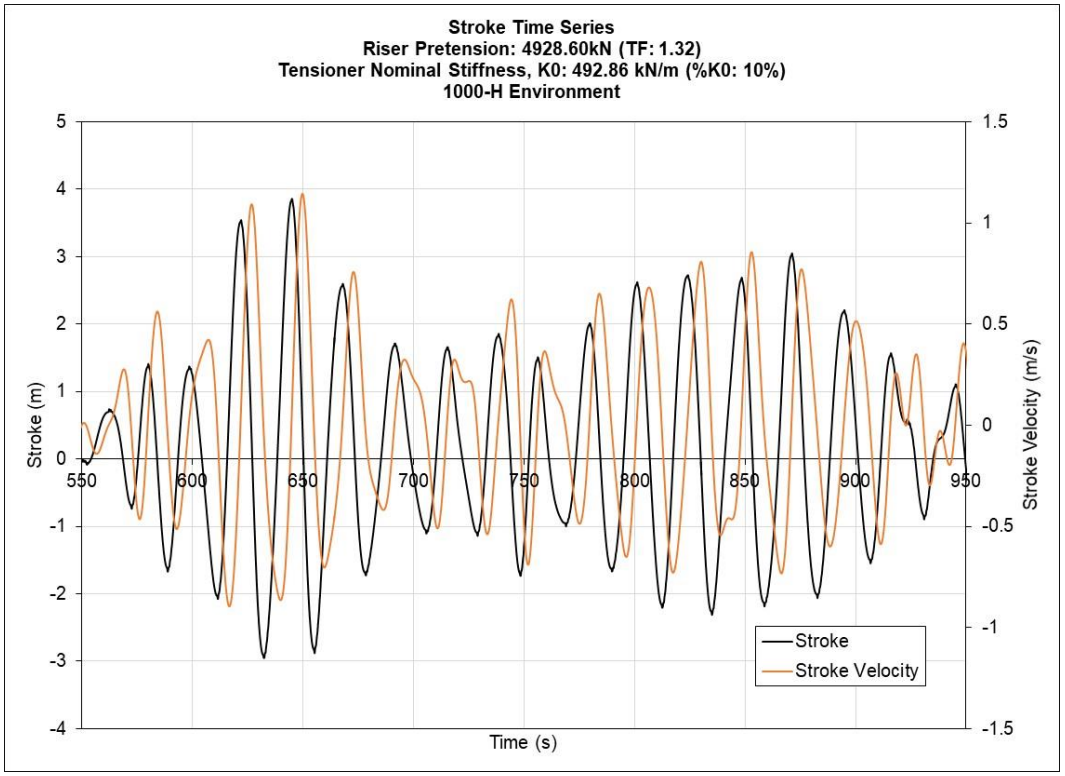

Figure 25 Case-2 stroke and stroke velocity time series (550s to 950s)

To have an effective use of MR Damper, it is imperative that MR Damper is engaged when stroke velocity is at large (recall MR Damper force is a function of stroke velocity).

Furthermore, the stroke fluctuates between downstroke and upstroke every few seconds and most of fluctuation peak are bigger than 1m. This necessitates the engagement of MR Damper for every peak. Therefore, it is required that in 1000-H storm event, that MR Damper is constantly engage and energize to make good use of its effectiveness in suppressing riser stroke peak.

5. ANALYSIS

5.1 Overview

As mentioned in section 1, the introduction of MR Damper in riser tensioner system is to reduce the riser stroke to a manageable level. The manageable level is considered to be 4.572m (15ft), as advised by Dr. Bhat from Shell. Having stroke at this level or lower reduces tensioner hardware, simplifying its manufacturing process especially the tensioner rod and tensioner barrel, and allows for a more compact topside design by having smaller deck spacing.

5.2 Design Objective

The analysis seek to investigate the MR Damper do-ability to restrict riser stroke. In addition to this, it also seeks to find the minimum damping coefficient that restricts the riser stroke to the desired level.

5.3 Metocean Data

Gulf-Of-Mexico 1000-H return period metocean is chosen to validate the performance of the semisubmersible and MR Damper in riser tensioner system. See Table 10 for Metocean details.

5.4 Loadcase Matrix

Various MR Damper damping coefficient were analyzed to understand the system performance and its effects on the riser and semisubmersible. The following is the loadcase matrix for MR Damper sensitivity studies:

Mode	Load Case	Metocean	C_f	Health Case	Nominal Tensioner Values				MR Damper Damping Coefficient (kN/ms^{-1})
					Top Tension (kN)	Tension Factor	Tensioner Stiffness (kN/m)	Tensioner Stiffness Fraction	
Drilling	8	1000-H	1.2	Intact	4928.60	1.32	492.86	10.00%	5,000
	9								6,000
	10								7,000
	11								8,000
	12								9,000
	13								10,000

Table 13 Loadcase matrix for MR damper sensitivity studies (SI unit)

Mode	Load Case	Metocean	C_f	Health Case	Nominal Tensioner Values				MR Damper Damping Coefficient (kip/fts^{-1})
					Top Tension (kip)	Tension Factor	Tensioner Stiffness (kip/ft)	Tensioner Stiffness Fraction	
Drilling	8	1000-H	1.20	Intact	1107.99	1.32	33.77	10.00%	343
	9								411
	10								480
	11								548
	12								617
	13								685

Table 14 Loadcase matrix for MR damper sensitivity studies (Imperial unit)

5.5 Riser Performance with Incorporation of MR Damper

5.5.1 Riser Stroke

The incorporation of MR Damper with linear damping reduces riser stroke in general (see Table 15 and Table 16). Total riser stroke is reduced from 7.55m (24.76ft) to 4.32m (14.16ft). The cases where riser stroke meets target stroke are Case 12, where the total stroke is 4.52m (14.81ft), and Case 13 where the total stroke is 4.32m (14.16ft).

The total stroke reduction is almost linear as shown in Figure 26 and Figure 27. Most reduction occurs in upstroke, where the upstroke reduces from 4.12m (13.5ft) to 1.95m (6.40ft). Reduction in downstroke is not significant. This is because the MR Damper has to counter larger force in downstroke event than in upstroke event (see tensioner system curve Figure 18 and Figure 19 in section 3.4.3). Consequently, further increase in damping coefficient may not be effective in suppressing the downstroke.

Mode	Load Case	Metocean	C_f	Health Case	Nominal Tensioner Values				MR Damper Damping Coefficient (kN/ms^{-1})	Stroke		
					Top Tension (kN)	Tension Factor	Tensioner Stiffness (kN/m)	Tensioner Stiffness Fraction		Max Upstroke (m)	Max Downstroke (m)	Total Stroke (m)
Drilling	2	1000-H	120.00%	Intact	4928.60	1.32	492.86	10.00%	N/A	4.12	-3.43	7.55
	8								5,000	3.21	-2.65	5.85
	9								6,000	2.81	-2.55	5.36
	10								7,000	2.54	-2.48	5.01
	11								8,000	2.32	-2.43	4.74
	12								9,000	2.12	-2.39	4.52
	13								10,000	1.95	-2.37	4.32

Table 15 Riser stroke with linear MR damper incorporated (SI unit)

Mode	Load Case	Metocean	C_f	Health Case	Nominal Tensioner Values				MR Damper Damping Coefficient (kip/fts^{-1})	Stroke		
					Top Tension (kip)	Tension Factor	Tensioner Stiffness (kip/ft)	Tensioner Stiffness Fraction		Max Upstroke (ft)	Max Downstroke (ft)	Total Stroke (ft)
Drilling	2	1000-H	1.2	Intact	1107.99	1.32	33.77	10.00%	N/A	13.50	-11.26	24.76
	8								343	10.52	-8.68	19.20
	9								411	9.20	-8.37	17.57
	10								480	8.32	-8.13	16.45
	11								548	7.60	-7.96	15.56
	12								617	6.97	-7.84	14.81
	13								685	6.40	-7.76	14.16

Table 16 Riser stroke with linear MR damper incorporated (Imperial unit)

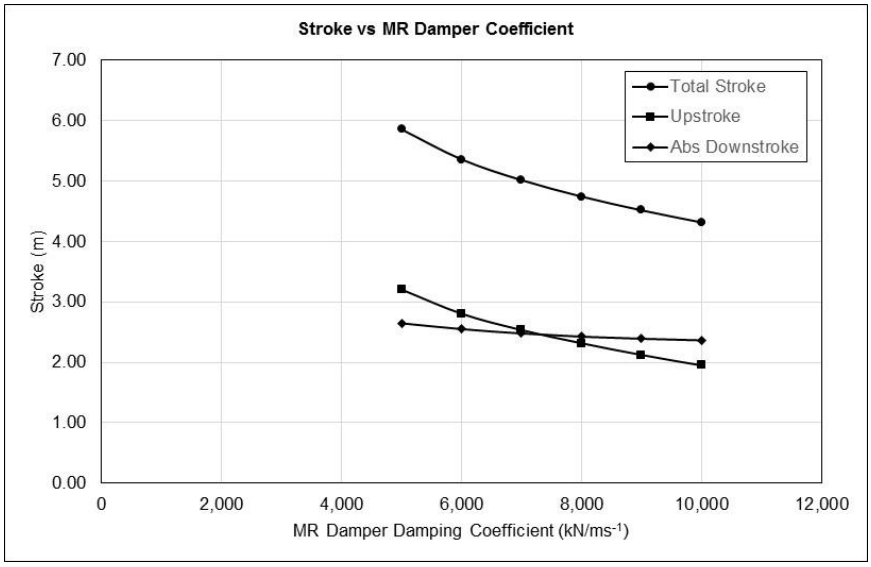

Figure 26 Plot of stroke vs damping coefficient (SI unit)

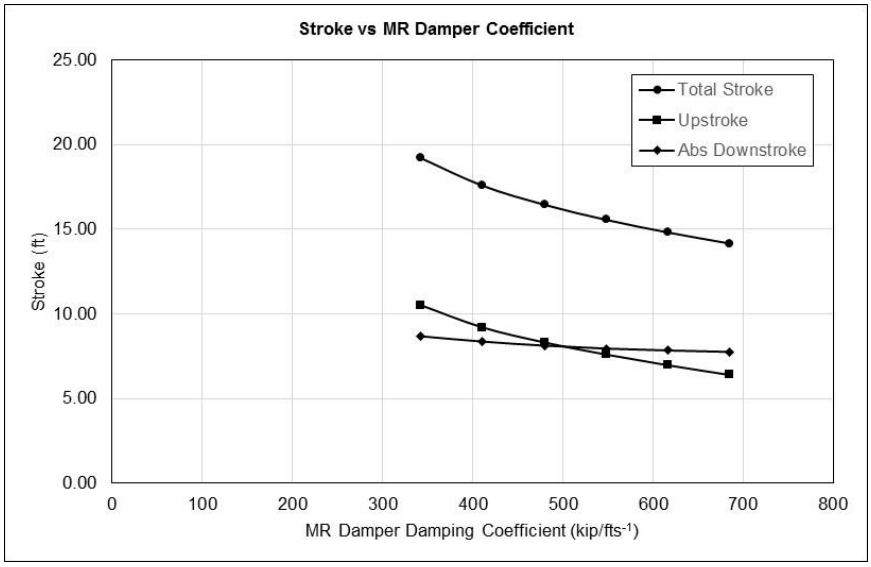

Figure 27 Plot of stroke vs damping coefficient (Imperial unit)

5.5.2 Riser Stroke Response Spectrum

Comparison of riser stroke spectrum between Case 2 (no MR Damper case) and Case 12 and Case 13 was performed. Case 12 and Case 13 are of interest because their total strokes are within the stroke limit.

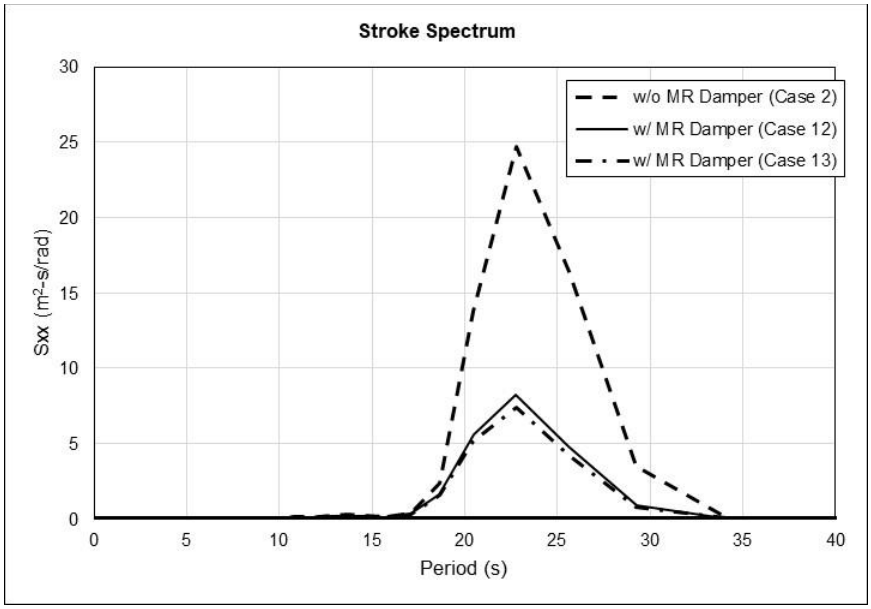

Figure 28 Stroke energy spectrum comparison for Case 2, Case 12 and Case 13

As shown in Figure 28, the peak spectrum reduces greatly with the introduction of MR Damper of coefficient 9000 kN/ms^{-1} (Case 12) and 10,000 kN/ms^{-1} (Case 13). The reduction of spectrum is due to energy dissipation by MR Damper in semisubmersible heave motion and riser top motion. Increasing MR Damper damping coefficient from 9000 kN/ms^{-1} (Case 12) to 10,000 kN/ms^{-1} (Case 13) is deemed ineffective as the energy reduced by the increase of damping coefficient is not significant, as illustrated by Case 13 spectrum curve in Figure 28. This confirms the finding discussed in section 5.5.1.

5.5.3 Tensioner and MR Damper Forces

The reduction of riser stroke affects the forces applied on the deck (see Figure 23). Evaluating the benefit of MR Damper from the tensioner and MR Damper forces are not straight forward as the maximum values of these components occur at a different phase. This is because tensioner force is a function of riser stroke (see Equation 81 and Equation 86) and MR Damper force is a function of riser stroke velocity (see Equation 95). Riser stroke and riser stroke velocity are orthogonal to each other, meaning that the maximum value of riser stroke occurs at the zero value of riser stroke velocity and vice-versa.

The reduction of riser stroke due to the introduction MR Damper results in the reduction of tensioner force. In Case 2 (no MR Damper case) the maximum tensioner force is 7,438kN (1,672kip), and the total stroke is 7.55m (24.76ft). In Case 13, where MR Damper with damping coefficient of 10,000 kN/ms^{-1} is introduced, the maximum tensioner force is 6,487kN (1,458kip), and the total stroke is 4.32m (14.16ft). However Case 13 has the presence of MR Damper force, which max force is 8,153kN (1833kip). Both forces are required to be considered in topside deck structural analysis.

The relationship between MR Damper force, and tensioner force and total riser stroke is illustrated in the plots in Figure 29 and Figure 30 below. The increase in MR Damper force leads to decrease in total stroke, with slight decrease in tensioner force. The evaluation of the benefit of having higher MR Damper force to compensate the riser stroke requires further analysis, and it is beyond the scope of this research.

Mode	Load Case	Metocean	C_f	Health Case	Nominal Tensioner Values				MR Damper Damping Coefficient (kN/ms^{-1})	Total Stroke (m)	Max Tensioner Force (kN)	Max MR Damper Force (kN)	Max MR Damper & Tensioner Force (kN)
					Top Tension (kN)	Tension Factor	Tensioner Stiffness (kN/m)	Tensioner Stiffness Fraction					
Drilling	2	1000-H	1.2	Intact	4928.60	1.32	492.86	10.00%	N/A	7.55	7438		
	8								5,000	5.85	6734	5017	9680
	9								6,000	5.36	6648	5889	10551
	10								7,000	5.01	6585	6580	11299
	11								8,000	4.74	6539	7234	12019
	12								9,000	4.52	6509	7680	12529
	13								10,000	4.32	6487	8153	13059

Table 17 Maximum tensioner and MR damper forces (SI unit)

Mode	Load Case	Metocean	C_f	Health Case	Nominal Tensioner Values				MR Damper Damping Coefficient (kip/fts^{-1})	Total Stroke (ft)	Max Tensioner Force (kip)	Max MR Damper Force (kip)	Max MR Damper & Tensioner Force (kip)
					Top Tension (kip)	Tension Factor	Tensioner Stiffness (kip/ft)	Tensioner Stiffness Fraction					
Drilling	2	1000-H	1.2	Intact	1107.99	1.32	33.77	10.00%	N/A	24.76	1672		
	8								342.59	19.20	1514	1128	2176
	9								411.11	17.57	1495	1324	2372
	10								479.63	16.45	1480	1479	2540
	11								548.15	15.56	1470	1626	2702
	12								616.67	14.81	1463	1727	2817
	13								685.18	14.16	1458	1833	2936

Table 18 Maximum tensioner and MR damper forces (Imperial unit)

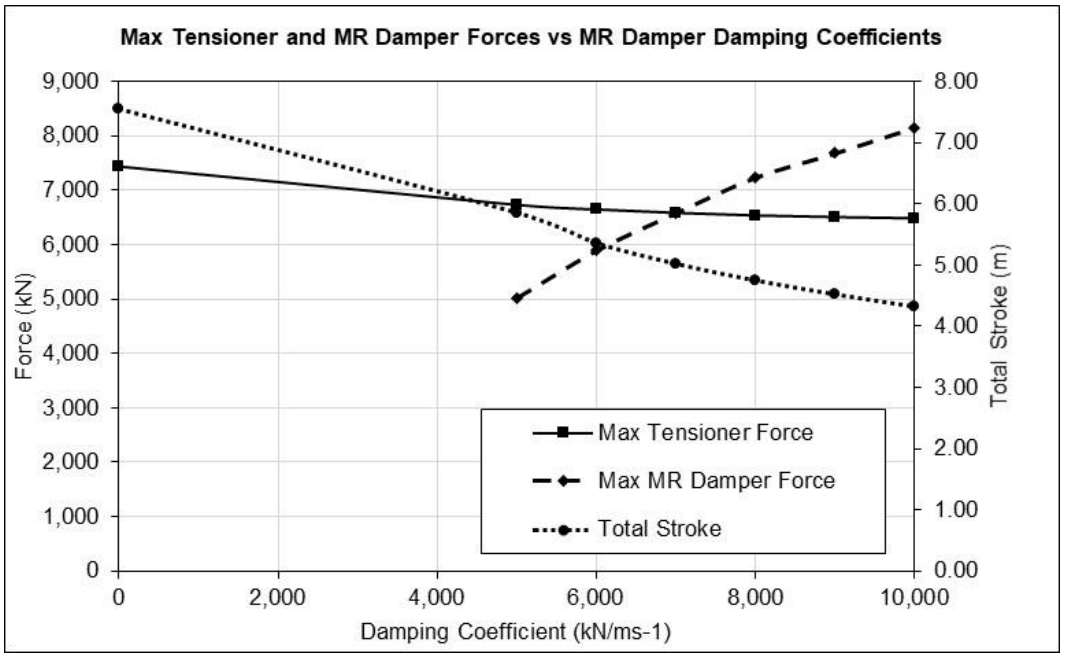

Figure 29 Maximum tensioner and MR damper forces vs damping coefficient (SI unit) (0 kN/ms^{-1} indicates No MR Damper Case/Case 2)

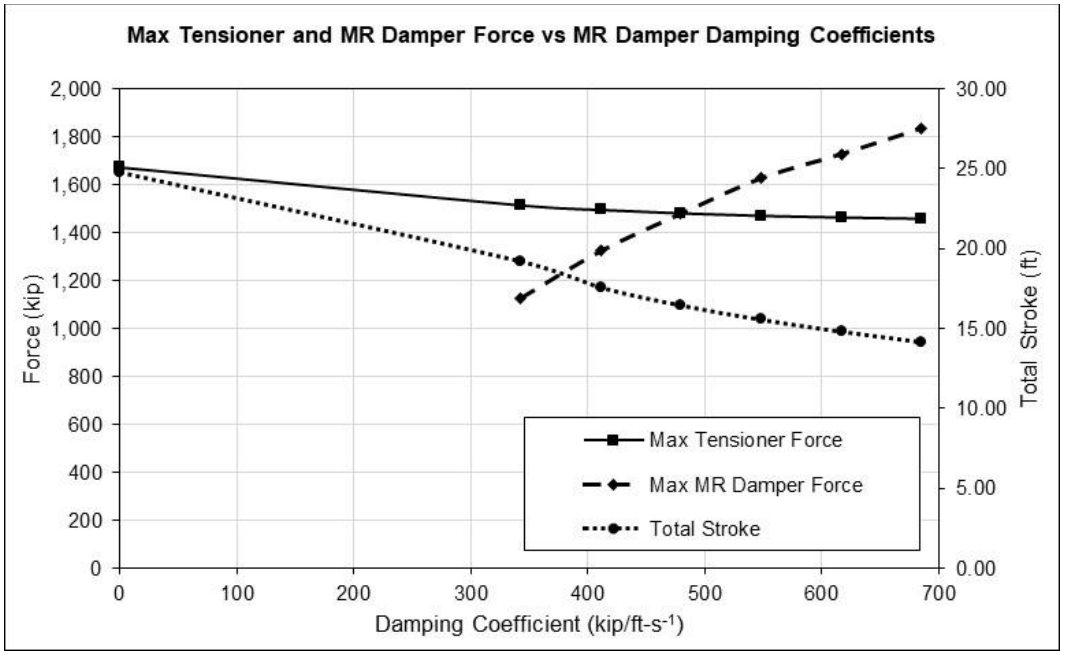

Figure 30 Maximum tensioner and MR damper forces vs damping coefficient (Imperial unit) (0 kip/fts^{-1} indicates No MR Damper Case/Case 2)

5.6 Semisubmersible Heave Performance with Incorporation of MR Damper

Semisubmersible heave performance is of great importance in riser stroke as it influences the riser stroke significantly (see section 4.2 and 4.3). The table below summarizes the heave motion for the MR Damper cases:

The heave motions in Table 19 and Table 20 show that the introduction of MR Damper significantly reduces the heave motion, and this consequently contribute to the reduction of riser stroke. The heave motion reduces from 7.90m (25.93ft) (Case 2) to 6.92m (22.70ft) (Case 8), a total of 0.98m (3.22ft) reduction. However, subsequent increase of damping coefficient did not provide significant reduction in heave motion. The heave motion reduces by 0.51m (1.67ft) from Case 8 (lowest damping coefficient) to Case 13 (highest damping coefficient), whilst the riser total stroke reduces by 1.53 m (5.02ft) from Case 8 to Case 13. The reduction in heave motion is illustrated in the plot below.

Mode	Load Case	Metocean	Nominal Tensioner Values			Heave Natural Period (s)	MR Damper Damping Coefficient (kN/ms^{-1})	Total Stroke (m)	Heave		
			Top Tension (kN)	Tension Factor	Tensioner Stiffness (kN/m)				Max Upward Heave (m)	Max Downward Heave (m)	Total Heave (m)
Drilling	2	1000-H	4928.60	1.32	492.86	24.25	0	7.55	3.69	-4.21	7.90
	8						5000	5.85	2.98	-3.94	6.92
	9						6000	5.36	2.89	-3.86	6.75
	10						7000	5.01	2.83	-3.78	6.61
	11						8000	4.74	2.81	-3.72	6.52
	12						9000	4.52	2.79	-3.66	6.45
	13						10000	4.32	2.80	-3.62	6.41

Table 19 Semisubmersible heave motion (SI unit)

Mode	Load Case	Metocean	Nominal Tensioner Values			Heave Natural Period (s)	MR Damper Damping Coefficient (kip/fts^{-1})	Total Stroke (ft)	Heave		
			Top Tension (kip)	Tension Factor	Tensioner Stiffness (kip/ft)				Max Upward Heave (ft)	Max Downward Heave (ft)	Total Heave (ft)
Drilling	2	1000-H	1107.99	1.32	30.47	24.25	0	24.76	12.12	-13.81	25.93
	8						342.59	19.20	9.77	-12.93	22.70
	9						411.11	17.57	9.48	-12.65	22.13
	10						479.63	16.45	9.30	-12.40	21.70
	11						548.15	15.56	9.20	-12.19	21.39
	12						616.67	14.81	9.16	-12.01	21.17
	13						685.18	14.16	9.18	-11.86	21.04

Table 20 Semisubmersible heave motion (Imperial unit)

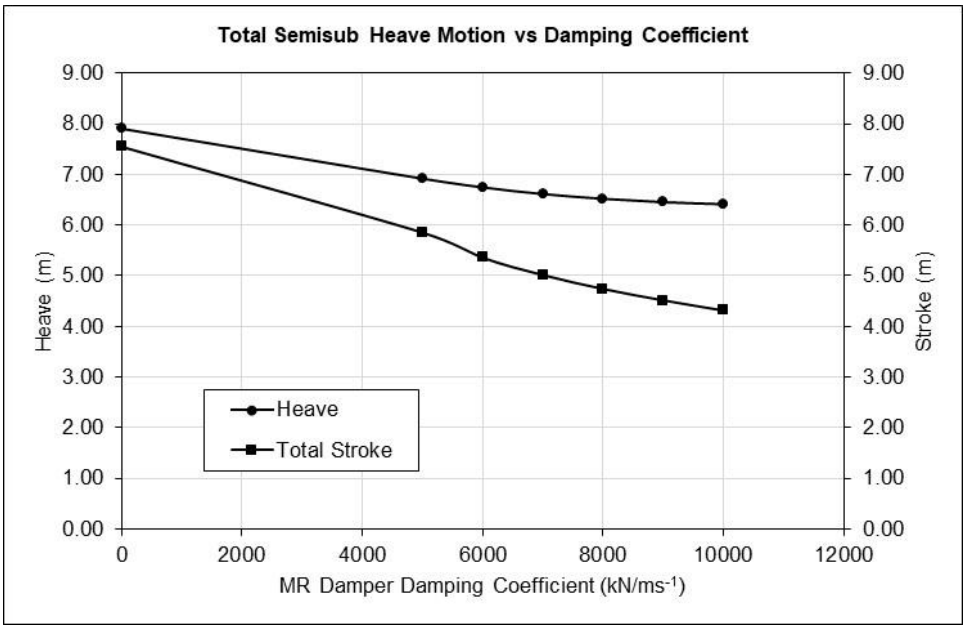

Figure 31 Plot of heave motion vs damping coefficient (SI unit) (0 kN/ms^{-1} indicates No MR Damper Case/Case 2)

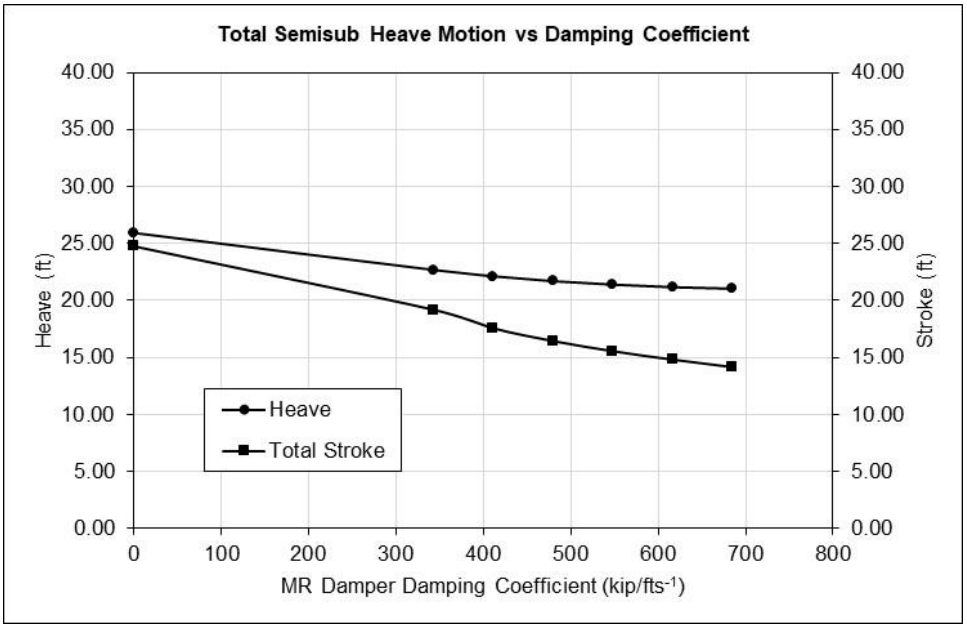

Figure 32 Plot of heave motion vs damping coefficient (Imperial unit) (0 kip/fts^{-1} indicates No MR Damper Case/Case 2)

5.6.1 Heave Spectrum with Incorporation of MR Damper

Comparison of heave spectrum between Case 2, Case 8, Case 12 and Case 13 were made to gain understanding of the MR Damper role in the heave motion (see Figure 33). The introduction of MR Damper dampened the energy in the heave motion, as can be seen by the reduction of spectrum peak between Case 2 and Case 8, or Case 2 and Case 12, or Case 2 and Case 13. This is due to the energy dissipation by MR Damper, leading to lower heave motion.

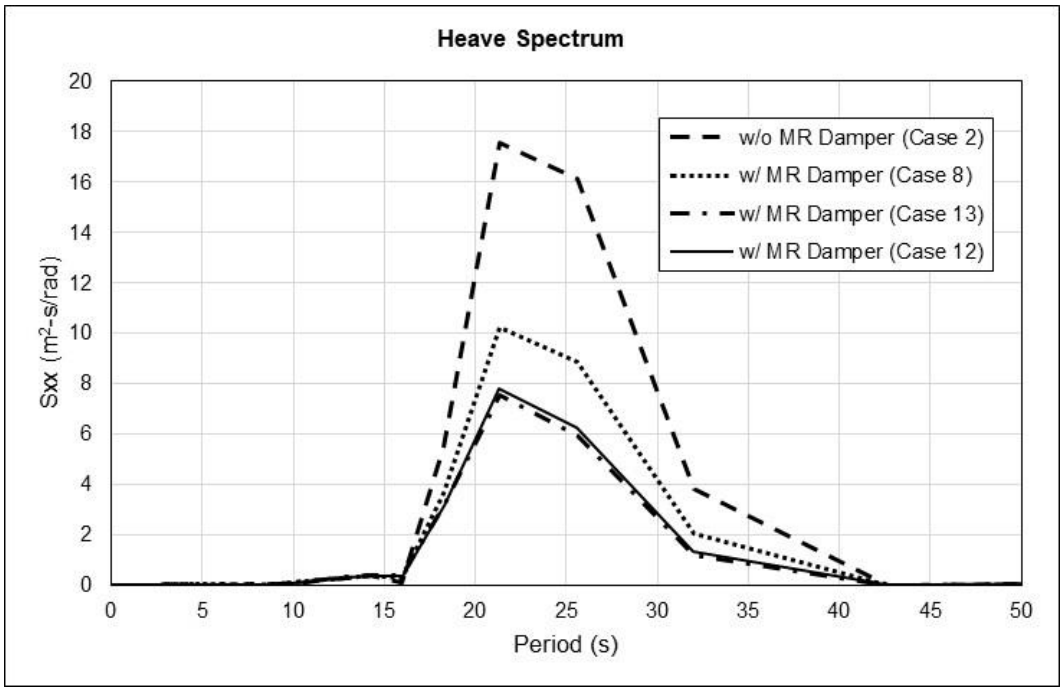

Figure 33 Heave Energy Spectrum

5.7 Incorporating Up-Scaled MR Damper Numerical Model

The result from linear damping analysis was used as basis to size the MR Damper model. Two MR Damper model was employed in the analysis: Bingham MR Damper Model

(see Equation 88), and Non-Linear Arctangent Model (see Equation 89). The parameters were determined based on best-fit curve and/or based on the required damping coefficient from linear damping analysis, which in this case is 9,000kN/ms^{-1} (Case 12). The table below summarizes the MR Damper model parameter coefficient.

Mode	Load Case	Metocean	Nominal Tensioner Values		MR Damper					
			Top Tension (kN)	Tensioner Stiffness Fraction	Numerical Model	Damping Coefficient (kN/ms^{-1})	Stiffness Coefficient (kN/m)	Engagement		Engaged Riser
								Upstroke (m)	Downstroke (m)	
Drilling	17	1000-H	4928.60	10.00%	Bingham	1,424	N/A	Constant		TTR-2
	18					9,400				
	19				NHAF	9,061	35			

Table 21 MR damper parameters (Bingham and non-linear arctangent function) (SI unit)

Mode	Load Case	Metocean	Nominal Tensioner Values		MR Damper					
			Top Tension (kip)	Tensioner Stiffness Fraction	Numerical Model	Damping Coefficient (kip/fts^{-1})	Stiffness Coefficient (kip/ft)	Engagement		Engaged Riser
								Upstroke (ft)	Downstroke (ft)	
Drilling	17	1000-H	1,107.99	10.00%	Bingham	97.55	N/A	Constant		TTR-2
	18					97.55				
	19				NHAF	97.55	2.40			

Table 22 MR damper parameters (Bingham and non-linear arctangent function) (Imperial unit)

Two Bingham models were considered, the first one exhibits the same system curve as an existing small-scale MR Damper, and another exhibits the same damping coefficient as linear damping coefficient. The Non-Linear Hysteretic Arctangent Function model is based on works performed by Kang (Kang 2015). The parameters are derived by manipulating the input current to achieve damping coefficient close to 9,000 kN/ms^{-1}. The plot below shows the MR Damper system curve:

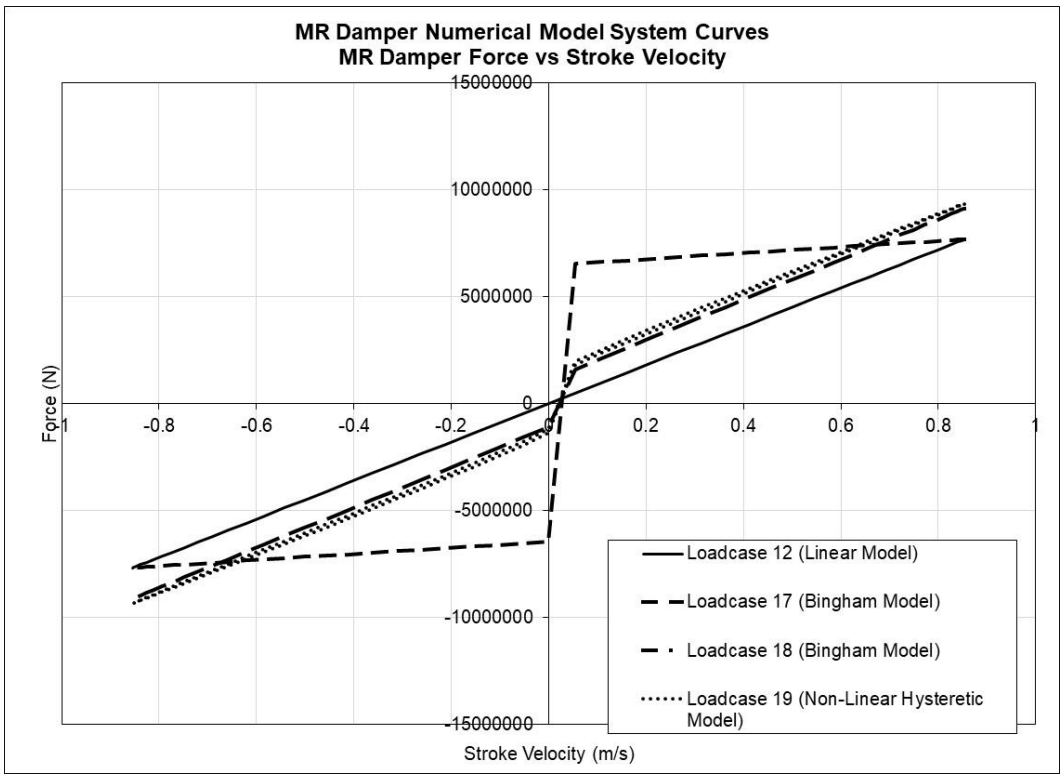

Figure 34 MR damper system curves

5.7.1 Stroke Results

The table below summarizes the stroke result from 1000-H storm time series simulation with MR Damper with Bingham and Non-Linear Hysteretic Arctangent Models.

The stroke results from Bingham model do not come close to the linear damping model. The resulting strokes is at 7.5m vicinity. This shows no total stroke reduction from the case without MR Damper. But the downstroke reduces, albeit the reduction is offset by the increase in upstroke, leaving insignificant change in total stroke. The Non-Linear Hysteretic Arctangent Model (NHAF) shows a stroke result that is close to the linear damping, that is 4.91m. The linear damping stroke result is 4.52m (Case 12). This shows that the numerical model of Non-Linear Hysteretic Arctangent model is closely resemble the linear damping damper.

Mode	Load Case	Metocean	Nominal Tensioner Values		MR Damper						Stroke		
			Top Tension (kN)	Tensioner Stiffness Fraction	Numerical Model	Damping Coefficient (kN/ms^{-1})	Stiffness Coefficient (kN/m)	Engagement		Engaged Riser	Max Upstroke (m)	Max Downstroke (m)	Total Stroke (m)
								Upstroke (m)	Downstroke (m)				
Drilling	17	1000-H	4928.60	10.00%	Bingham	1,424	N/A	Constant		TTR-2	5.57	-1.86	7.43
	18					9,400					6.22	-1.32	7.55
	19				NHAF	9,061	35				2.99	-1.92	4.91

Table 23 Stroke results from MR damper numerical model (SI unit)

Mode	Load Case	Metocean	Nominal Tensioner Values		MR Damper						Stroke		
			Top Tension (kip)	Tensioner Stiffness Fraction	Numerical Model	Damping Coefficient (kip/fts^{-1})	Stiffness Coefficient (kip/ft)	Engagement		Engaged Riser	Max Upstroke (ft)	Max Downstroke (ft)	Total Stroke (ft)
								Upstroke (ft)	Downstroke (ft)				
Drilling	17	1000-H	1,107.99	10.00%	Bingham	97.55	N/A	Constant		TTR-2	18.27	18.27	18.27
	18					97.55					18.27	18.27	18.27
	19				NHAF	97.55	2.40				18.27	18.27	18.27

Table 24 Stroke results from MR damper numerical model (Imperial unit)

5.7.2 Semisubmersible Heave Results

The reduction of riser stroke affects the semisubmersible heave motion (see section 5.5 for linear damping). Table 25 below summarizes the semisubmersible heave motion for riser equipped with MR Damper with actual MR Damper numerical model. The Bingham model with damping coefficient of 9,400 kN/ms^{-1} and Non-Linear Hysteretic Arctangent Model with damping coefficient of 9,061 kN/ms^{-1} have the significant heave reductions.

Mode	Load Case	Metocean	Nominal Tensioner		MR Damper					Heave		
			Top Tension (kN)	Tensioner Stiffness Fraction	Numerical Model	Damping Coefficient (kN/ms^{-1})	Stiffness Coefficient (kN/m)	Engagement		Max Upward Heave (m)	Max Downward Heave (m)	Total heave (m)
								Upstroke (m)	Downstroke (m)			
Drilling	17	1000-H	4928.60	10.00%	Bingham	1,424	N/A	Constant		2.84	-4.62	7.46
	18					9,400				2.73	-3.73	6.45
	19				NHAF	9,061	35.00			2.47	-3.58	6.05

Table 25 Semisubmersible motion with riser tensioner with MR damper (SI unit)

Mode	Load Case	Metocean	Nominal Tensioner		MR Damper					Stroke		
			Top Tension (kip)	Tensioner Stiffness Fraction	Numerical Model	Damping Coefficient (kip/fts^{-1})	Stiffness Coefficient (kip/ft)	Engagement		Max Upward Heave (ft)	Max Downward Heave (ft)	Total Heave (ft)
								Upstroke (ft)	Downstroke (ft)			
Drilling	17	1000-H	1,107.99	10.00%	Bingham	98	N/A	Constant		9.31	-15.16	24.47
	18					644				8.94	-12.22	21.16
	19				NHAF	621	2.40			8.09	-11.76	19.85

Table 26 Semisubmersible motion with riser tensioner with MR damper (Imperial unit)

5.7.3 Tensioner and MR Damper Forces with Bingham and Non-Linear Arctangent Hysteretic Numerical Model

Table 27 summarizes maximum forces of tensioner and MR Damper. The Non-Linear Hysteretic Arctangent Model has the highest Maximum MR Damper force and Maximum Combined Tensioner-MR Damper Forces. Compare to linear damping model with damping coefficient of 9,000 kN/ms^{-1}, the Non-Linear Hysteretic Arctangent Model forces are significantly high. The forces are 59,570 kN for maximum MR Damper force and 65,708kN for maximum combined force. The linear damping with damping coefficient of 9,000 kN/ms^{-1} has 7,680 kN maximum MR Damper force and 12,529 kN maximum combined tensioner-MR Damper force.

Mode	Load Case	Metocean	MR Damper						Total Stroke (m)	Max Tensioner Force (kN)	Max MR Damper Force (kN)	Max MR Damper & Tensioner Force (kN)
			Numerical Model	Damping Coefficient (kN/ms^{-1})	Stiffness Coefficient (kN/m)	Engagement		Engaged Riser				
						Upstroke (m)	Downstroke (m)					
Drilling	17	1000-H	Bingham	1,424	N/A	Constant		TTR-2	7.43	12,550	13,370	25,050
	18			9,400					7.55	15,110	18,160	32,280
	19		NHAF	9,061	35				4.91	9,170	59,570	65,708

Table 27 Tensioner and MR damper maximum forces with MR damper Bingham and Non-Linear Hysteretic Arctangent Model (SI unit)

Mode	Load Case	Metocean	MR Damper						Total Stroke (ft)	Max Tensioner Force (kip)	Max MR Damper Force (kip)	Max MR Damper & Tensioner Force (kip)
			Numerical Model	Damping Coefficient (kip/fts^{-1})	Stiffness Coefficient (kip/ft)	Engagement		Engaged Riser				
						Upstroke (ft)	Downstroke (ft)					
Drilling	17	1000-H	Bingham	97.55	N/A	Constant		TTR-2	24.36	2,821.35	3,005.70	5,631.47
	18			644.07					24.76	3,396.86	4,082.53	7,256.83
	19		NHAF	620.88	2.40				16.11	2,061.50	13,391.87	14,771.75

Table 28 Tensioner and MR damper maximum forces with MR damper Bingham and Non-Linear Hysteretic Arctangent Model (Imperial unit)

5.8 Sensitivity Analysis on MR Damper Engagement Interval

Three sensitivity analysis were performed to investigate MR Damper effectiveness in suppressing riser stroke with the MR Damper engaged at certain stroke ranges. The stroke ranges of interest are 1) stroke exceeding -2m (downstroke 2m or more), 2) stroke exceeding +/-2m (upstroke 2m or more, or downstroke 2m or more), and stroke exceeding +/-1m (upstroke 1m or more, or downstroke 1m or more). Linear damping of 9,000 kN/ms^{-1} is used for comparison with constant engagement case (Case 12). The stroke result of the analysis is tabulated below.

Overall the total strokes in Table 29 are higher than Case 12 total stroke, which is 4.52m. This demonstrates that engaging MR Damper at certain stroke range (not at zero stroke or nominal, see section 4.4) does not make good use of MR Damper.

Mode	Load Case	Metocean	Nominal Tensioner		MR Damper						Stroke		
			Top Tension (kN)	Tensioner Stiffness Fraction	Numerical Model	Damping Coefficient (kN/ms^{-1})	Stiffness Coefficient (kN/m)	Engagement		Engaged Riser	Max Upstroke (m)	Max Downstroke (m)	Total Stroke (m)
								Upstroke (m)	Downstroke (m)				
Drilling	14	1000-H	4928.60	10.00%	Linear	9,000	N/A	N/A	-2.00	TTR-2	4.18	-3.24	7.42
	15							2.00	-2.00		3.39	-3.11	6.50
	16							1.00	-1.00		2.87	-2.72	5.59

Table 29 Loadcase matrix for MR damper engagement interval sensitivity analysis (SI unit)

Mode	Load Case	Metocean	Nominal Tensioner		MR Damper					Stroke		
			Top Tension (kip)	Tensioner Stiffness Fraction	Numerical Model	Damping Coefficient (kip/fts^{-1})	Stiffness Coefficient (kip/ft)	Engagement		Max Upstroke (ft)	Max Downstroke (ft)	Total Stroke (ft)
								Upstroke (ft)	Downstroke (ft)			
Drilling	17	1000-H	1,107.99	10.00%	Bingham	98	N/A	Constant		9.31	-15.16	24.47
	18					644				8.94	-12.22	21.16
	19				NHAF	621	2.40			8.09	-11.76	19.85

Table 30 Loadcase matrix for MR damper engagement interval sensitivity analysis (Imperial unit)

6. CONCLUSIONS

Reduction in riser stroke can be achieved by optimizing semisubmersible hull design. The offset pontoon hull (Mid-Case) originally design by Muehlner (Muehlner and Banumurthy 2015), modified for shallower draft, has lower heave motion than the generic Base Case hull. This in turn results in lower stroke motion which is more favorable to MR Damper. This inline with the effort of reducing riser stroke, which help reducing the deck spacing.

The introduction of linear damping MR Damper on riser tensioner system in Mid-Case semisubmersible greatly reduced the riser stroke to be within the desired stroke, which is 4.572m (15ft) in 1000-H Gulf-of-Mexico Storm. The minimum required damping coefficient to achieve this is 9000 kN/ms^{-1} (617 $kips/fts^{-1}$) (Case-12), which result in total stroke of 4.52m (14.81ft), a reduction of 3.03m (9.94ft) from no-MR Damper case (Case-2). The total stroke for Case-2 is 7.55m (24.76ft). Having this reduction significantly reduce the required deck spacing.

The stroke reduction is primarily caused by the reduction in semisubmersible heave motion. The total heave motion for Case-12 is 6.45m (21.17ft), a reduction of 1.45m (4.78ft), almost half of the stroke reduction. This demonstrates that the MR Damper not only restrict riser motion, it also restricts semisubmersible heave motion.

A spectrum analysis revealed that the reduction in stroke motion is due to dissipation in energy from wave action and from semisubmersible action due to the MR Damper. The semisubmersible heave motion reduction is also due to the energy dissipated by the MR Damper.

The introduction of MR Damper generates a new force to the topside deck and riser structure, which is the MR Damper force. The max MR Damper force for damping coefficient 9000 kN/ms^{-1} is 7,880 kN (1,727kip). In comparison the maximum tensioner force for the same case is 6,509 kN (1,463kip), which is roughly 1,000kN less than MR Damper force. The effect of having MR Damper force on topside deck requires evaluation in the future.

The MR Damper numerical model of Non-Linear Hysteretic Arctangent Model provides the resulting total stroke close to that of linear damping model, albeit with larger resultant MR Damper forces. The Non-Linear Arctangent Model of damping coefficient 9,061 kN/ms^{-1} provides the total stroke of 4.91m, close to total stroke of linear damping model (damping coefficient 9,000 kN/ms^{-1}), which is 4.52m. The maximum MR Damper force of Non-Linear Arctangent Model is 59,570 kN, whereas the maximum MR Damper of Linear Damping Model is lower that is 7,680 kN.

Engaging MR Damper at certain stroke range reduces the MR Damper effectiveness in suppressing riser stroke. MR Damper engaged at stroke range -2m or lower results in total

stroke of 7.42m. MR Damper engaged at stroke range +/- 2m or higher results in total stroke of 6.50m. And MR Damper engages at stroke range +/-1m or higher results in total stroke of 5.59m. In comparison, the total stroke of constant MR Damper engagement is 4.52m

REFERENCES

Ajimoko, Tayo. 2016. "Comparative Analysis of Well Efficiencies Achievable between Mooring and Dynamic Positioning for Deepwater Station Keeping." Offshore Technology Conference Proceedings OTC-26843-MS on 22-25 Mar 2016. Kuala Lumpur: Offshore Technology Conference. 1.

Ambrose, Billy, Matthew Childs, and Russell Krohn. 2001. "Application of a Deepwater Riser Risk Analysis to Drilling Operations and Riser Design." Offshore Technology Conference Proceedings OTC-12954 on 30 Apr to 3 May 2001. Houston: Offshore Technology Conference. 1.

Bitaraf, Maryam, Osman E. Ozbulut, Stefan Hurlebaus, and Luciana Barroso. 2009. "Application of semi-active control strategies for seismic protection of buildings with MR dampers." Engineering Structures 32 (Elsevier Sci Ltd) 3040-3041.

Chen, Cheng-Yo, Xiaoming Mei, and Trevor Mills. 2007. "Effect of Heave Plate on Semisubmersible Response." International Offshore and Polar Engineering Conference Proceedings of the Sixteenth (2007) on 1-6 Jul 2007. Lisbon: The International Society of Offshore and Polar Engineers(ISOPE). 2218-2219.

Dominguez, A., R. Sedaghati, and I. Stiharu. 2007. "Modeling and application of MR dampers in semi-adaptive structures." Computers and Structures 86 407-415.

Faltinsen, O. M. 1990. Sea Loads on Ships and Offshore Structures. Cambridge: Cambridge University Press.

Kang, Hooi-Siang. 2015. "Semi-Active Magneto-Rheological Damper and Applications in Tension Leg Platform/Semi-Submersible, PhD, Texas A&M University-College Station." Dissertation.

Minerals Management Service, Gulf of Mexico OCS Region. 2000. "Gulf of Mexico OCS Region Publications." Bureau of Ocean Energy Management. Minerals Management Service, U.S. Department of the Interior. May. Accessed November 30, 2017. https://www.boem.gov/BOEM-Newsroom/Library/Publications/2000/2000-001.aspx.

Muehlner, Edmund, and Surya Banumurthy. 2015. "Low-Heave Semi-Submersible Enabling Dry-Tree Field Development." Offshore Technology Conference Proceedings - OTC-25666-MS on 4-7 May 2015. Houston: Offshore Technology Conference. 5-6.

Mungall, Chris, Kevin Haverty, Shankar Bhat, David Andersen, Indranil Sarkar, Jack Wu, and Nils Mårtensson. 2004. "Semisubmersible Based Dry Tree Platform with Compliant Vertical Access Risers." Offshore Technology Conference Proceedings OTC-16199 on 3-6 May 2004. Houston: Offshore Technology Conference. 1-3.

Symans, D. Michael, and C. Michael Constantinou. 1997. "Semi-active control systems for seismic protection of structures: a state-of-the-art review." Engineering Structures 21 (Elsevier Science Ltd) 469-487.

Tse, T, and C. C. Chang. 2002. "Seismic Protection of Base-isolated Structures Using Semi-Active MR Dampers." Advances in Building Technology 1: 529-531.

WAMIT. 2015. WAMIT User Manual. 7.1. Chestnut Hill, MA: WAMIT, Inc.

Yang, Guangqiang, Billie F. Spencer, Hyung-Jo Jung, and J. David Carlson. 2004. "Dynamic Modeling of Large-Scale Magnetorheological Damper Systems for Civil Engineering

Applications." Journal of Engineering Mechanics ASCE (Journal of Engineering Mechanics) 130: 1-8.

Yang, Meng-Gang, Chun-Yang Li, and Zheng-Qing Chen. 2013. "A new simple non-linear hysteretic model for MR damper and verification of seismic response reduction experiment." Engineering Structures 52 (Elsevier Ltd) 434-445.

APPENDIX 1

Semisubmersible Hull Layout

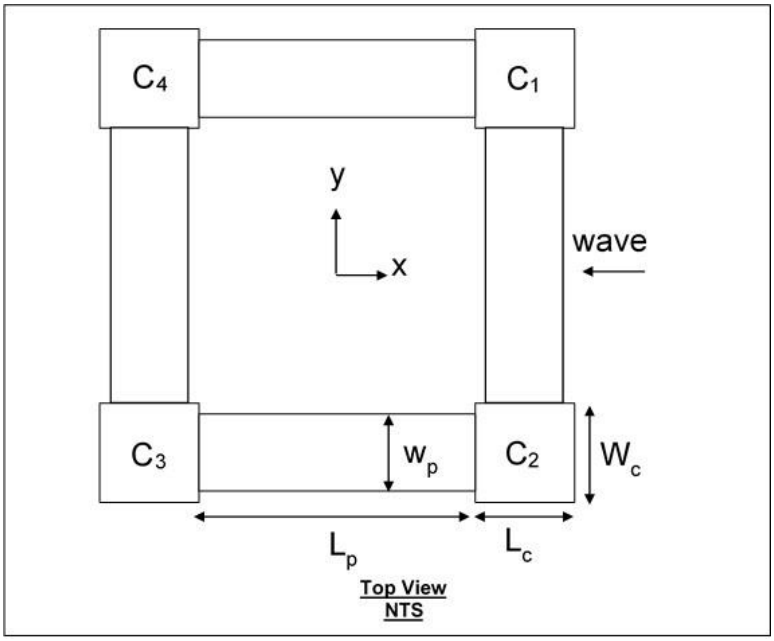

Figure 35 Top view of semisubmersible

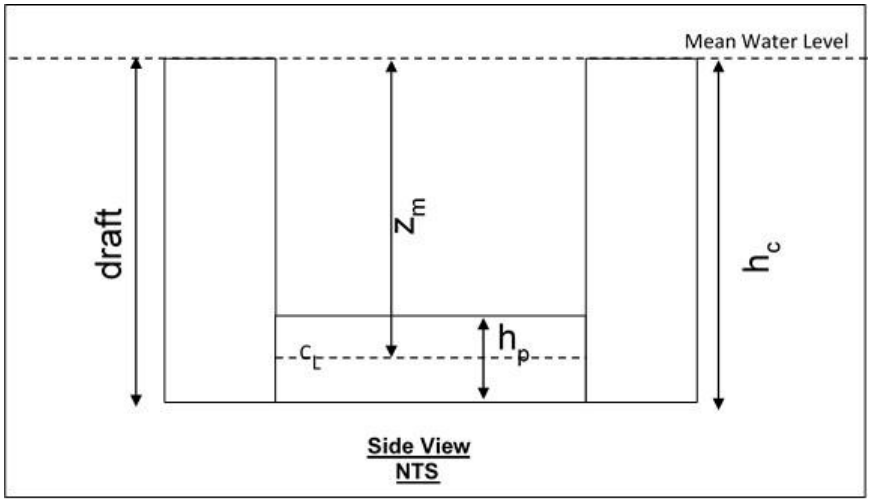

Figure 36 Side view of semisubmersible

Basic Parameters

Incident wave velocity potential:

$$\phi_1 = -\frac{\xi_a g e^{kz}}{\omega} sin(kx + \omega t)$$

Equation 129

Free surface elevation:

$$\xi = \xi_a cos(kx + \omega t)$$

Equation 130

Horizontal wave speed:

$$u = \frac{\partial \phi_1}{\partial x} = -\frac{\xi_a g k e^{kz}}{\omega} cos(kx + \omega t)$$

Equation 131

Vertical wave speed

$$w = \frac{\partial \phi_1}{\partial z} = -\frac{\xi_a g k e^{kz}}{\omega} sin(kx + \omega t)$$

Equation 132

Horizontal wave acceleration:

$$a_1 = \frac{\partial u}{\partial t} = \frac{\partial^2 \phi_1}{\partial t \partial x} = \xi_a g k e^{kz} cos(kx + \omega t)$$

Equation 133

Vertical wave acceleration:

$$a_3 = \frac{\partial w}{\partial t} = \frac{\partial^2 \phi_1}{\partial t \partial z} = -\xi_a g k e^{kz} cos(kx + \omega t)$$

Equation 134

Deriving excitation force for pontoon P_1 and P_3

Pontoon P1 and P3 are submerged and wave number (k) is larger than pontoon width. Therefore we can use equation 3.38 in (Faltinsen 1990):

$$F_3 = \left(\rho A_p + A_{33}^{(2D)}\right) ds \; a_3$$

Equation 135

Equation 135 is excitation and diffraction force for one pontoon. Excitation force is measured at pontoon geometrical center, that is:

$$z = -z_m$$

Equation 136

Inserting acceleration Equation 7 and z elevation Equation 136 into Equation 135:

$$F_3 = -\left(\rho A_p + A_{33}^{(2D)}\right) \xi_a g k e^{-kz_m} cos(kx + \omega t) \int_{-\frac{L_P}{2}}^{\frac{L_P}{2}} dy$$

Equation 137

$$F_3 = -\left(\rho A_p + A_{33}^{(2D)}\right) \xi_a g k L_P e^{-kz_m} cos(kx + \omega t)$$

Equation 138

Pontoon P_1 centerline in x-direction:

$$x_{P_1} = \frac{L_P}{2} + \frac{L_C}{2}$$

Equation 139

Therefore, pontoon P_1 excitation force is:

$$F_{3_{P_1}} = -\left(\rho A_p + A_{33}^{(2D)}\right)\xi_a g k L_P e^{-kz_m} cos\left(k x_{P_1} + \omega t\right)$$

Equation 140

$$F_{3_{P_1}} = -\left(\rho A_p + A_{33}^{(2D)}\right)\xi_a g k L_P e^{-kz_m} cos\left(k(\frac{L_P}{2} + \frac{L_C}{2}) + \omega t\right)$$

Equation 141

$$F_{3_{P_1}} = -\left(\rho A_p + A_{33}^{(2D)}\right)\xi_a g k L_P e^{-kz_m} cos\left(\frac{k}{2}(L_P + L_C) + \omega t\right)$$

Equation 142

Pontoon P_3 centerline in x-direction:

$$x_{P_3} = -\frac{L_P}{2} - \frac{L_C}{2}$$

Equation 143

Therefore, pontoon P_3 excitation force is:

$$F_{3_{P_1}} = -\left(\rho A_p + A_{33}^{(2D)}\right)\xi_a g k L_P e^{-kz_m} cos\left(k x_{P_3} + \omega t\right)$$

Equation 144

$$F_{3_{P_1}} = -\left(\rho A_p + A_{33}^{(2D)}\right)\xi_a g k L_P e^{-kz_m} cos\left(k(-\frac{L_P}{2} - \frac{L_C}{2}) + \omega t\right)$$

Equation 145

$$F_{3_{P_3}} = -\left(\rho A_p + A_{33}^{(2D)}\right)\xi_a g k L_P e^{-kz_m} cos\left(-\frac{k}{2}(L_P + L_C) + \omega t\right)$$

Equation 146

Pontoon 1 and pontoon 3 overall excitation and diffraction force is:

$$F_{3_{P_{1+P_3}}} = F_{3_{P_1}} + F_{3_{P_3}}$$

Equation 147

$$F_{3_{P_{1+P_3}}} = -\left(\rho A_p + A_{33}^{(2D)}\right)\xi_a g k L_P e^{-kz_m}[cos\left(\frac{k}{2}(L_P + L_C) + \omega t\right)$$

$$+ cos\left(-\frac{k}{2}(L_P + L_C) + \omega t\right)]$$

Equation 148

Using trigonometry identity to simplify cosine terms in Equation 148:

$$cos\left(\frac{k}{2}(L_P + L_C) + \omega t\right) + cos\left(-\frac{k}{2}(L_P + L_C) + \omega t\right)$$

$$= \cos\left(\frac{k}{2}(L_P + L_C)\right)\cos(\omega t) - \sin\left(\frac{k}{2}(L_P + L_C)\right)\sin(\omega t)$$

$$+ \cos\left(\frac{k}{2}(L_P + L_C)\right)\cos(\omega t) + \sin\left(\frac{k}{2}(L_P + L_C)\right)\sin(\omega t)$$

Equation 149

$$cos\left(\frac{k}{2}(L_P + L_C) + \omega t\right) + cos\left(-\frac{k}{2}(L_P + L_C) + \omega t\right) = 2\cos\left(\frac{k}{2}(L_P + L_C)\right)\cos(\omega t)$$

Equation 150

$$F_{3_{P_{1+P_3}}} = -\left(\rho A_p + A_{33}^{(2D)}\right)\xi_a g k L_P e^{-kz_m}[2\cos\left(\frac{k}{2}(L_P + L_C)\right)\cos(\omega t)]$$

Equation 151

$$F_{3_{P_{1+P_3}}} = -2\left(\rho A_p + A_{33}^{(2D)}\right)\xi_a g k L_P e^{-kz_m}\cos\left(\frac{k}{2}(L_P + L_C)\right)\cos(\omega t)$$

Equation 152

$$F_{3_{P_{1+P_3}}} = -2\rho\xi_a g k L_P\left(A_p + \frac{A_{33}^{(2D)}}{\rho}\right)e^{-kz_m}\cos\left(\frac{k}{2}(L_P + L_C)\right)\cos(\omega t)$$

Equation 153

Deriving excitation force for pontoon P_2 and P_4

From equation 3.38 in (Faltinsen 1990)

$$F_3 = \left(\rho A_P + A_{33}^{(2D)}\right) ds \; a_3$$

Equation 154

From Equation 7, and $s = x$:

$$F_3 = \int_{\frac{-L_P}{2}}^{\frac{L_P}{2}} \left(\rho A_P + A_{33}^{(2D)}\right)\left(-\xi_a g k e^{kz} cos(kx + \omega t)\right) dx$$

Equation 155

$$F_3 = \left(\rho A_P + A_{33}^{(2D)}\right)\left(-\xi_a g k e^{kz} \frac{\sin(kx + \omega t)}{k}\right)_{x=\frac{-L_P}{2}}^{x=\frac{L_P}{2}}$$

Equation 156

$$F_3 = -\left(\rho A_P + A_{33}^{(2D)}\right)\xi_a g e^{kz}\left(\sin\left(k\frac{L_P}{2} + \omega t\right) - \sin\left(k\left(\frac{-L_P}{2}\right) + \omega t\right)\right)$$

Equation 157

Using trigonometry identity to simplify sine terms:

$$\sin\left(k\frac{L_P}{2} + \omega t\right) - \sin\left(k\left(\frac{-L_P}{2}\right) + \omega t\right)$$

$$= \sin\left(k\frac{L_P}{2}\right)\cos(\omega t) + \cos\left(k\frac{L_P}{2}\right)\sin(\omega t) - \cos\left(k\frac{L_P}{2}\right)\sin(\omega t)$$

$$+ \sin\left(k\frac{L_P}{2}\right)\cos(\omega t)$$

Equation 158

$$\sin\left(k\frac{L_P}{2}+\omega t\right)-\sin\left(k\left(\frac{-L_P}{2}\right)+\omega t\right)=2\sin\left(k\frac{L_P}{2}\right)\cos(\omega t)$$

Equation 159

$$F_3=-\left(\rho A_P+A_{33}^{(2D)}\right)\xi_a g e^{kz}\left(2\sin\left(k\frac{L_P}{2}\right)\cos(\omega t)\right)$$

Equation 160

$$F_3=-2\left(\rho A_P+A_{33}^{(2D)}\right)\xi_a g e^{kz}\sin\left(k\frac{L_P}{2}\right)\cos(\omega t)$$

Equation 161

$$z=-z_M$$

Equation 162

$$F_3=-2\left(\rho A_P+A_{33}^{(2D)}\right)\xi_a g e^{-kz_M}\sin\left(k\frac{L_P}{2}\right)\cos(\omega t)$$

Equation 163

P_2 and P_4 have the same excitation force, hence:

$$F_{3_{P_2+P_4}}=2F_3$$

Equation 164

$$F_{3_{P_2+P_4}}=-4\left(\rho A_P+A_{33}^{(2D)}\right)\xi_a g e^{-kz_M}\sin\left(k\frac{L_P}{2}\right)\cos(\omega t)$$

Equation 165

$$F_{3_{P_2+P_4}} = -4\rho\xi_a g\left(A_P + \frac{A_{33}^{(2D)}}{\rho}\right)e^{-kz_M}\sin\left(k\frac{L_P}{2}\right)\cos(\omega t)$$

Equation 166

Deriving excitation force for columns

Deriving Column 1 excitation force:

$F_{3_{C1}} = \iint_S pn_3 dS$ (Froude-Kriloff force)

Equation 167

$$p = -\rho\frac{\partial\phi_1}{\partial t}$$

Equation 168

$$\frac{\partial\phi_1}{\partial t} = -\xi_a g e^{kz}cos(kx + \omega t)$$

Equation 169

$$p = \rho\xi_a g e^{kz}cos(kx + \omega t)$$

Equation 170

$$n_3 = 1$$

Equation 171

Substitute Equation 169 and Equation 171 into Equation 167:

$$F_{3_{C1}} = \iint_S \rho \xi_a g e^{kz} cos(kx + \omega t) dS$$

Equation 172

$$F_{3_{C1}} = \rho \xi_a g e^{kz} \cos(kx + \omega t)(L_c w_c)|_{x=\frac{L_P + L_C}{2}}$$

Equation 173

Where

$$z = -h_{draft}$$

Equation 174

Therefore column C_1 excitation force is:

$$F_{3_{C1}} = \rho \xi_a g L_c w_c e^{-kh_{draft}} \cos\left(k\left(\frac{L_P + L_C}{2}\right) + \omega t\right)$$

Equation 175

Similar derivation is employed for column C_2, C_3 and C_4.

$$F_{3_{C2}} = \rho \xi_a g L_c w_c e^{-kh_{draft}} \cos\left(k\left(\frac{L_P + L_C}{2}\right) + \omega t\right)$$

Equation 176

$$F_{3_{C3}} = \rho \xi_a g L_c w_c e^{-kh_{draft}} \cos\left(-k\left(\frac{L_P + L_C}{2}\right) + \omega t\right)$$

Equation 177

$$F_{3_{C4}} = \rho \xi_a g L_c w_c e^{-kh_{draft}} \cos\left(-k\left(\frac{L_P + L_C}{2}\right) + \omega t\right)$$

Equation 178

Total column excitation force is

$$F_{3_C} = F_{3_{C1}} + F_{3_{C2}} + F_{3_{C3}} + F_{3_{C4}}$$

Equation 179

or

$$F_{3_C} = 2\rho \xi_a g L_c w_c e^{-kh_{draft}} \left(\cos\left(k\left(\frac{L_P + L_C}{2}\right) + \omega t\right) + \cos\left(-k\left(\frac{L_P + L_C}{2}\right) + \omega t\right)\right)$$

Equation 180

Using trigonometry identity to simplify cosine terms in Equation 180:

$$\cos\left(k\left(\frac{L_P + L_C}{2}\right) + \omega t\right) + \cos\left(-k\left(\frac{L_P + L_C}{2}\right) + \omega t\right) = 2\cos\left(\frac{k}{2}(L_P + L_C)\right)\cos(\omega t)$$

Equation 181

$$F_{3_C} = 2\rho \xi_a g L_c w_c e^{-kh_{draft}} \left(2\cos\left(\frac{k}{2}(L_P + L_C)\right)\cos(\omega t)\right)$$

Equation 182

$$F_{3_C} = 4\rho \xi_a g L_c w_c e^{-kh_{draft}} \cos\left(\frac{k}{2}(L_P + L_C)\right)\cos(\omega t)$$

Equation 183

Total hull excitation force

Combining Equation 153, Equation 166 and Equation 183 to get the total excitation force of the hull:

$$F_3 = F_{3_{P_{1+P_3}}} + F_{3_{P_{2+P_4}}} + F_{3_C}$$

Equation 184

Substitute Equation 153, Equation 166 and Equation 183 into Equation 184:

$$F_3 = -2\rho\xi_a g k L_P \left(A_p + \frac{A_{33}^{(2D)}}{\rho}\right) e^{-kz_m} \cos\left(\frac{k}{2}(L_P + L_C)\right)\cos(\omega t)$$
$$- 4\rho\xi_a g \left(A_P + \frac{A_{33}^{(2D)}}{\rho}\right) e^{-kz_M} \sin\left(k\frac{L_P}{2}\right)\cos(\omega t)$$
$$+ 4\rho\xi_a g L_c w_c e^{-kh_{draft}} \cos\left(\frac{k}{2}(L_P + L_C)\right)\cos(\omega t)$$

Equation 185

$$F_3 = \rho\xi_a g e^{-kz_m}\cos(\omega t)\left[\left(-2kL_P\cos\left(\frac{k}{2}(L_P + L_C)\right) - 4\sin\left(k\frac{L_P}{2}\right)\right)\left(A_P + \frac{A_{33}^{(2D)}}{\rho}\right)\right.$$
$$\left. + 4L_c w_c e^{-k(h_{draft} - z_m)} \cos\left(\frac{k}{2}(L_P + L_C)\right)\right]$$

Equation 186

Note that in Equation 186, $A_{33}^{(2D)}$ is pontoon 2-dimensional added mass.

Pontoon added mass estimation

From figure 3.10 (Faltinsen 1990), 2D added mass is determined to be:

$$\frac{A_{33}^{(2D)}}{\rho\pi a^2} \approx C$$

Equation 187

$$A_{33}^{(2D)} = \rho\pi a^2 C$$

Equation 188

Deriving Semisubmersible Heave Motion

The semisubmersible heave equation of motion is as following:

$$(M + A_{33})\ddot{\eta}_3 + B_{33}\dot{\eta}_3 + C_{33}\eta_3 = F_3$$

Equation 189

Note that A_{33} in Equation 189 is the hull heave 3-dimensional added mass.

Assuming long wave:

$$B_{33}\dot{\eta}_3 \ll (M + A_{33})\ddot{\eta}_3$$

Equation 190

Simplifying the equation of motion:

$$(M + A_{33})\ddot{\eta}_3 + C_{33}\eta_3 = F_3$$

Equation 191

$$\ddot{\eta}_3 = -\omega^2\eta_3$$

Equation 192

$$C_{33} = \rho g A_w$$

Equation 193

$$A_w = 4L_C w_c$$

Equation 194

$$-\omega^2(M + A_{33})\eta_3 + (4\rho g L_C w_c)\eta_3 = F_3$$

Equation 195

$$\eta_3 = \frac{F_3}{-\omega^2(M + A_{33}) + 4\rho g L_C w_c}$$

Equation 196

Substitute Equation 186 into Equation 196 to get the heave motion:

$$\eta_3 = \frac{\rho \xi_a g e^{-kz_m} \cos(\omega t)\left[\begin{array}{c}\left(-2kL_P \cos\left(\frac{k}{2}(L_P + L_C)\right) - 4\sin\left(k\frac{L_P}{2}\right)\right)\left(h_P w_P + \frac{A_{33}^{(2D)}}{\rho}\right) + \\ 4L_c w_c e^{-k(h_{draft} - z_m)} \cos\left(\frac{k}{2}(L_P + L_C)\right)\end{array}\right]}{-\omega^2(M + A_{33}) + (4\rho g L_C w_c + k_{riser} + k_{mooring})}$$

Equation 197

The amplitude of heave motion:

$$\overline{\eta_3} = \frac{\rho\xi_a g e^{-kz_m}\left[\begin{array}{c}\left(-2kL_P\cos\left(\frac{k}{2}(L_P+L_C)\right)-4\sin\left(k\frac{L_P}{2}\right)\right)\left(h_P w_P+\frac{A_{33}^{(2D)}}{\rho}\right)+\\ 4L_c w_c e^{-k(h_{draft}-z_m)}\cos\left(\frac{k}{2}(L_P+L_C)\right)\end{array}\right]}{-\omega^2(M+A_{33})+4\rho g L_C w_c}$$

Equation 198

APPENDIX 2

Base Case Semisubmersible

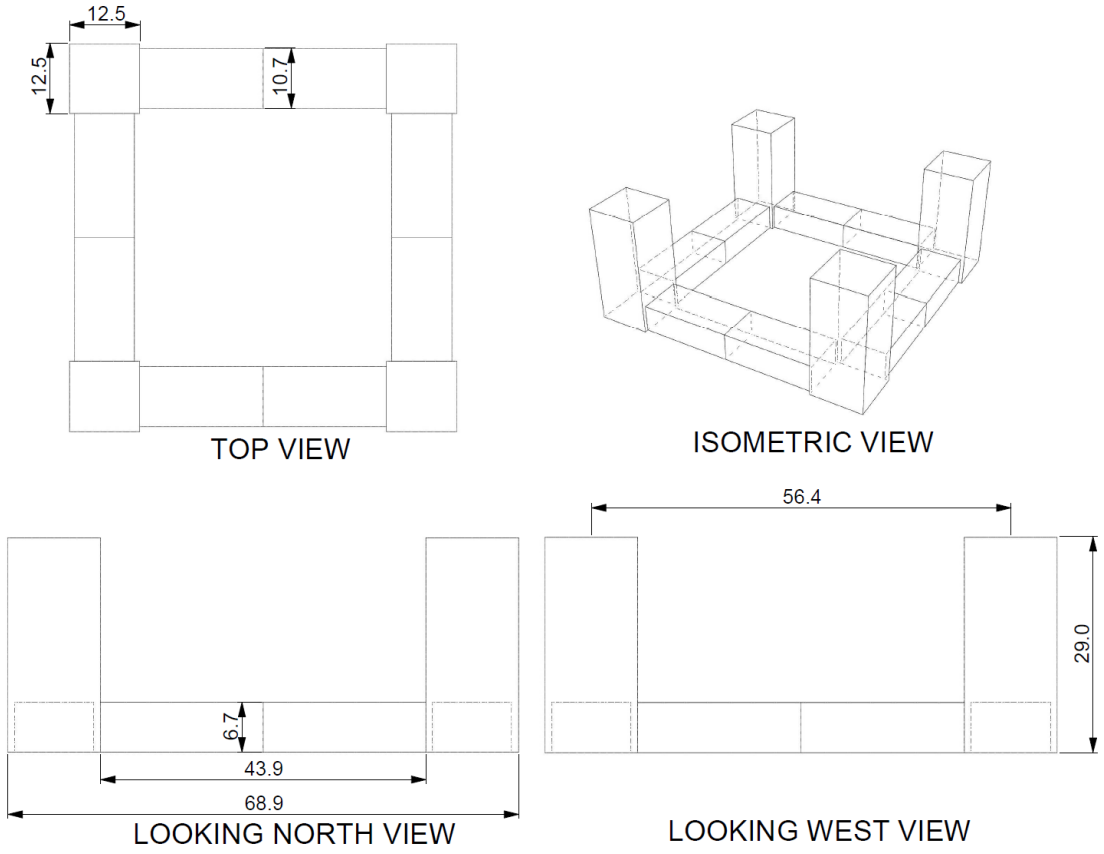

Figure 37 Base Case semisubmersible layout (Kang 2015)

Option-1 McDermott Deepdraft Semisubmersible (Chen, Mei, & Mills, 2007)

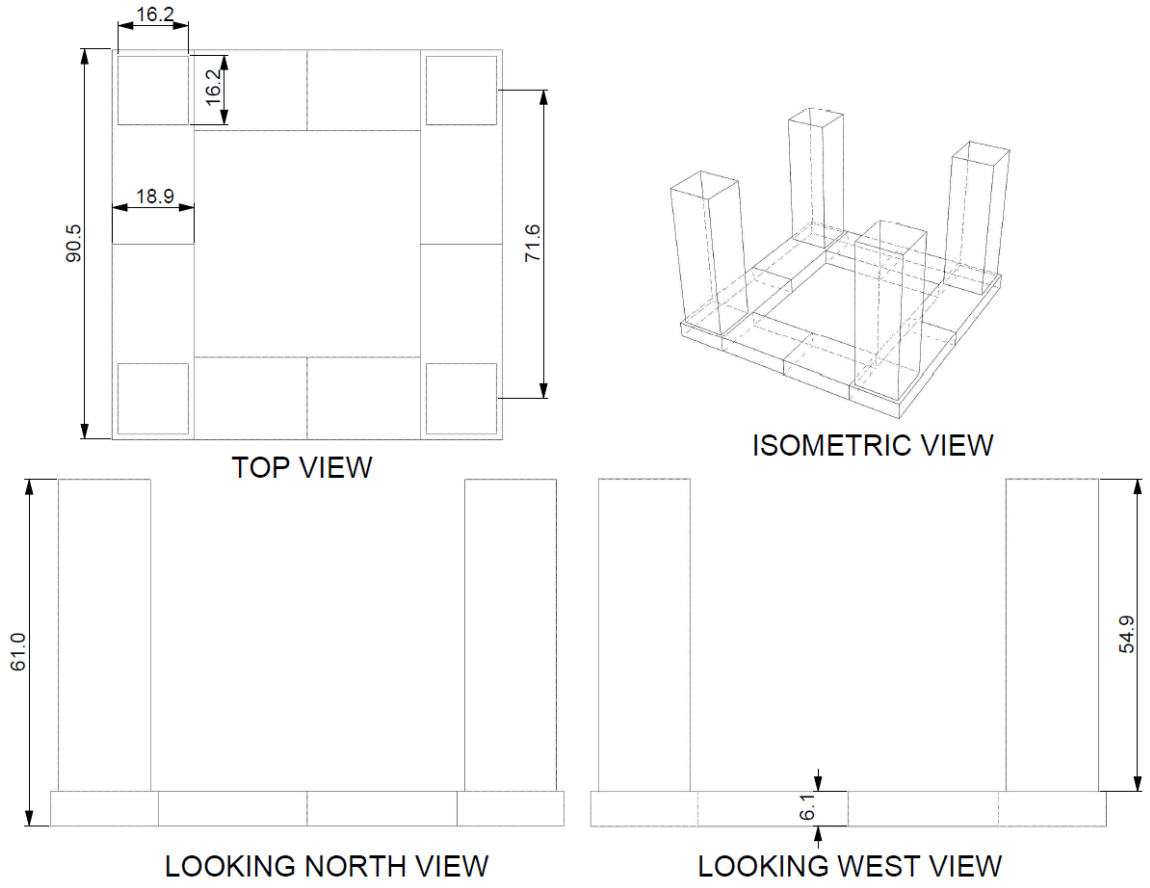

Figure 38 Option-1 semisubmersible layout (Chen, Mei and Mills 2007)

Option-2 Floatec Offset-Pontoon Semisubmersible

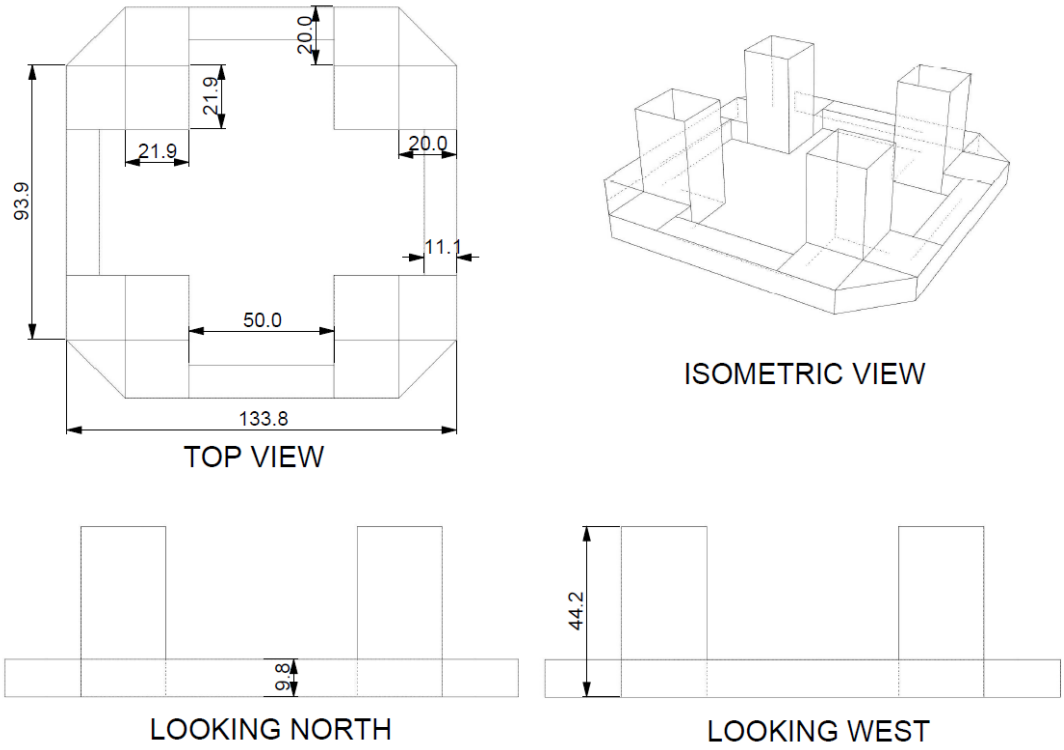

Figure 39 Option-2 semisubmersible layout (Muehlner and Banumurthy 2015)

Mid-Case Semisubmersible

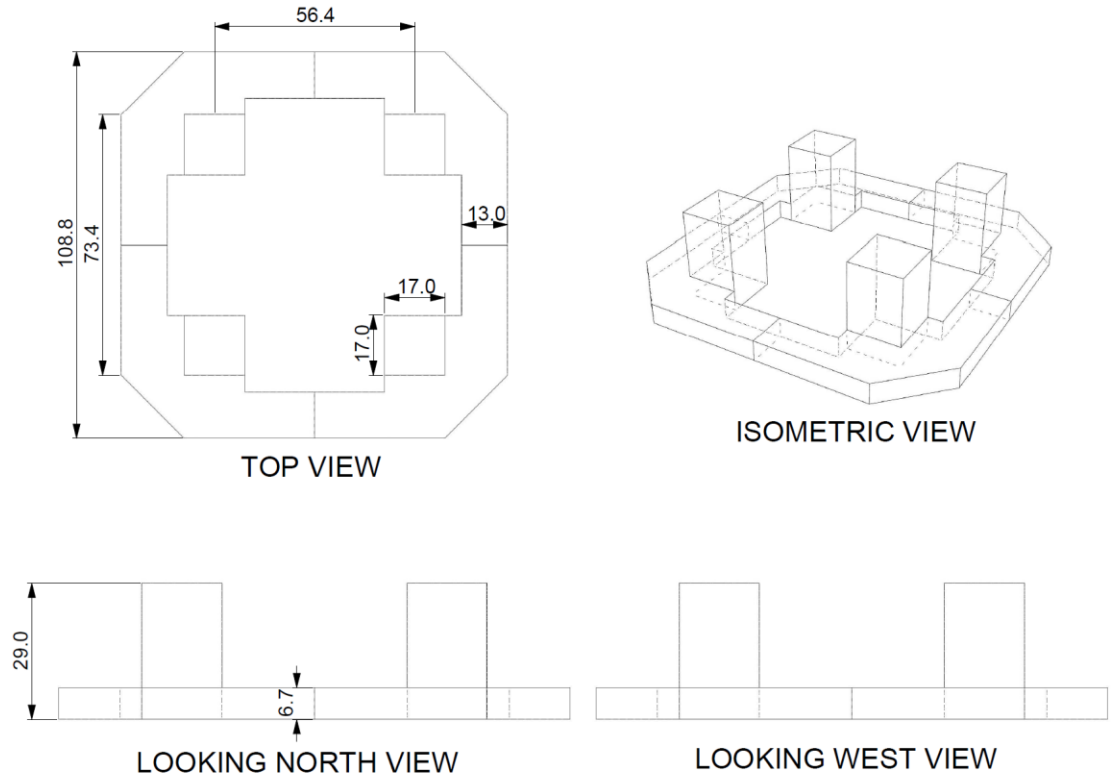

Figure 40 Mid-Case semisubmersible layout

APPENDIX 3

Leg #	Top Hang Off Point (m)			Pretension (kN)
	x	y	z	
Leg 01	47.67	51.91	-22.25	2030.00
Leg 02	49.79	49.79	-22.25	2030.00
Leg 03	51.91	47.67	-22.25	2030.00
Leg 04	51.91	-47.67	-22.25	2030.00
Leg 05	49.79	-49.79	-22.25	2030.00
Leg 06	47.67	-51.91	-22.25	2030.00
Leg 07	-47.67	-51.91	-22.25	2030.00
Leg 08	-49.79	-49.79	-22.25	2030.00
Leg 09	-51.91	-47.67	-22.25	2030.00
Leg 10	-51.91	47.67	-22.25	2030.00
Leg 11	-49.79	49.79	-22.25	2030.00
Leg 12	-47.67	51.91	-22.25	2030.00

Table 31 Mooring leg top-hang off points and pretension

TTR #	Top Hang Off Point (m)			Nominal Top-Tension (kN)
	x	y	z	
TTR-1	-5	0	22.25	4928.60
TTR-2	5	0	22.25	4928.60

Table 32 Top-tensioned riser top-hang off points and nominal top-tension

APPENDIX 4

Plot of Tensioner System Curves for Case-1 through Case-5

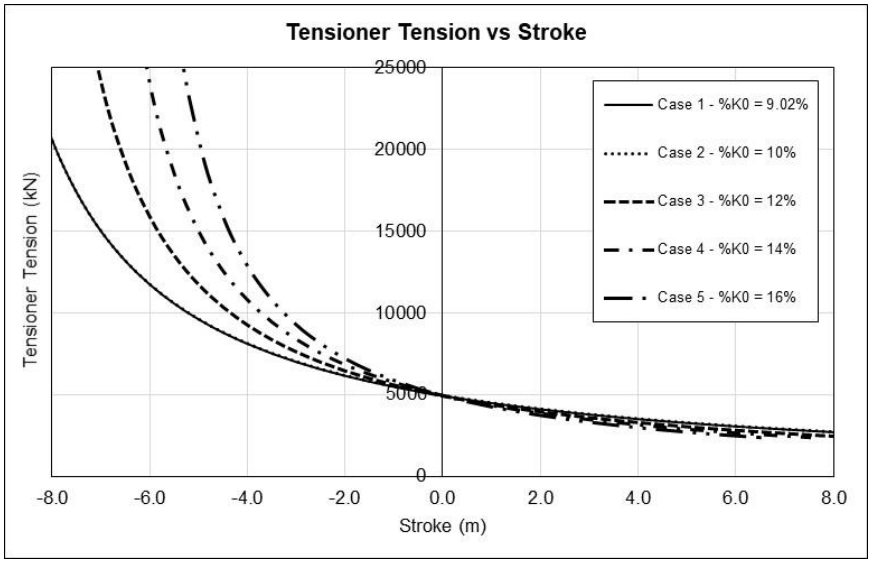

Figure 41 Plot of tensioner tension vs stroke Case-1 through Case-5

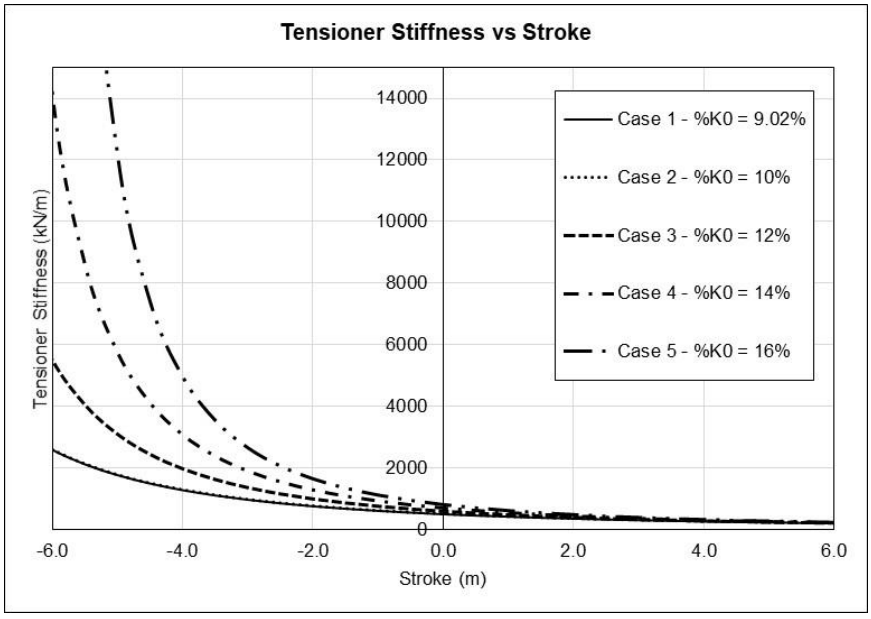

Figure 42 Plot of tensioner stiffness vs stroke Case-1 through Case-5

Comparison Plot between Case-2 Tensioner with Backside Pressure and Without Backside Pressure

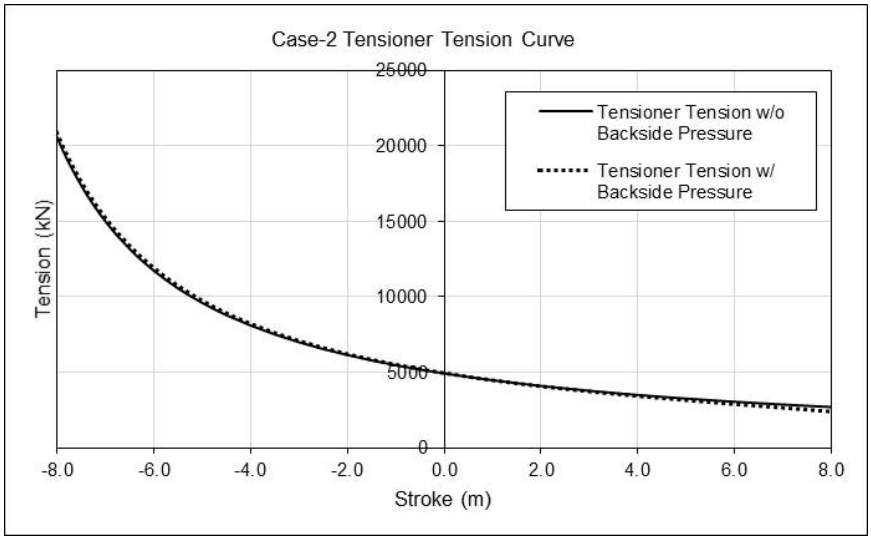

Figure 43 Comparison plot between tensioner tension with backside pressure and without backside pressure

APPENDIX 5

Motion Mode	Base Case			Case-2 Floatec			Mid-Case		
	Max	Min	Total	Max	Min	Total	Max	Min	Total
Surge	-0.83 m (-2.72 ft)	-35.41 m (-116.18 ft)	34.58 m (113.45 ft)	-0.01 m (-0.03 ft)	-28.05 m (-92.02 ft)	28.04 m (91.99 ft)	0.00 m (-0.02 ft)	-34.62 m (-113.58 ft)	34.61 m (113.57 ft)
Sway	-0.13 m (-0.43 ft)	-0.20 m (-0.64 ft)	0.06 m (0.21 ft)	0.06 m (0.18 ft)	0.00 m (0.00 ft)	0.06 m (0.18 ft)	0.11 m (0.37 ft)	0.00 m (0.00 ft)	0.11 m (0.37 ft)
Heave	6.59 m (21.64 ft)	-8.20 m (-26.91 ft)	14.80 m (48.55 ft)	2.65 m (8.70 ft)	-2.80 m (-9.19 ft)	5.45 m (17.89 ft)	3.70 m (12.14 ft)	-4.21 m (-13.81 ft)	7.91 m (25.95 ft)
Pitch	5.73 deg	-3.27 deg	9.00 deg	3.47 deg	-1.38 deg	4.86 deg	4.75 deg	-1.87 deg	6.63 deg
Roll	0.50 deg	0.36 deg	0.14 deg	0.03 deg	0.00 deg	0.04 deg	0.05 deg	-0.01 deg	0.05 deg
Yaw	0.13 deg	0.02 deg	0.11 deg	0.15 deg	0.00 deg	0.15 deg	0.21 deg	0.00 deg	0.21 deg

Table 33 Base-Case, Floatec Option-2 and Mid-Case semisubmersibles' displacement

Motion Mode	Base Case		Case-2 Floatec		Mid-Case	
	Max	Min	Max	Min	Max	Min
Surge	4.32 m/s (14.16 ft/s)	-4.38 m/s (-14.38 ft/s)	2.25 m/s (7.39 ft/s)	-2.37 m/s (-7.77 ft/s)	2.30 m/s (7.54 ft/s)	-2.49 m/s (-8.18 ft/s)
Sway	0.01 m/s (0.02 ft/s)	-0.01 m/s (-0.02 ft/s)	0.00 m/s (0.01 ft/s)	0.00 m/s (-0.01 ft/s)	0.00 m/s (0.02 ft/s)	0.00 m/s (-0.01 ft/s)
Heave	3.02 m/s (9.92 ft/s)	-2.78 m/s (-9.13 ft/s)	0.65 m/s (2.14 ft/s)	-0.61 m/s (-2.00 ft/s)	1.27 m/s (4.17 ft/s)	-1.15 m/s (-3.78 ft/s)
Pitch	0.03 rad/s (1.84 deg/s)	-0.03 rad/s (-1.61 deg/s)	0.02 rad/s (1.17 deg/s)	-0.01 rad/s (-0.75 deg/s)	0.02 rad/s (1.02 deg/s)	-0.02 rad/s (-0.95 deg/s)
Roll	0.00 rad/s (0.02 deg/s)	0.00 rad/s (-0.02 deg/s)	0.00 rad/s (0.01 deg/s)	0.00 rad/s (0.00 deg/s)	0.00 rad/s (0.01 deg/s)	0.00 rad/s (-0.01 deg/s)
Yaw	0.00 rad/s (0.01 deg/s)	0.00 rad/s (-0.01 deg/s)	0.00 rad/s (0.01 deg/s)	0.00 rad/s (-0.01 deg/s)	0.00 rad/s (0.01 deg/s)	0.00 rad/s (-0.01 deg/s)

Table 34 Base-Case, Floatec Option-2 and Mid-Case semisubmersibles' velocity

Motion Mode	Base Case		Case-2 Floatec		Mid-Case	
	Max	Min	Max	Min	Max	Min
Surge	1.68 m/s² (5.51 ft/s²)	-1.87 m/s² (-6.13 ft/s²)	0.88 m/s² (2.90 ft/s²)	-0.96 m/s² (-3.16 ft/s²)	0.88 m/s² (2.90 ft/s²)	-0.98 m/s² (-3.21 ft/s²)
Sway	0.00 m/s² (0.01 ft/s²)	0.00 m/s² (-0.01 ft/s²)	0.00 m/s² (0.00 ft/s²)	0.00 m/s² (0.00 ft/s²)	0.00 m/s² (0.00 ft/s²)	0.00 m/s² (0.00 ft/s²)
Heave	1.19 m/s² (3.90 ft/s²)	-1.31 m/s² (-4.28 ft/s²)	0.19 m/s² (0.63 ft/s²)	-0.20 m/s² (-0.65 ft/s²)	0.40 m/s² (1.30 ft/s²)	-0.42 m/s² (-1.39 ft/s²)
Pitch	0.02 rad/s² (0.87 deg/s²)	-0.01 rad/s² (-0.80 deg/s²)	0.01 rad/s² (0.31 deg/s²)	-0.01 rad/s² (-0.31 deg/s²)	0.01 rad/s² (0.38 deg/s²)	-0.01 rad/s² (-0.38 deg/s²)
Roll	0.00 rad/s² (0.01 deg/s²)	0.00 rad/s² (-0.01 deg/s²)	0.00 rad/s² (0.00 deg/s²)	0.00 rad/s² (0.00 deg/s²)	0.00 rad/s² (0.00 deg/s²)	0.00 rad/s² (0.00 deg/s²)
Yaw	0.00 rad/s² (0.00 deg/s²)	0.00 rad/s² (0.00 deg/s²)	0.00 rad/s² (0.00 deg/s²)	0.00 rad/s² (0.00 deg/s²)	0.00 rad/s² (0.00 deg/s²)	0.00 rad/s² (0.00 deg/s²)

Table 35 Base-Case, Floatec Option-2 and Mid-Case semisubmersibles' acceleration